Heat balance and temperature regulation in complex biological systems

Dissertation

der Mathematisch-Naturwissenschaftlichen Fakultät
der Eberhard Karls Universität Tübingen
zur Erlangung des Grades eines
Doktors der Naturwissenschaften
(Dr. rer. nat.)

vorgelegt von
Dipl.-Ing. (FH) Ulf Fischbach, M.Eng.
aus Dernbach

Tübingen
2017

Gedruckt mit der Genehmigung der Mathematisch-Naturwissenschaftlichen Fakultät der Eberhard Karls Universität Tübingen.

Tag der mündlichen Qualifikation:	25.04.2017
Dekan:	Prof. Dr. Wolfgang Rosenstiel
1. Berichterstatter:	Prof. Dr. David Wharam
2. Berichterstatter:	Prof. Dr. Ulrich Gärtner

Teile der Inhalte aus den Kapiteln 2, 3 und 5 der vorliegenden Arbeit sind bereits in der Dissertation "Ökophysiologische Konsequenzen und Bewältigung hoher Habitattemperaturen bei mediterranen Landschnecken" (Dr. Andreas Dieterich, Universität Tübingen, 2015) enthalten. Dies begründet sich in unserer Zusammenarbeit innerhalb eines "Twinning Projektes" der Universität Tübingen und der Hochschule Esslingen. Mein Eigenanteil an diesen Kapiteln beträgt wie folgt:

Kapitel	wissenschaftliche Konzeption	Daten-generierung	Analyse und Interpretation	Schriftliche Ausarbeitung
2	75 %	98 %	99 %	98 %
3	60 %	60 %	95 %	99 %
5	80 %	60 %	95 %	99 %

meiner Tochter.

"Simplicity is the ultimate sophistication"
Leonardo da Vinci

Danksagung

Herrn Prof. Dr.-Ing. Ulrich Gärtner, Leiter des Instituts für Angewandte Forschung Energetische Systeme an der Hochschule Esslingen, danke ich für die hervorragende Zusammenarbeit, die äußerst konstruktiven Diskussionen sowie die wohlwollende Förderung meiner Arbeit. Seine fachliche und persönliche Unterstützung haben ein Umfeld geschaffen, in dem ich immer gerne gearbeitet habe. Ebenso danke ich Herrn Prof. Dr.-Ing. Stefan Rösler, der bei allen thermo- und fluiddynamischen Fragen ebenfalls stets ein offenes Ohr für mich hatte.

Herrn Prof. Dr. David Wharam danke ich für die ausgezeichnete Betreuung und für seine stetige Diskussionsbereitschaft; ohne ihn wäre die gesamte Arbeit nicht zustande gekommen. Das persönliche Verhältnis, das er zu all seinen Doktoranden pflegt, habe ich sehr zu schätzen gelernt und hatte großen Einfluss auf den Fortgang dieser Arbeit.

Herrn Prof. Dr. Heinz-R. Köhler, Dr. Andreas Dieterich, Dr. Christophe Mazzia und Dr. Yvan Capowiez möchte ich ganz besonders für das Feedback, die Anregungen und Denkanstöße rund um alle biologischen Fragen danken.

Ein ganz besonderer Dank gilt der Mathematisch-Naturwissenschaftlichen Fakultät der Eberhard Karls Universität Tübingen, durch deren finanzielle Förderung im Rahmen des Twinning Projektes mir die Möglichkeit zu dieser Arbeit überhaupt erst gegeben wurde.

An dieser Stelle darf natürlich Dipl.-Ing. (FH) Markus Ludwig auch nicht unerwähnt bleiben. Die ehrlichen und offenen Gespräche während unserer gemeinsamen Zeit waren mir immer wieder eine Unterstützung und Motivation.

Darüber hinaus möchte ich mich bei allen Mitarbeitern des Labors für Wärme- und Strömungstechnik, insbesondere Herrn Dipl-Ing. Frank Bühler und Herrn Joachim Herz, für die gute Zusammenarbeit bei den Messungen zum Sauerstoffverbrauch bedanken.

Für die Unterstützung bei den kalorischen Untersuchungen und die Bereitstellung des Thermal Activity Monitors gilt mein Dank Herrn Prof. Dr. Günter Gauglitz und Dr. Felix Kolarov der Universität Tübingen.

In gleicher Weise gilt mein Dank Herrn Volker Lehmann der Bruker-Biospin GmbH in Rheinstetten. Sein großes Interesse an diesem Forschungsgebiet hat

einen entscheidenden Baustein für die vorliegende Arbeit geliefert.

Vor allem danke ich meinen Projektstudenten, ohne deren Hilfe meine Arbeit nicht auf diese Art und Weise zustande gekommen wäre.

Der größte Dank gilt jedoch meiner gesamten Familie, die mir auch in schwierigen Lebenslagen stets den nötigen moralischen und finanziellen Rückhalt gegeben hat. Insbesondere danke ich meiner Frau Nadine, die mir in schwierigen Phasen dieser Arbeit immer wieder Kraft und Mut zugesprochen hat.

Abstract

The present work gives an insight into the internal heat management system of the terrestrial snail *Xeropicta derbentina*, which has to cope with extreme climate conditions in its habitat. The oxygen consumption of inactive animals was investigated in order to clarify if the entire metabolism is adapted to high ambient temperatures. It was found that particularly medium-sized individuals show a significant reduction in oxygen consumption when exposed to high temperatures. Additionally, the extrapolation of measured data revealed theoretical upper and lower temperature limits. These were associated with arousal of the animal and the temperature of maximum heat shock protein (Hsp70) production that serves as a molecular protection system. The metabolic scaling exponent was found to decrease for increasing temperatures.

Calorimetric investigations of two size groups have shown that small individuals react more sensitive to increasing temperatures. Active and inactive metabolic energy was separated and the active share was found to decrease for both size groups as temperature increases. The comparison of mass ratio and ratio of change of time spent in activity when temperature increases from 20 °C to 30 °C showed an inverse proportionality indicating that mass and exposition to ambient temperature influence the behavior of the animal.

NMR measurements were performed that provided data of the vein system, the lung volume and the heart volume of *X. derbentina*. Combining these geometrical data and the measured oxygen consumption and calorimetric data facilitated the calculation of additional physiological parameters.

A surrogate model of the vein system was constructed and the active diffusive surface of capillaries and main vein was calculated and confirmed by geometrical measurements. Finally, a model was presented that is able to validate the measured oxygen consumption by the use of the Colburn analogy between mass and momentum transfer. By combining basic diffusion laws with the momentum transfer, i.e. wall shear stress, at the inner wall of capillaries and main vein the progression of oxygen mass fraction inside the hemolymph can be visualized.

Xeropicta derbentina, terrestrial snail, heat balance, oxygen consumption, metabolic scaling, calorimetry, diffusion, Colburn analogy

Zusammenfassung

Die vorliegende Arbeit gibt einen Einblick in den Wärmehaushalt der Landschnecke *Xeropicta derbentina*, die in ihrem Habitat mit extremen klimatischen Bedingungen konfrontiert ist. Der Sauerstoffverbrauch von inaktiven Tieren wurde untersucht, um zu prüfen, inwieweit der gesamte Stoffwechsel der Tiere an hohe Umgebungstemperaturen angepasst ist. Es wurde speziell bei Schnecken mittlerer Größe ein signifikanter Rückgang im Sauerstoffverbrauch gemessen wenn diese einer hohen Temperatur ausgesetzt werden. Darüber hinaus hat die Extrapolation der gemessenen Daten ein oberes und unteres theoretisches Temperaturlimit aufgezeigt. Diese wurden mit der Aktivierung des Stoffwechsels der Tiere und mit der Temperatur des maximal induzierbaren Hitzeschockproteins (Hsp70) in Verbindung gebracht.

Kalorische Messungen an zwei Größengruppen haben ergeben, dass kleine Tiere sensibler auf eine Temperaturerhöhung reagieren. Der aktive und inaktive Anteil des Gesamtumsatzes wurde separiert und es ergab sich ein reduzierter aktiver Anteil bei beiden Größengruppen. Der Vergleich des Massenverhältnisses mit dem der zeitlichen Reduktion der Aktivität beider Größengruppen hat eine inverse Proportionalität gezeigt. Dies deutet darauf hin, dass das Körpergewicht und die Umgebungstemperatur das Verhalten der Tiere beeinflussen.

NMR Messungen lieferten geometrische Informationen zu Adersystem, Volumen der Lunge und dem Volumen des Herzens von *X. derbentina*. Durch die Verknüpfung dieser Werte mit den gemessenen Sauerstoffverbräuchen und kalorischen Daten wurden zusätzliche physiologische Parameter ermittelt.

Ein Ersatzmodell des Adersystems wurde konstruiert und die aktive diffusive Oberfläche des Adersystems berechnet und mithilfe geometrischer Messungen bestätigt. Schließlich wurde ein Modell vorgestellt, das auf der Colburn Analogie zwischen Massen- und Impulsaustausch basiert. Mit dessen Hilfe war es möglich, den gemessenen Sauerstoffverbrauch zu validieren. Durch die Kombination grundlegender Diffusionsgesetze mit dem wandnahen Impulsaustausch (Wandschubspannung) im Inneren des Adersystems konnte der Verlauf des Sauerstoffmassenanteils in der Hämolymphe dargestellt werden.

Xeropicta derbentina, Landschnecke, Wärmehaushalt, Sauerstoffverbrauch, Allometrie, Kalorimetrie, Diffusion, Colburn Analogie

Contents

List of Figures

List of Tables

Nomenclature

Dimensionless Numbers

Symbol	Description	Definition
Nu	Nusselt number	$\frac{\alpha \cdot L}{\lambda} = \frac{q_w \cdot L}{\lambda \cdot \Delta T}$
Pr	Prandtl number	$\frac{\nu}{a}$
Re	Reynolds number	$\frac{u_\infty \cdot L}{\nu}$
Sc	Schmidt number	$\frac{\nu}{D}$
Sh	Sherwood number	$\frac{\beta \cdot L}{D} = \frac{j_w \cdot L}{\rho \cdot D \cdot \Delta \omega}$

Greek Symbols

Symbol	Description	Dimensions	Units
α	scaling exponent	–	1
α	heat transfer coefficient	$\mathsf{MT}^{-3}\Theta^{-1}$	$\mathrm{W \cdot m^{-2} \cdot K^{-1}}$
β	mass transfer coefficient	LT^{-1}	$\mathrm{m \cdot s^{-1}}$
ΔH_{vap}	molar enthalpy of vaporization	$\mathsf{ML}^2\mathsf{T}^{-2}\mathsf{N}^{-1}$	$\mathrm{J \cdot mol^{-1}}$
$\Delta O_{2_{\mathrm{breath}}}$	oxygen reduction per breath	–	%
λ	thermal conductivity	$\mathsf{MLT}^{-3}\Theta^{-1}$	$\mathrm{W \cdot m^{-1} \cdot K^{-1}}$

λ	flow coefficient	$-$	1
μ	dynamic viscosity	$\mathsf{ML^{-1}T^{-1}}$	$\mathrm{Pa \cdot s}$
ν	kinematic viscosity	$\mathsf{L^2T^{-1}}$	$\mathrm{m^2 \cdot s^{-1}}$
ϕ	relative humidity	–	$\%$
Φ	raise of O_2 concentration due to chemical bonding	–	1
ρ	density	$\mathsf{ML^{-3}}$	$\mathrm{kg \cdot m^{-3}}$
ω	mass fraction	$-$	1
τ	shear stress	$\mathsf{ML^{-1}T^{-2}}$	$\mathrm{N \cdot m^{-2}}$
ξ	decrease of O_2 mass fraction in the lung due to inhalation effects	$-$	1

Roman Symbols

Symbol	Description	Dimensions	Units
A	area	$\mathsf{L^2}$	$\mathrm{m^2}$
a	thermal diffusivity	$\mathsf{L^2T^{-1}}$	$\mathrm{m^2 \cdot s^{-1}}$
c	concentration	$\mathsf{NL^{-3}}$	$\mathrm{mol \cdot m^{-3}}$
CE	calorimetric equivalent	$\mathsf{ML^{-1}T^{-2}}$	$\mathrm{kJ \cdot l^{-1}}$
c_f	friction coefficient	$-$	1
c_v	specific heat capacity at constant volume	$\mathsf{L^2T^{-2}\Theta^{-1}}$	$\mathrm{J \cdot kg^{-1} \cdot K^{-1}}$
CV	caloric value	$\mathsf{ML^2T^{-2}N^{-1}}$	$\mathrm{kJ \cdot mol^{-1}}$
D	diffusion coefficient, diffusivity	$\mathsf{L^2T^{-1}}$	$\mathrm{m^2 \cdot s^{-1}}$

D	diameter	L	m
d	distance	L	m
e	internal energy	$\mathsf{ML}^2\mathsf{T}^{-2}$	J
e	eulerian number	–	1
$e_{(T)}$	saturated vapor pressure	$\mathsf{ML}^{-1}\mathsf{T}^{-2}$	Pa
f	frequency	T^{-1}	Hz
f_b	breathing frequency	T^{-1}	min^{-1}
J	diffusion mass flow	MT^{-1}	$\mathrm{kg} \cdot \mathrm{s}^{-1}$
j	diffusion flux	$\mathsf{NL}^{-2}\mathsf{T}^{-1}$	$\mathrm{mol} \cdot \mathrm{m}^{-2} \cdot \mathrm{s}^{-1}$
$k_{\mathrm{H,cp}}$	henry constant	$\mathsf{M}^{-1}\mathsf{NL}^{-2}\mathsf{T}^{2}$	$\mathrm{mol} \cdot \mathrm{l}^{-1} \cdot \mathrm{atm}^{-1}$
L	characteristic length	L	m
l	length	L	m
q	heat flux	MT^{-3}	$\mathrm{W} \cdot \mathrm{m}^{-2}$
m	amount of mol O_2 to turnover 1 mol of glucose	–	1
m	mass, body weight	M	kg
MR	metabolic rate	NT^{-1}	$\mathrm{mol} \cdot \mathrm{s}^{-1}$
$\dot{n}_{O_2}$	oxygen consumption	NT^{-1}	$\mathrm{mol} \cdot \mathrm{s}^{-1}$
n	amount of substances	N	mol
n	number of specimens, number of segments	–	1
P	cardiac performance	$\mathsf{ML}^2\mathsf{T}^{-3}$	W
p	pressure	$\mathsf{ML}^{-1}\mathsf{T}^{-2}$	Pa
p	probability value	–	1

P_{th}	thermal output	$\mathsf{ML^2T^{-3}}$	W
R	radius	L	m
R	universal gas constant	$\mathsf{ML^2T^{-2}N^{-1}\Theta^{-1}}$	$\mathrm{J \cdot mol^{-1} \cdot K^{-1}}$
r	correlation coefficient	–	1
r	ratio of lung volume to breathing volume	–	1
r	spatial fraction of substances	–	1
R^2	coefficient of determination	–	1
T	temperature	$\mathsf{\Theta}$	K
T_1	time constant of spin-lattice relaxation	T	s
T_2	time constant of decay of magnetization M_{xy}	T	s
T_E	echo time	T	s
t	time	T	s
T_R	repetition time	T	s
u	velocity in x direction	$\mathsf{LT^{-1}}$	$\mathrm{m \cdot s^{-1}}$
$\vec{v}$	velocity vector	$\mathsf{LT^{-1}}$	$\mathrm{m \cdot s^{-1}}$
v	velocity in y direction	$\mathsf{LT^{-1}}$	$\mathrm{m \cdot s^{-1}}$
V	volume	$\mathsf{L^3}$	$\mathrm{m^3}$
$\dot{V}_b$	breathing volume per minute	$\mathsf{L^3T^{-1}}$	$\mathrm{m^3 \cdot s^{-1}}$
V_b	breathing volume	$\mathsf{L^3}$	$\mathrm{m^3}$
V_l	lung volume	$\mathsf{L^3}$	$\mathrm{m^3}$
V_m	molar volume	$\mathsf{L^3N^{-1}}$	$\mathrm{m^3 \cdot mol^{-1}}$

$\dot{V}_{O_2}$	volume flow of oxygen	$\mathsf{L}^3\mathsf{T}^{-1}$	$\mathrm{m}^3 \cdot \mathrm{s}^{-1}$
w	velocity in z direction	LT^{-1}	$\mathrm{m} \cdot \mathrm{s}^{-1}$
X	concentration fraction passing from physical solubility to chemical bonding	$-$	1

Chapter 1

Introduction

The present work has been conducted in the faculty of Mechanical Engineering at the Esslingen University of Applied Sciences and is part of the "Twinning Project" "Wärmeflüsse, Thermodynamik und ökophysiologische Konsequenzen hoher Temperaturen bei mediterranen Landschnecken" of the Eberhard Karls University Tübingen under the supervision of Prof. H.-R. Köhler. The project is structured as a co-operation between the faculty of Mechanical Engineering of the Esslingen University of Applied Sciences and the department of Biology at the University of Tübingen with the objective of promoting interdisciplinary research between the two universities. The overall aim is the investigation of the evolutionary pressure on a particular species of living organism, the land snail *Xeropicta derbentina*. The extremely warm climatic conditions in its habitat directly hamper its survival and this investigation yields a very descriptive example of climatic conditions influencing the evolutionary fitness as well as the genetic variability and adaptability of a specific species.

Xeropicta derbentina (Krynicki 1836) (Gastropoda, Hygromiidae) is a terrestrial, pulmonate snail abundant in southern France, whence it was introduced from the eastern Mediterranean. In southern France, *X. derbentina* was first reported in 1949 [Aubry et al., 2006, Kiss et al., 2005, Van Regteren Altena, 1960] presumably having been introduced into southern France during the Second World War. Although this species has to cope with hot and dry conditions in its habitat it has been spreading northwards ever since. In southern France it is often found in areas with scarce vegetation and high sun exposure. In order to survive under these conditions this animal has had to

develop physiological as well as behavioral mechanisms that have allowed it to populate such regions.

X. derbentina is an annual species that reaches adult shell sizes up to approximately 15 mm. Its outer shell morphology is dominated by a uniformly white color [Dieterich et al., 2013], but a smaller percentage of individuals also shows a darkly pigmented banding [Dieterich et al., 2014]. The development of a calcified shell helps to minimize the effective area for water loss and to keep the mucous layer between the shell and the interior of the snail [Dieterich, 2015]. During its locomotion ashore large amounts of mucous are disseminated. Especially in hot and dry regions land snails, therefore, need to ensure a sufficient water intake to compensate for this loss. As their water content is higher than 75 % [Reuner et al., 2008], desiccation and overheating pose a major threat to their survival. Thus, the overall energy balance of *X. derbentina* is characterized by the trade-off between evaporative water loss needed for convective cooling and the demand to minimize total water loss.

During July and August in southern France air temperatures a few centimeters above the ground reach values up to 45 °C and can even exceed values of 55 °C on the soil surface, which constitute hostile conditions for snails. Detailed measurements of temperature, air velocity, and humidity have shown that this snail species withstands ambient temperatures of over 40 °C for a whole day [Ludwig, 2012]. As a behavioral reaction to these conditions the snails climb vertical objects, such as blades of grass or other vegetation, as can often be observed early in the morning as its habitat heats up and humidity decreases. Such climbing behavior is believed to be a part of the snails' survival strategy by protecting them from unfavorable conditions near the ground and is one of the reasons for *X. derbentina*'s rapid spread throughout southern France [Aubry et al., 2006]. Once individuals have reached cooler conditions at positions high above the ground they become inactive and retract into their shells to avoid desiccation. For food and fluid intake most land snails, therefore, become active during the cooler and moister phases in the evening and at night-time.

During hot and dry summer days *X. derbentina* remains inactive for long periods of time, develops an epiphragm to seal its aperture and thus further minimize water loss by evaporation, and may form clusters of hundreds of

individuals at positions distant from the soil surface. The structure of the epiphragm is constituted in such a way that diffusion of oxygen is ensured [Barnhart, 1983] allowing them to stay inactive for as long as several months with very little water loss.

Next to these behavioral reactions of *X. derbentina* both metabolic and physiological adaptations have been ascertained that facilitate a survival under unfavorable conditions. *Otala lactea* (Müller 1774) for example remains inactive during the whole summer and passes into the phase of aestivation in order to reduce its metabolic activity towards a minimum [Herreid, 1977]. In the present work the term aestivation should describe a short- to medium-term reduction of metabolic activity to overcome disadvantageous conditions such as hot and dry phases. Additionally aestivation in snails is often associated with a reduction in heartbeat and breathing frequency [Rees and Hand, 1990, Rizzatti and Romero, 2001].

In the context of physiological adaptations it has been shown that another common mechanism in *X. derbentina* is the production of heat shock proteins (Hsp) that serve as a primary defense to protect cells from proteotoxic damage [Dieterich et al., 2013]. Heat shock proteins possess the ability of correctly refolding a certain proportion of proteins after they are exposed to a cellular stressor, such as temperature or heavy metals [Köhler et al., 1992, Triebskorn et al., 1997]. Their task of stabilization after a stress impulse protects cellular proteins from denaturation and accelerates the degradation of damaged proteins. This protection mechanism is, however, only functional up to a certain maximum of stress impulses. If the intensity of the stress exceeds this capacity the Hsp level decreases again and the protection mechanism can no longer be guaranteed [Eckwert et al., 1997]. Based on their molecular weight different families of Hsp have been characterized of which the Hsp70 family is best-researched to date.

Not only the molecular stress response but rather the entire metabolism needs to be adapted to high ambient temperatures in order that these snails are able to withstand severe climatic conditions over short periods of time. Several biological investigations on *X. derbentina* have been undertaken by researchers of the department of Biology at the University of Tübingen that already provide a deep insight into protein related mechanisms that are influ-

enced by climatic conditions, such as ambient temperature and general heat exposure of the animal [Dieterich et al., 2013, 2014, Köhler, 2009, Troschinski et al., 2014]. These mechanisms will not be further considered in the present work. However, the use of engineering and physical techniques such as high-precision measurements of metabolism and the numerical simulations of fluid- and thermodynamics in combination with the biological approach of protein analysis and behavioral studies results in a very integrated view of the complex mechanisms of heat management taking place in the investigated organism.

In order to provide further contributions from the physical part of the co-operation, the overall heat management system of *X. derbentina* has been investigated. The present work thus aims at providing additional information to understand the highly developed physiological survival mechanisms of *X. derbentina*. As a first step, oxygen consumption was used as a proxy for metabolic activity to investigate possible metabolic regulation processes that take place at high temperatures. Based on a previous study from Riddle [1977] it is known that temperature has a large influence on the metabolism of snails, and may even trigger aestivation. At the same time snails adapted to hot and dry conditions consistently show lower values of oxygen consumption. This type of metabolic regulation has not previously been found in the investigated species. The fact that these individuals occupy large rural sections in southern France and are obviously very well adapted to the harsh Mediterranean climate highlights the importance of this measurement for *X. derbentina*. In order to measure the oxygen consumption of these small animals a sophisticated micro-respirometer has been constructed. The measurements of different size groups at different temperatures permitted the investigation of the allometry relationship between weight and metabolic rate of the animal. This correlation is mainly dominated by a characteristic exponent shared for all animals belonging to a distinct class. Its dependence upon temperature for *X. derbentina*, however, is still not fully clear and is also addressed.

Additionally, an attempt has been made to investigate possible physiological regulation effects over a comparable temperature range by high-precision direct calorimetry measurements of the overall metabolic turnover. With this technique all aerobic and anaerobic metabolic processes that produce heat are measured and integrated to deliver the thermal output of the individuals. By

applying this technique detailed insights into duration and output level of active and inactive phases can be obtained that provide valuable information about how long these phases last under varying thermal conditions and for different sizes of snails. Considering the fact that the geometrical size of the animals directly corresponds to their age permits the investigation of metabolic activity under varying temperatures in between different life stages of the animals and possible metabolic adaptations during the latter.

Under the assumption of an aerobic metabolism both datasets, oxygen consumption and metabolic turnover via direct calorimetry, are quantitatively consistent with each other and permit the construction of an integrative physiological model of *X. derbentina*. In order to obtain additional values for the relevant parameters breathing frequency, breathing volume and oxygen reduction per breath, the geometry of the snail including its most important organs had to be acquired. Due to the animals high water content this was realized by a Nuclear Magnetic Resonance (NMR) measurement that has a high sensitivity to the local water concentrations. As this snail species only grows to a size of approximately 10–15 mm these measurements and their interpretation constitute a significant challenge. The derived integrative physiological model provides ranges for the aforementioned values and helps to further characterize the physiological state of the animal without the need to directly measure the corresponding parameters.

Based on these physiological values, the geometrical data of the lung and the heart as well as additional information derived from similar snail species, the oxygen concentrations in artery and vein are calculated as well as the amount of active diffusive surface of the animal's lung. These calculations subsequently lead to a range for the heartbeat frequency of *X. derbentina* as the volume flow of hemolymph, the snail's blood, is directly linked to the amount of the absorbed oxygen concentration during the respiration of the animal.

Subsequently a method is presented to calculate oxygen concentration along the venous system of *X. derbentina* that is based on a surrogate model of the venous system derived from the NMR measurements and utilizes the analogy between local shear stress in the venous system and mass transfer between the snail's lung and its hemolymph known as the Colburn analogy. The molar diffusion flow through all capillaries and the main vein is then compared to the

measured oxygen consumption of *X. derbentina* for validation of the model. Finally the cardiac performance of the snail is investigated.

In conclusion this research provides a better understanding of the metabolic processes that take place in the highly adapted organism of this species. The development of behavioral and physiological strategies allows *X. derbentina* to populate a region that is at first glance completely unsuitable for terrestrial land snails and in many ways restricts their lifestyle.

Chapter 2

Oxygen consumption and metabolic scaling of *X. derbentina*

2.1 Introduction

The influence of temperature on oxygen consumption in snails has been investigated by Mason [1971], who recorded respiration rates of twelve species at 5 °C, 10 °C, and 15 °C. His findings suggest a general rise in the metabolic rate with increasing temperature with only a single species displaying stagnant oxygen consumption at the highest test temperature. Mason confirmed these results for the species *Hygromia striolata* and *Discus rotundatus*. This tendency has also been confirmed by Rising and Armitage [1969] for two different species of slugs, *Limax maximus* and *Philomycus carolinianus*.

Schmidt-Nielsen et al. [1971] investigated the influence of temperature on *Sphincterochila boissieri*, a snail inhabiting the deserts of the Middle East and thus facing a very dry and hot climate. The authors showed that higher temperatures resulted in higher oxygen consumption and that this relationship mirrored the data recorded for non-desert snails. They concluded that no metabolic adaptation to temperatures up to 35 °C was present, but, as the lethal temperature for *S. boissieri* is known to be 50–55 °C, higher experimental temperatures up to this limit should be investigated. Furthermore, they noticed remarkable variations in consumption ("oxygen burst") which appeared periodically and were believed to be intrinsic since they occurred under constant external conditions and may, therefore, be characteristic for the

metabolism of *S. boissieri*. Herreid [1977] has also observed this behavior for *Otala lactea* obtained from Morocco. His results showed highly variable oxygen consumption rates of six individuals after arousal from dormancy which was triggered by increased humidity.

Riddle [1977] compared oxygen consumption between the desert snail *Rabdotus schiedeanus* and the garden snail *Helix aspersa* and found a general rise in oxygen consumption for temperatures up to 25 °C. Beyond 25 °C a metabolic regulation became visible for both species, and oxygen consumption declined, contrary to the results of Schmidt-Nielsen et al. [1971]. Riddle concluded that the "depressed metabolism (...) at high temperatures is adaptive in conserving metabolizable energy". This was especially evident for the desert snail *R. schiedeanus* that in general showed a lower oxygen demand. These studies were confirmed by Dallas et al. [1991] showing that individuals of *Trigonephrus sp.* had a significantly higher oxygen demand at 15 °C than at 25 °C, corresponding to an "active" and an "inactive" state of these Namibian desert snails. In comparison with *Helix aspersa* and *Otala lactea*, both snails of similar size, oxygen consumption was significantly lower showing the metabolic adaptation of *Trigonephrus* to much warmer climatic conditions.

Riddle [1975] demonstrated that atmospheric humidity has a strong influence on the oxygen consumption of the desert snail *R. schiedeanus*, resulting in significantly higher consumption for increasing relative humidity. The comparison with *Helix aspersa* additionally revealed the lower metabolic rates for the desert snail at high temperatures when humidity was very low [Riddle, 1977].

Comparative oxygen measurements by Steigen [1979] for banded and unbanded morphs of *Cepaea hortensis* revealed the oxygen consumption to generally increase between 5–15 °C and to stagnate for the unbanded morph at 25 °C.

Nopp [1965] reported the difference in oxygen consumption between starving, dry-sleeping, and "active" pulmonates. Starving *Arianta arbustorum* individuals showed significantly lower oxygen consumption rates than fresh-fed conspecifics. Furthermore, dry-sleeping individuals further reduced their oxygen consumption to approximately half of the "hungry-level". Nopp [1965] mentioned that this dry-sleep level is only reached after 2–4 days of inactiv-

ity. Blazka [1955] and Nopp [1965] also report that oxygen consumption in pulmonate land snails drops drastically at the beginning of estivation and subsequently remains almost constant from the second week of estivation onwards.

The absolute body size of an organism and therefore its weight is a very important factor in determining the rate of metabolic processes. This correlation is a classic topic of physiology. At the end of the 19th century Rubner [1883] noticed that the weight-specific metabolic rate of homoeothermic animals decreases with increasing body size. If, however, metabolic rate is calculated per unit body surface almost constant values can be obtained. This is known as the "surface rule" stating that the surface of two geometrically similar bodies can be expressed by the 2/3 power of weight multiplied by a constant (the cubic root of the volume is a linear value and its square, therefore, has the dimension of a surface).

A general mathematical expression for the dependency between metabolic rate and weight, the metabolic scaling, is given by the well-known allometry formula:

$$MR = b \cdot m^{\alpha} \tag{2.1}$$

where MR is the metabolic rate, expressed by oxygen consumption, m is the body weight, α is the scaling exponent, and b is a specific constant. Equation 2.1 can also be written as:

$$\log MR = \log b + \alpha \cdot \log m \tag{2.2}$$

This results in a linear relationship between $\log MR$ and $\log m$ with the slope α. If α=1 Equation 2.2 represents an isometric relationship, which results in a doubling of the metabolic rate as the weight doubles. If α=2/3 one directly obtains the relationship corresponding to the surface rule. Kleiber [1947] reviewed applications of the surface law in zoophysiology and showed that, for a certain group of mammals, the metabolic rate was proportional to the 0.756th[1] power of body weight. According to Kleiber [1947] the surface rule cannot be the sole explanation for the metabolic activity of animals but the behavior of a species has to be considered as well. Another general review of metabolism and body size is given by Bertalanffy [1957]. The author supposed that three

[1]Despite the fact that a power law derived from a rather small weight-spectrum may not result in such an accurate value, the three digits are presented anyway.

different "metabolic types" exist and that each species essentially belongs to one of these types. In the first type metabolism and growth is described in such a way that metabolic rate is proportional to the surface or the 2/3 power of weight following the assumptions of the surface rule. In the second type the rate is proportional to weight itself and, in the third type, an intermediate proportionality between surface and weight is found with $1>\alpha>2/3$. In recent years the generality of the 2/3 or the 3/4 power of weight metabolic scaling has been questioned [Chown et al., 2007, Kozłowski et al., 2003]. Glazier [2005] reviewed published data and showed that significant deviation exists from the 2/3 or 3/4 scaling model among mammals (0.38–1.11), squamate reptiles (0.27–1.26) and invertebrates (−1.2–2.05) (α became negative when juveniles were included). These deviations could not be explained by theoretical models, such as the resource-transport-network model [West and Brown, 2005, West et al., 1997], which predicts an exponent α of 0.75, from molecules to whole organisms, and describes the way "materials are transported through space-filling fractal networks of branching tubes". An alternative model based on cell size describes the change in metabolic scaling as a result of the way body size changes. Growth driven by an increasing cell number results in an isometric scaling of metabolism, whereas growth via an increasing cell size results in an exponent α=0.67 [Kozłowski et al., 2003]. The results of Chown et al. [2007] showed a broad variation of α (0.67–1) for an interspecific analysis of eight ant species, which also corresponded to the cell growth types of Kozłowski et al. [2003]. Furthermore, ontogenetic factors were investigated, such as phases of fast growth and reproduction that increase metabolic scaling, resulting in the finding that the exponent α may change during the course of ontogeny [Glazier, 2006]. Recently Glazier [2009] reviewed data of 19 ectothermic species and showed that the mean value of the metabolic exponent α was significantly higher for "active" animals (0.918) compared to "inactive" ones (0.768).

For poikilothermic invertebrates contradictory results concerning the exponent α have been published. Liebsch [1929] investigated three species of *Helicidae* showing a direct proportionality to weight and hence α=1, and the measurements carried out with *Cepaea vindobonensis* by Bertalanffy and Müller [1943] support this relationship. This was confirmed by the findings of Kienle

and Ludwig [1956] who measured oxygen consumption in *Helicella candicans*. In contrast to these results Wesemeier [1960] found the average slope of the curve in a log-log plot for four different species of land snails to be α=0.76. Wesemeier also criticized the results of Liebsch [1929] for not taking the state of locomotion into account. By comparing *Helix pomatia* at different levels of activity he showed that phases of resting and movement have an influence on the slope α resulting in values of 0.8 for moving snails and 0.71 for resting individuals. Furthermore he noted that Liebsch [1929] had calculated the regression coefficient as an average value for different species without accounting for interspecific variation. The results of Wesemeier [1960] for α in pulmonate land snails varied between 0.71 and 0.85 showing that there might not be an exact correlation between weight and metabolism, such as stated by the surface law, but rather a species-specific relationship. In addition the author confirmed the result of Kienle [1957] where the lung surface of *Helix pomatia* was found to be proportional to $W^{0.74}$. However, it is still unclear whether this is an intrinsic and therefore species-specific genetically fixed feature or if metabolism itself is limiting the growth of the lung surface. Steigen [1979] presented results of *Cepaea hortensis* for energy metabolism at temperatures from 5–25 °C showing a continuous decrease of α for increasing temperatures for banded (except for 20 °C) and unbanded morphs ranging from 1.06–1.23 and 0.96–1.60, respectively.

Mason [1971] found a linear relationship on a double log plot between weight and oxygen consumption in an interspecific comparison between twenty terrestrial snail species. However, this trend was only found for species with large adult size. Mason [1971] presented regression coefficients of 0.74, 0.65, and 0.71 for their slope at 5 °C, 10 °C, and 15 °C, respectively.

Czarnołęski et al. [2008] showed that phases of slow and fast growth in ontogeny affect the relationship between metabolism and size in *H. aspersa* resulting in an almost isometric relation (α=1) for the initial fast-growing ontogenetic phase and a lower value of α for the slow-growing phase. Similar variations in α due to different developmental stages of 421 individuals of *Cornu aspersum* were documented by Gaitán-Espitia et al. [2013].

Air-breathing water snails (*Basommatophora*) have been investigated by Berg and Ockelmann [1959] who found variations in α ranging from 0.45 to

1.0. They concluded that seasonal changes were the reason for this and also pointed out that "the relation, oxygen consumption to body size, is not a fixed, unchangeable quantity characteristic for all species (...)". Additionally, Duerr [1967] presented measurements for *Lymnaea stagnalis appressa*, another air-breathing water snail, and found a direct proportionality of respiration to its weight.

Acclimation to different temperatures within an appropriate time span is known to pose a physiological problem for some species that may result in different oxygen consumption rates, as reported by a number of authors [Herreid, 1977, Rising and Armitage, 1969, Schmidt-Nielsen et al., 1971, Segal, 1961, Steigen, 1979]. This effect, however, is not addressed in the current study.

Clearly, the discussion of the interrelationship of temperature, body size, and metabolism in terrestrial snails has a long-standing tradition. In this context, the present investigation is aimed at answering the following questions:

1. Does a change in temperature affect the oxygen consumption of *X. derbentina*?

2. If so, does the metabolism of individuals of different shell diameter react to the same extent?

3. If so, does the metabolism of "active" and "inactive" individuals react in the same way when temperature is changed?

4. What is the value of the exponent α for *X. derbentina* and how does it depend upon the ambient temperature?

2.2 Material and methods

2.2.1 Test organism

The present investigation uses *X. derbentina* (Krynicki 1836), a hygromiid land snail. Specimens were collected from an untreated meadow on private property close to Modène, department Vaucluse, southern France (N44°6.055′ E5°7.937′) between August and early November 2013. The owner neither applied any pesticides to the landsite nor used it as farm land. All snails collected were carried to the laboratory, kept hydrated and fed lettuce and baby porridge (Hipp Gute Nacht BIO oat & apple, Pfaffenhofen, Germany).

To assure constant starting conditions for all measurements snails were preconditioned in a separate climate chamber that reproduced the 24h humidity and temperature cycle characteristic for an average day in August in southern France. Immediately before the measurements, the individuals' masses and shell diameters were measured. In this study only "uniformly white" morphs were used in accordance with the shell coloration pattern classification used by Köhler et al. [2009].

Measurements were carried out for 20 °C, 30 °C, and 38 °C for three different size-groups of snails, group 1 with 0.65–0.85 cm shell diameter (n=23), group 2 with 0.9–1.0 cm (n=22) and group 3 with 1.0–1.25 cm (n=25). For each size-group and for each temperature at least n=7 snails were analyzed to assure a minimum of required statistical reliability. Due to the highly time-consuming procedure a larger number of individuals could not be analyzed.

2.2.2 Oxygen consumption measurement

The necessity to both observe the snails and measure oxygen consumption in parallel as well as the need for a high accuracy required a de novo-construction of a purpose-built micro-respirometer. For the measurement of oxygen consumption a cylindrical aluminum chamber containing a defined air volume was constructed. To capture both "inactive" and "active" phases independently, snails were measured individually. The top of the chamber was equipped with an oxygen sensor O_2 Tracer (ProChem Analytik, Xanten, Germany) which is based on an electrochemical cell with a sensitivity of 0.01 % O_2. The principle

of this sensor is similar to a battery or a fuel cell, where chemical energy is transformed into a continuous electric current. A varying concentration of the reactant oxygen results in a variable corresponding current. For a constant total pressure, which is essential for the measurements, a defined rate of oxygen, according to the partial pressure of oxygen p_{O_2}, diffuses through a membrane and participates in the reaction.

The top of the chamber was sealed with acrylic glass that allows the observation of the snail's activity. A custom plastic cover was designed, in which a small webcam and an LED were integrated for the recording of the animal's activity. This permitted the separate determination of oxygen consumption rates both in "active" and "inactive" phases. The entire respirometer chamber was then placed in a water bath to adjust the environment for the different test temperatures. To minimize the thermal impact of the observation webcam and, therefore, to allow stable oxygen signals to be recorded, only 10 pictures per hour with a flashing LED were taken, otherwise LED and webcam were turned off. Furthermore, gas pressure (PAA-33X, Keller, Jestetten, Germany), temperature (miniature PT100, Electronic Sensor, Heilbronn, Germany) and humidity (SHT21, Sensirion, Staefa, Switzerland) inside the chamber were monitored. On the basis of the measured relative humidity the dry gas pressure was calculated by subtracting the water vapor pressure from the total pressure. The water vapor pressure is defined by the following product of relative humidity ϕ and saturated vapor pressure $e_{(T)}$:

$$p_{\text{water vapor}} = \phi \cdot e_{(T)} \tag{2.3}$$

The saturated vapor pressure and its dependency upon temperature is described by Clausius-Clapeyron equation:

$$\frac{de_{(T)}}{dT} = \frac{\Delta H_{\text{vap}} \cdot e_{(T)}}{R \cdot T^2} \tag{2.4}$$

with ΔH_{vap} as the molar enthalpy of vaporization and R as the universal gas constant. Due the dependency of ΔH_{vap} upon temperature the integration of Equation 2.4 is very difficult. Therefore, typically an approximation formula is used to determine $e_{(T)}$, the so-called Magnus formula. A large number of these approximation formulas is available and very commonly used is the one from Sonntag [1990]:

$$e_{(T)}[Pa] = 6.112 \cdot e^{\frac{17.62 \cdot T}{243.12+T}} \cdot 100 \tag{2.5}$$

with the temperature T given in degree Celsius. Total dry gas pressure, temperature and air volume finally revealed the total molar amounts of the substances n_{total} inside the chamber, as stated by the ideal gas equation:

$$p_{\text{total,dry}} \cdot V_{\text{chamber}} = n_{\text{total}} \cdot R \cdot T_{\text{chamber}} \tag{2.6}$$

Using Dalton's law and the definition of the spatial fraction of oxygen r_{O_2} in the mixture, one obtains for the amount of oxygen:

$$n_{O_2} = \frac{p_{O_2} \cdot V_{\text{chamber}}}{R \cdot T_{\text{chamber}}} = \frac{r_{O_2} \cdot p_{\text{total,dry}} \cdot V_{\text{chamber}}}{R \cdot T_{\text{chamber}}} \tag{2.7}$$

The time evolution of each measurement revealed the variation of the amount of oxygen in the units of $[\text{mol} \cdot \text{s}^{-1}]$, which is equal to the oxygen consumption of each specimen.

The automatic LED and webcam power switch was realized by using a separate LabView program that controlled a National Instruments (Austin, TX, USA) NI-9472 Card connected to the LED and to a relay that linked the USB-connection from the webcam to the computer. Pictures were taken automatically by the open-source software iSpy. Signals for oxygen, gas pressure, and temperatures were acquired every ten seconds by an Agilent (Santa Clara, CA, USA.) 34972A LXI Data Acquisition/Data Logger Switch Unit and saved as *.`csv`-files for further analysis. Humidity signals were taken with the software from Sensirion that was included with the Evaluation Kit. Relative humidity was not controlled during the experiments but was always in the range of 25–50 % depending on ambient conditions and the measured snail.

The validity of the measurements was confirmed by a baseline record of a constant level of oxygen for the empty chamber at each temperature.

The oxygen sensor, which was directly screwed into the acrylic glass at the chamber's top, was provided with a hardware implementation for temperature correction, integrated in its outer casing, and thus located outside the measurement chamber. To minimize environmental temperature gradients in this hardware that would immediately influence the oxygen signal, the measurement took place in an insulated Rittal (Herborn, Germany) cabinet. The measurement chamber was then placed in an additional plastic case that was used as a water bath and the water circulation was realized via an external setup. This arrangement resulted in a very stable microclimate inside the cabinet since the measurement chamber was conditioned by the temperature of the

circulating water and was properly insulated from external influences (Figure 2.1).

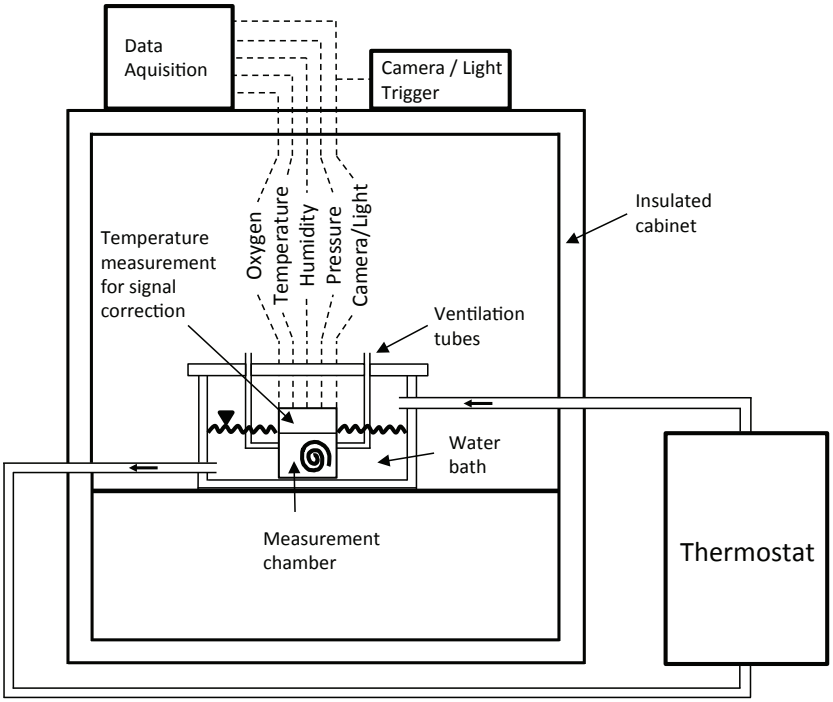

Figure 2.1: Schematic depiction of the developed camera-equipped micro-respirometry system

Additionally, baseline measurements were taken with an empty chamber and a linear correlation ($r=-0.856$, Pearson) was obtained between the oxygen signal and the temperature that was measured at the position of the outer casing of the oxygen sensor (compare Figure 2.1). This was subsequently used to correct the measured oxygen signal for unavoidable temperature drifts. With this correction the oxygen signals for baseline measurements were shown to vary in a range of $\pm 0.01\,\%\ O_2$ level, representing the maximum accuracy of the oxygen sensor and demonstrating the high accuracy of the measurements.

The gas pressure sensor was placed directly above the water level to reduce the hose length outside of the water bath, and thus minimize the influence of slight temperature gradients.

In order to avoid the impact of different movement activity on the measurements, only data recorded for individuals in their "inactive" phases were used for this study.

2.2.3 Statistics

Data were checked for normal distribution using the Shapiro-Wilk W-Test in JMP 11.0 (SAS Institute Inc.). In order to obtain a normal distribution, data for oxygen consumption had to be transformed by calculation of the 4^{th} root.[2] In the following, the original data will always be presented together with the transformed data on two vertical axes but statistical analyses were exclusively applied to the transformed data. Additionally, homogeneity of variances was guaranteed by non-significance in Levene's tests. Significance was then checked by ANOVA with a post-hoc Tukey-Kramer test.

If not specified otherwise $p \leq 0.05$ was defined significant (*), $p \leq 0.01$ was highly significant (**), and $p \leq 0.001$ was conclusively (***) (very highly) significant.

On the basis of fitted power series a two-parameter function has been determined with Excel 2010 (Microsoft Inc., Redmond, WA, USA) representing oxygen consumption depending on shell free weight and temperature to unify both dependencies.

2.3 Results

2.3.1 Influence of shell size on the oxygen consumption

Shell size was significantly and positively associated with oxygen consumption, independent of the investigated temperatures (ANOVA, Tukey-Kramer HSD test between all groups, Figure 2.2). Mean values for each size group were $(0.44 \pm 0.27) \times 10^{-10}\,\text{mol} \cdot \text{s}^{-1}$ (group 1, small), $(1.06 \pm 0.59) \times 10^{-10}\,\text{mol} \cdot \text{s}^{-1}$

[2]Most biological data do not follow a normal distribution and require the shifted or skewed distribution of the entire data to be transformed into a normal one. This is usually accompanied by trial and error until a proper transformation is found. This does not change the contained information as the entire data is transformed and the ANOVA only compares the mean values between groups.

(group 2, medium) and $(2.00 \pm 1.18) \times 10^{-10}\,\mathrm{mol \cdot s^{-1}}$ (group 3, large) for the non-transformed data. Mean shell sizes were $(0.74 \pm 0.06)\,\mathrm{cm}$, $(0.95 \pm 0.03)\,\mathrm{cm}$ and $(1.17 \pm 0.06)\,\mathrm{cm}$ for shell size categories 1, 2, and 3, respectively.

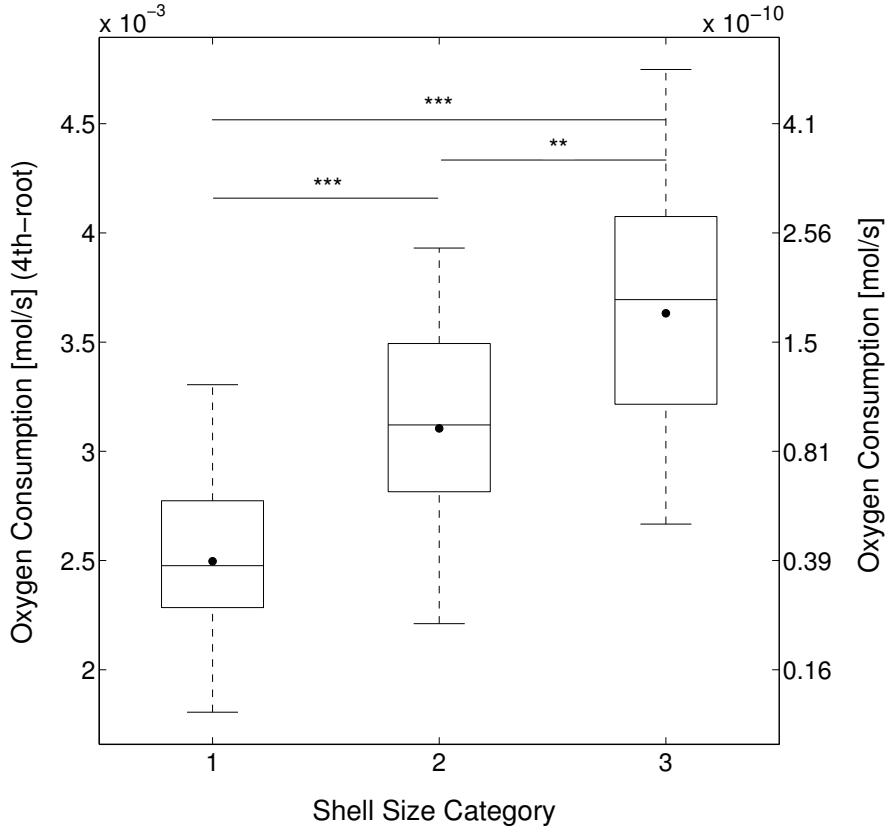

Figure 2.2: Oxygen consumption for shell size groups 1, 2, and 3 (left axis: transformed data, right axis: original data). Black dots represent means. Box plots represent 25 %, medians and 75 % quartiles

2.3.2 Influence of temperature on the oxygen consumption

To account for the different investigated temperatures a two-way ANOVA was applied with the two factors "shell size category" and "temperature". This analysis, however, showed the interaction between shell size category and temperature to be close to the limit of significance (p=0.053). Hence, a one-way ANOVA with subsequent Tukey-Kramer HSD test was applied for each

shell size category. The results for shell size category 1 (the "small" individuals) did not show any significant differences between the three different test temperatures 25 °C, 30 °C, and 38 °C (Tukey-Kramer HSD, $p>0.99$ for all temperatures, Figure 2.3). Means are $(3.99 \pm 1.48) \times 10^{-11}\,\mathrm{mol \cdot s^{-1}}$, $(4.74 \pm 3.67) \times 10^{-11}\,\mathrm{mol \cdot s^{-1}}$, and $(4.51 \pm 2.91) \times 10^{-11}\,\mathrm{mol \cdot s^{-1}}$ for 25 °C, 30 °C and 38 °C, respectively.

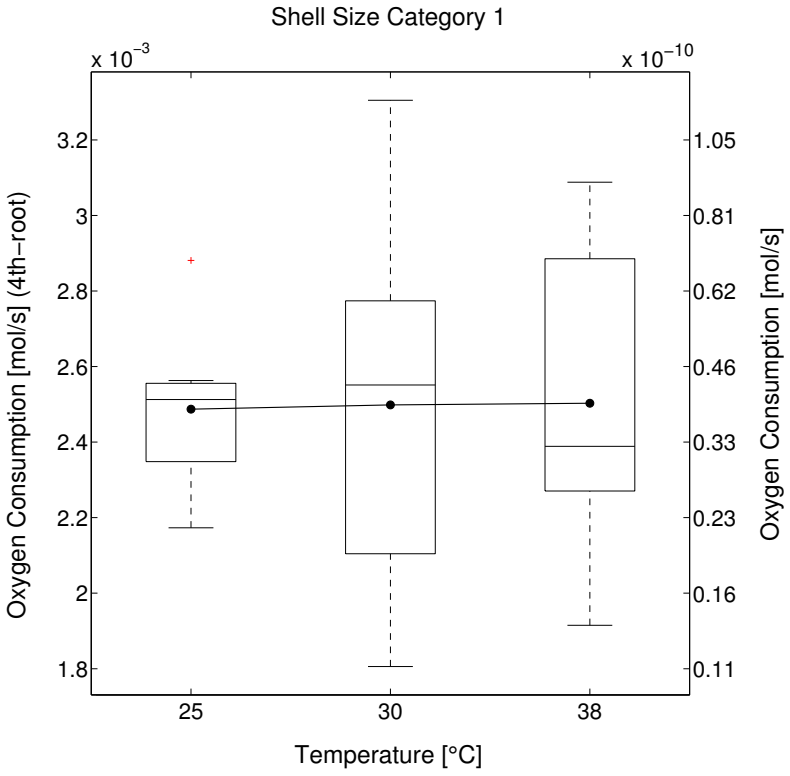

Figure 2.3: Oxygen consumptions for the three tested temperatures, shell size category 1 (left axis: transformed data, right axis: original data)

The data obtained for shell size category 2 (Figure 2.4), however, revealed a very highly significant decrease (Tukey-Kramer HSD, $p<0.001$) in oxygen consumption at the temperature of 38 °C ($(0.51 \pm 0.33) \times 10^{-10}\,\mathrm{mol \cdot s^{-1}}$ compared to the temperature of 30 °C ($(1.56 \pm 0.55) \times 10^{-10}\,\mathrm{mol \cdot s^{-1}}$). A highly significant (Tukey-Kramer HSD, $p<0.01$) decrease in oxygen consumption at 38 °C could also be found vs. 25 °C ($(1.04 \pm 0.25) \times 10^{-10}\,\mathrm{mol \cdot s^{-1}}$).

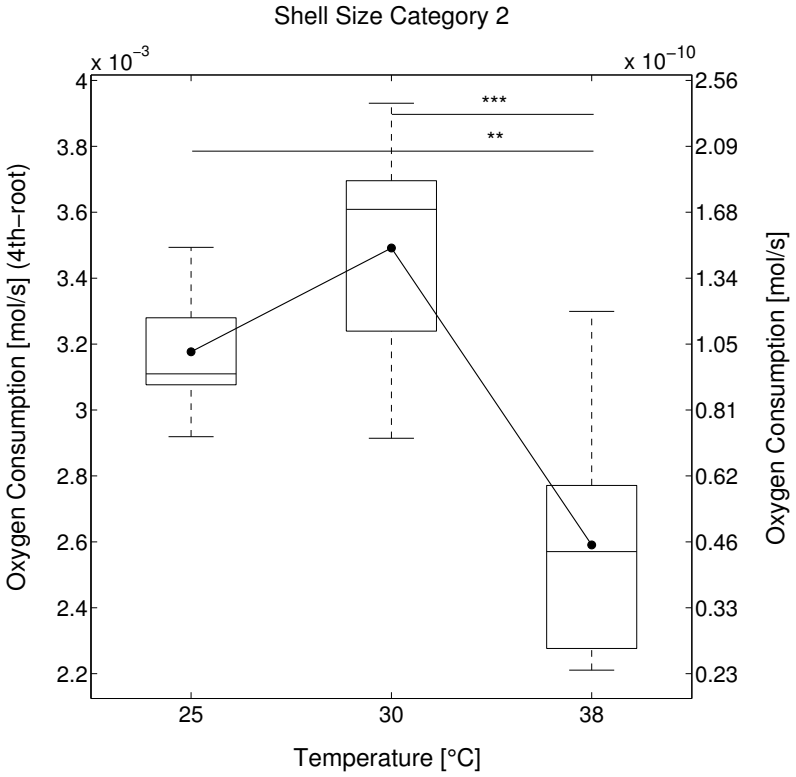

Figure 2.4: Oxygen consumptions for the three tested temperatures, shell size category 2 (left axis: transformed data, right axis: original data)

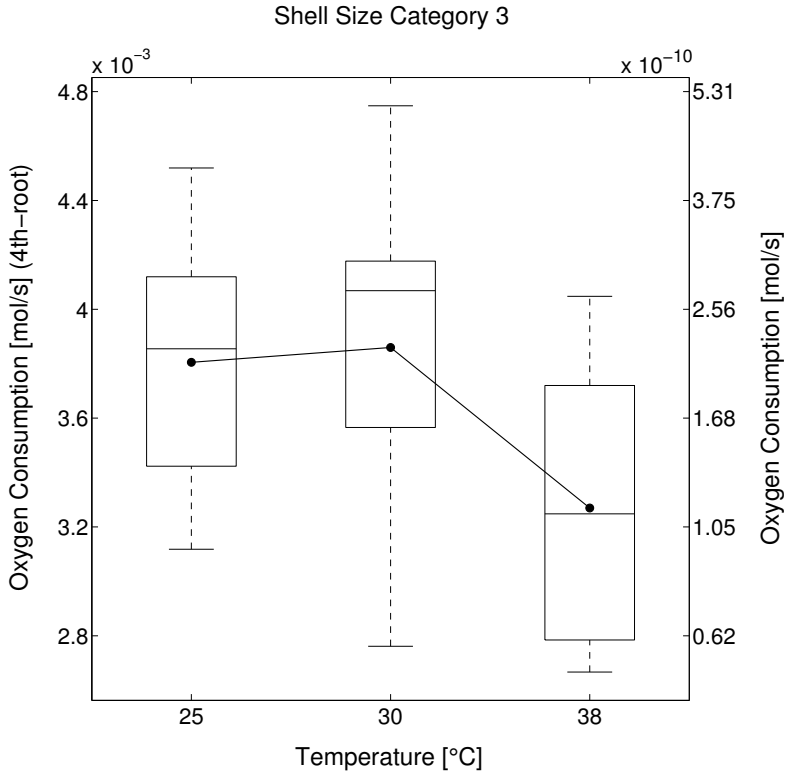

Figure 2.5: Oxygen consumptions for the three tested temperatures, shell size category 3 (left axis: transformed data, right axis: original data)

Data recorded for the "large" individuals, those of shell size category 3 (Figure 2.5) showed a similar drop in oxygen consumption at the highest temperature, 38 °C. Between 25 °C and 30 °C no decline in metabolism was visible. Despite lacking significance, the oxygen consumption rates at 38 °C revealed a trend towards reduced metabolism at that temperature (Tukey-Kramer HSD, p=0.07). Means for 25 °C, 30 °C, and 38 °C were $(2.27 \pm 1.11) \times 10^{-10}\,\mathrm{mol \cdot s^{-1}}$, $(2.48 \pm 1.33) \times 10^{-10}\,\mathrm{mol \cdot s^{-1}}$, and $(1.30 \pm 0.78) \times 10^{-10}\,\mathrm{mol \cdot s^{-1}}$, respectively.

2.3.3 Influence of weight on the metabolism at different temperatures

This potential interrelationship was investigated using the shell-free weight of each animal. Therefore, empty shells of *X. derbentina* were weighed and correlated to their outer shell diameter yielding an approximately cubic fit (n=26, R^2=0.981) that was used to subtract the shell weight from each specimen.

The analysis of intraspecific weight influence on oxygen consumption required appropriate fitting of the data points, which was achieved with the software package MATLAB R2013b (Mathworks, Natick, MA, USA).[3]

For 25 °C the fitting procedure resulted in α=1.221 and b=2.835×10^{-13} with R^2=0.875 (Figure 2.6). The uncertainty in coefficients is given by the 95 % confidence intervals of 1.000–1.442 and 9.856×10^{-14}–8.157×10^{-13} for α and b, respectively.

[3]To minimize the uncertainty of the resulting fit coefficients, the basic dataset, which can be approached by a non-linear power function $MR = b \cdot m^{\alpha}$, was transformed by plotting the data in a double logarithmic diagram. By doing so the power function is transformed into a straight line with the slope α. MATLAB performed the fit with a linear least-squares minimization technique to calculate the coefficients b and α. The resulting uncertainty for the fitted coefficients is also calculated by MATLAB. Additionally, the upper and lower prediction bounds (95 % confidence) for the fitted curve were calculated. Calculation has been applied with the original data since a transformation by the 4^{th} root would result in different fit coefficients that are not comparable to the existing literature.

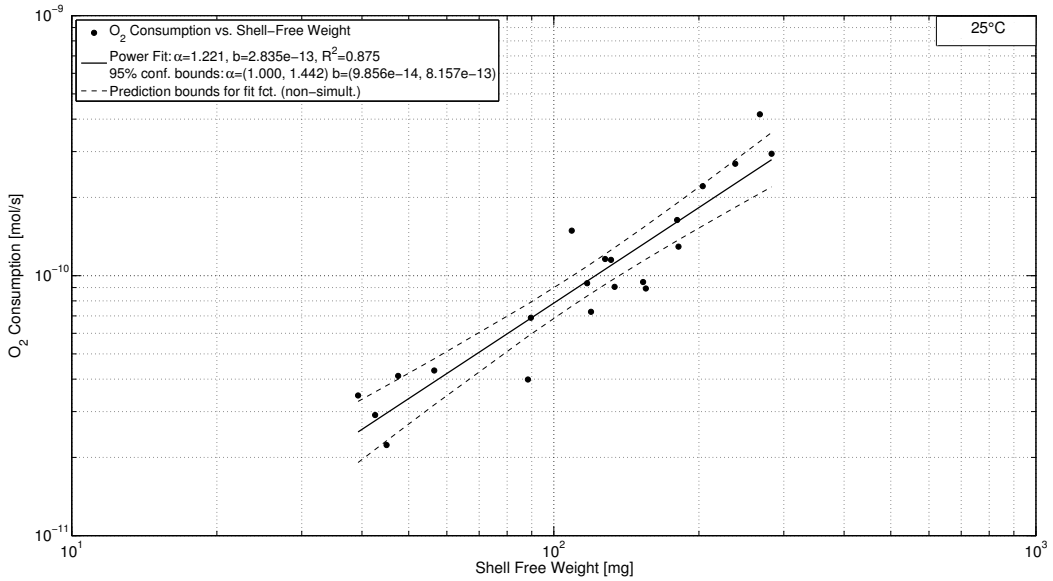

Figure 2.6: Oxygen consumption vs. shell free weight for 25 °C, logarithmic scaling

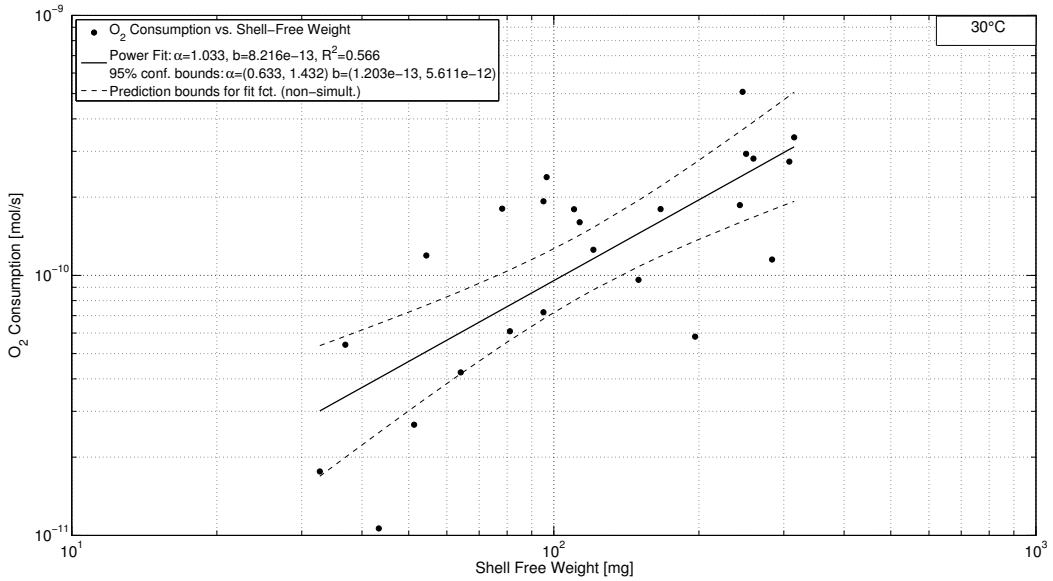

Figure 2.7: Labels as in Fig. 2.6. Oxygen consumption vs. shell free weight for 30 °C, logarithmic scaling

The fit for 30 °C resulted in R^2=0.566 for α=1.033 and b=8.216×10^{-13} (Figure 2.7). The uncertainties for α and b were higher due to the lower R^2 value compared to the measurements at 25 °C given by the intervals of 0.633–1.432 and 1.203×10^{-13}–5.611×10^{-12} for α and b, respectively.

The power fit function for 38 °C revealed its maximum of R^2=0.362 for α=0.689 and b=2.18×10^{-12} (Figure 2.8). As mentioned before, uncertainty in both coefficients is high as R^2 is even lower than calculated for the data at 30 °C (0.294–1.083 and 3.291×10^{-13}–1.444×10^{-11} for α and b, respectively).

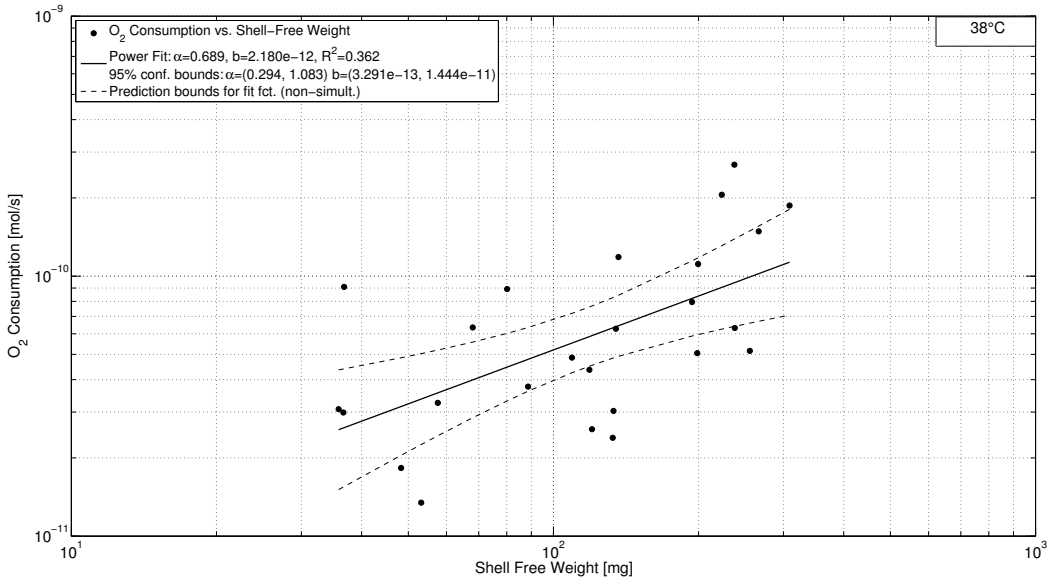

Figure 2.8: Labels as in Fig. 2.6. Oxygen consumption vs. shell free weight for 38 °C, logarithmic scaling

2.4 Discussion

A population of *Xeropicta derbentina* from southern France (Modène, Vaucluse) was used to investigate the oxygen consumption at three different ambient temperatures. Additionally three shell size groups were differentiated and the influence of temperature was studied separately for each group. Finally, the effect of mass on metabolic rate was analyzed, which is expressed by the characteristic curve of oxygen consumption over shell-free weight for each

temperature.

In order to classify the measured oxygen consumption of *X. derbentina* results of some of the previously discussed oxygen consumption studies on other snail species are given in Table 2.1. To allow for a proper comparison only those studies were chosen which used the shell-free weight of the corresponding snail species to calculate weight-specific consumptions. Shell-free weight-specific values of the present work have been calculated for the mean oxygen consumption value of each size group at a test temperature of 25 °C.

The comparison shows that the measured values of oxygen consumption on *X. derbentina* agree well with the results of other snail species being of the same magnitude. Though the specific consumption is rather higher in general taking the natural spread in biological experiments into account the determined values of *X. derbentina* are reasonable. This becomes especially clear when comparing the results for *O. lactea* that differ significantly for the presented studies.

2.4.1 Effect of shell size

Independent of the temperature, an increase in oxygen consumption with increasing shell size was found. This relation is plausible since larger snails have greater energy demands and therefore higher metabolic rates. The development of the mean values for each shell size category shows a more or less constant trend suggesting a linear relation for the data when the temperature influence is neglected. However, no statistical evidence can be derived from this relation as the data for "shell size category" contains non-uniformly distributed values of the shell diameter.

2.4.2 Effect of temperature for each shell size group

In southern France *X. derbentina* has to face xeric and hot conditions during the day. As reported by Dieterich et al. [2013] snails are almost entirely "inactive" during the day, which limits their food and water uptake to times of activity on the ground at night and in the early morning when cooler temperatures prevail. By climbing vertical objects the snails escape from lethal ground temperatures during daytime and quickly become "inactive" to avoid

Table 2.1: Overview of oxygen consumption values for different snail species

Species	**Condition**	**Specific oxygen consumption [mol/(mg s)]**	**Reference**
X. derbentina	25 °C, group 1, dormant	7.013×10^{-13}	Fischbach, present work
	25 °C, group 2, dormant	8.297×10^{-13}	
	25 °C, group 3, dormant	1.008×10^{-12}	
B. dealbatus	22 °C, dormant	2.271×10^{-13}	Horne [1973]
R. schiedeanus	25 °C, dormant	3.179×10^{-13}	Riddle [1975]
	73 % rel. humidity		
H. aspersa	25 °C, dormant	4.996×10^{-13}	Riddle [1977]
	60 % rel. humidity		
R. schiedeanus	25 °C, dormant	2.044×10^{-13}	
	60 % rel. humidity		
O. lactea	20 °C, dormant	2.767×10^{-13}*	Herreid [1977]
O. lactea	23–25 °C, dormant	1.555×10^{-13}	Barnhart and McMahon [1987]
	32 % rel. humidity		

* specific consumption was calculated based on the provided average shell weight

desiccation. Schmidt-Nielsen et al. [1971] argued that in very harsh habitats the major physiological threats for snails are thermal death, desiccation and starvation. The solution to these problems basically includes metabolic regulation at high temperatures, control of water loss during inactivity, and low metabolic rates during dormancy [Riddle, 1975]. A metabolic adaption of snails at higher temperatures has been reported by a number of researchers [Dallas et al., 1991, Riddle, 1977, Steigen, 1979].

The results for shell size category 1 indicate that no thermal regulation is present for small individuals of *X. derbentina* mirrored by the lack of any significant differences for all investigated temperatures (Figure 2.3). Apparently, this effect is related to the animals' young age and their ongoing adolescence. Young individuals may tolerate higher temperatures before regulation of metabolism takes place. This argument, however, has still to be confirmed. Effects of increased oxygen consumption due to locomotion can be precluded since every recorded individual was "inactive" during the measurements.

The results for shell size category 2 (Figure 2.4), however, are in good agreement with the results of Riddle [1977] who detected strong regulations for both of his test species, *Rabdotus schiedeanus* and the garden snail *Helix aspersa*, beyond 25 °C. A similar result was presented by Steigen [1979] who showed temperature compensation of *C. hortensis* in a temperature range of 15–25 °C.

Snails belonging to shell size category 3 (Figure 2.5) showed a non-significant trend similar to that of category 2 snails. The reasons for the differences between distinct sizes – and respectively ages – of *X. derbentina* may be explained by their general capacity to adjust physiological processes to external temperatures at different life stages. Given that the induction of stress proteins reflects a snail's ability to modify metabolic processes, it should be taken into account that 70-kD stress protein (Hsp70) levels are reduced in older individuals and that it is more difficult to induce Hsp70 in old individuals [Köhler, 2009, Mayer and Bukau, 2005]. This reduced capability to physiologically counteract heat stress is probably based upon accumulated stress effects in individuals of old age at the end of summer [Dieterich et al., 2013] and the energetic trade-off between maintaining the molecular stress response system and reproduction [Mizrahi et al., 2011]. It is plausible that this physiological limitation is not

restricted to stress protein induction but extends to other basic metabolic processes, such as the O_2 consumption. Consequently, "older" individuals of *X. derbentina* may not be able to maintain high metabolic activity in the heat, due to a general "weakening", while younger individuals can. Yengkokpam et al. [2008] showed that, in particular, a connection between oxygen consumption and Hsp70 production exists as he reported for the fish *Labeo rohita*.

Variation in oxygen consumption, resulting in a rather high standard deviation in all test groups, may be due to irregular pneumostome opening and periodical release of CO_2 during measurements as it was described by Barnhart and McMahon [1987].

The conclusion is drawn that a change in ambient temperature affects the oxygen consumption of *X. derbentina*. The degree of this impact, however, depends upon their age, i.e. individuals in phases of strong growth and ongoing adolescence do not show any metabolic downregulation at higher temperatures, whereas individuals of medium and large size, and hence of older age, show a clear metabolic shift in response to high temperatures. However, the question as to what extent "active" individuals also showed metabolic adaptations and how far size/age affected activity in general cannot be answered, since all measurements were performed on individuals in their "inactive" phases.

2.4.3 Weight-/metabolism relationship

The relation between metabolism and body size, respectively body weight, of living organisms has been under intense discussion for almost 175 years. With respect to homeotherms, particularly mammals, the results according to Kleiber [1947] suggest that their metabolic rate grows with approximately 0.75 the power of weight. Bertalanffy [1957] distinguishes between three different growth types, those obeying the surface rule (α=2/3), those growing proportionally to their weight (α=1) and an intermediate type ($2/3<\alpha<1$). In his detailed review he states that snails of the family of *Helicidae* belong to the second group with a metabolic rate directly proportional to weight, hence α=1.

The results in the present study demonstrate a clear relationship with temperature, similar to the one observed by Steigen [1979], namely a decrease in α for increasing temperatures. For 25 °C the value of α was 1.22, which is higher

than 1.0 and outside the range postulated by Bertalanffy [1957]. For 30 °C the value of α is approximately 1 indicating a direct proportionality to weight consistent with the results of Liebsch [1929] and also Kienle and Ludwig [1956]. At the highest temperature of 38 °C, α declines even further to the value of approximately 0.69 that is close to the value for animals obeying the surface rule.

Wesemeier [1960] presented results for both "active" and "inactive" specimens of *Helix pomatia* and reported an increased value of α for the "active" individuals that he could not explain. For *Xeropicta derbentina* it is well known that these snails become more and more "inactive" as temperatures increase. Even though no "active" snail was measured in the present study, it is conceivable that snails at the lower test temperatures may have a higher state of "internal" activity than the ones measured at the highest temperature, which are trying to lower their metabolism as much as possible. It is therefore possible that the state of activity, indirectly triggered by temperature, has an influence on α.

It has to be mentioned that measurements become less accurate at high temperatures due to unavoidable methodological reasons and, therefore, an evaluation of the goodness of fit is difficult to interpret. The first reason for this is due to the lower oxygen consumptions at higher temperatures and the increasing sensitivity of the respirometric system at higher temperature differences between measurement chamber and the outer environment. The second reason may be due to increased thermal stress on *X. derbentina* that arises at higher temperatures. Under the assumption that this effect starts primarily in only a few individuals and not in the entire group of animals at the same time, the overall variance increases and therefore R^2 declines.

A complete view of the dependence of oxygen consumption upon temperature and body size is given in Figure 2.9A.[4] The changing curvature of the

[4]The resulting equations of the power fits from Figures 2.6-2.8 have been used to calculate oxygen consumptions for each temperature using the mean shell free weights of each shell size category (compare Figure 2.2) resulting in 3x3 data-points. For the representation of oxygen consumption of each size category over temperature a quadratic fit was generated. The three coefficients for the absolute (a_1, a_2, a_3), linear (b_1, b_2, b_3), and quadratic term (c_1, c_2, c_3) of each size category were subsequently plotted vs. the mean shell-free weights and interpolated again with a quadratic fit yielding $a_{(m)}$, $b_{(m)}$, and $c_{(m)}$ each containing three coefficients. The surface for oxygen consumption can then be represented by a function of the form: $\dot{O}_2 = a_{(m)} + b_{(m)} \cdot T + c_{(m)} \cdot T^2$

surface at elevated temperatures is related to the trend towards lower exponents α (solid lines for T=25 °C, 30 °C and 38 °C corresponding to the measured data). The exponent α represents the curvature of the solid line at each section and clearly shows a value <1 (negative curvature for increasing body weight) for T=38 °C and increases further up to a value >1 for the lowest temperature.

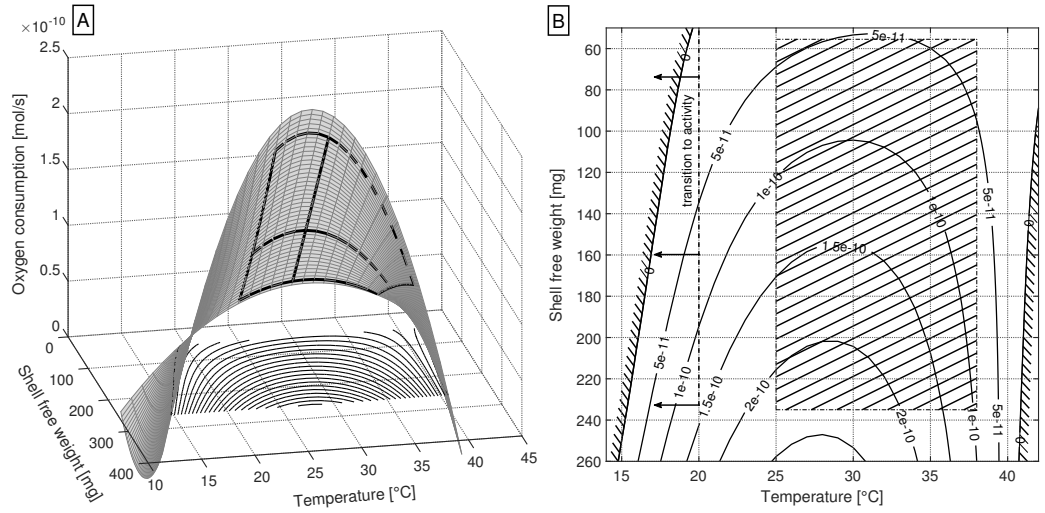

Figure 2.9: A: Response surface calculated for oxygen consumption vs. temperature and shell free weight. B: Two-dimensional plot of constant O_2 consumptions (isoboles) in a temperature vs. shell free weight diagram. Zero isoboles represent the theoretical limits (zero O_2 consumption) deduced by extrapolation. The hatched area shows the region of interpolation.

For given shell free weights (dashed lines) the surface includes the results from Figures 2.3, 2.4, and 2.5 showing the decline in metabolism with increasing temperatures, particularly for high body weight. Here, the response surface has been extrapolated to temperatures beyond the upper and lower limits chosen in this study (14–42 °C). The resulting plot reveals conditions under which the oxygen consumptions theoretically would yield negative values, representing possible limits of physiology. Additionally, isobolic curves of constant oxygen consumptions are depicted in Figure 2.9B displaying the "regions" of predicted physiological limits (zero or negative oxygen consumptions for both very low and very high ambient temperatures). Even though these "limits"

derive from extrapolations and are, thus, purely theoretical they fit rather well to behavioral and biochemical adaptations of *X. derbentina* to environmental temperatures. The lower temperature "limit" (15–20 °C) corresponds to conditions triggering arousal from inactivity resulting in the transition into active movement and feeding activity. However this region is associated with a high degree of uncertainty due to its rather distant extrapolation from measured data as indicated by the hatched surface. The upper temperature "limit" (slightly above 40 °C) corresponds astonishingly well to the temperature that induces the maximum Hsp70 response after 8h exposure [Troschinski et al., 2014]. For even higher temperatures, the Hsp70 response in *X. derbentina* starts to be overwhelmed, indicating the biochemical limits of this species, as also extrapolated for the O_2 consumption in the presented model.

The mathematical description of the response surface in Figure 2.9 is given by the following Equation 2.8:

$$\begin{aligned} \dot{O}_2 = \quad & (a_{1(m)} + a_{2(m)} \cdot m + a_{3(m)} \cdot m^2) \\ + \quad & (b_{1(m)} + b_{2(m)} \cdot m + b_{3(m)} \cdot m^2) \cdot T \\ + \quad & (c_{1(m)} + c_{2(m)} \cdot m + c_{3(m)} \cdot m^2) \cdot T^2 \end{aligned} \tag{2.8}$$

This equation can also be rearranged to express oxygen consumption as a linear combination of an absolute, linear and quadratic term of weight:

$$\begin{aligned} \dot{O}_2 = \quad & (a_{1(m)} + b_{1(m)} \cdot T + c_{1(m)} \cdot T^2) \\ + \quad & (a_{2(m)} + b_{2(m)} \cdot T + c_{2(m)} \cdot T^2) \cdot m \\ + \quad & (a_{3(m)} + b_{3(m)} \cdot T + c_{3(m)} \cdot T^2) \cdot m^2 \end{aligned} \tag{2.9}$$

The coefficients $a_{1-3(m)}$, $b_{1-3(m)}$ and $c_{1-3(m)}$ can be found in Table 2.2:

Table 2.2: Coefficients of the calculated response surface

	1	**2**	**3**
$a_{i(m)}$	-1.1549×10^{-11}	-5.9971×10^{-6}	9.2619×10^{-3}
$b_{i(m)}$	-6.5462×10^{-13}	4.6534×10^{-7}	-4.9078×10^{-4}
$c_{i(m)}$	3.2832×10^{-14}	-7.7807×10^{-9}	6.2120×10^{-6}

In conclusion, using a highly sophisticated micro-respirometer constructed especially for the investigation of "inactive" snails it could be shown that the

relation between oxygen consumption and size of *X. derbentina* is not quantitatively fixed but is directly dependent upon ambient temperatures. This may well be associated with the observed metabolic depression at higher temperatures for medium-sized and large snails.

Chapter 3

Energy metabolism measured by direct calorimetry

3.1 Introduction

The oxygen consumption measurements presented in Chapter 2 revealed that elevated temperatures lead to a significant decrease in oxygen consumption for mid-level sized individuals of *X. derbentina* with intact capability to physiologically counteract thermal stress. Therefore, an approach has been made to further investigate the effects of metabolic adaptations at higher temperatures by direct calorimetry.

The metabolic rate (energy demand) of living organisms can be captured indirectly by measuring the rate of oxygen consumption or directly from the rate of heat production. All processes that are involved with energy turnover produce heat and, therefore, direct calorimetry gives an integral view of all effects taking place in the sample, including side effects such as any combination of aerobic and anaerobic metabolism, resulting in an integral thermic signal. Only in cases of complete aerobic metabolism data on oxygen consumption can directly be transformed into metabolic rates by using a fixed oxy-calorific equivalent (also called "calorimetric equivalent") depending on the composition of food, i.e. carbohydrates, lipids, and protein [Gnaiger et al., 1989]. The complex relationship between energetics and oxygen consumption has been described by Gnaiger [1980] and Grainger [1968]. According to Gnaiger, the use of an oxy-calorific equivalent requires "a detailed thermochemical analysis

of the biochemical pathways" to allow for an interpretation in terms of ATP-turnover and depends on whether the organism is in an aerobic or anaerobic state. In the latter case the caloric equivalent of ATP-turnover is reduced by up to 30% for the fermentation of glucose. In the anaerobic state of an animal the measurement of metabolic activity in terms of oxygen consumption would result in a significant discrepancy to the true metabolic activity since it only captures aerobic rates of energy turnover. The use of direct calorimetry is, therefore, essential for the study of anaerobic metabolism of animals that are frequently exposed to low oxygen conditions. Peakin [1973] additionally stated that for hygrophilous animals direct calorimetry has the advantage of avoiding physiological stress due to desiccation by providing more natural conditions while measuring.

Direct calorimetry has been applied on a wide range of biological systems such as microbial cultures but also facilitates the monitoring of complete ecological entities such as forests, sediments, and lakes, and their interaction with adjacent units due to toxicological interference [Drong and Lamprecht, 1993]. An overview of investigated fields of calorimetric experiments as well as the different calorimetric equipment is given in Drong and Lamprecht [1993]. Direct calorimetry measurements of small animals have been reported by Lamprecht [1998], measurements on poikilothermic animals have been reported among others for honeybee workers [Fahrenholz et al., 1989] and some reptiles [Lamprecht and Matuschka, 1985]. Furthermore direct calorimetry is applicable for the investigation of changes in metabolic activity of animals that came into contact with harmful substances, such as cadmium [Joachimsohn et al., 1989].

Among the few researchers that investigated snails with direct calorimetry are Becker and Lamprecht [1977]. They identified oxygen consumption and heat production in the snail *Biomphalaria glabrata* to be significantly higher if the animals were infected with the parasite *Schistosoma mansoni*. Additionally, the comparison of transformed values of oxygen consumption with values of heat production showed that the metabolism of infected and uninfected individuals was always in the aerobic state.

In a further study Becker [1980] demonstrated that infected specimens of *Biomphalaria glabrata* ($0.96\,\mu W \cdot mg^{-1}$ wet weight) did not show a higher heat production than uninfected individuals ($1.02\,\mu W \cdot mg^{-1}$ wet weight). But

when locomotion was specifically prevented the thermal output for infected snails ($0.3\,\mu W \cdot mg^{-1}$ wet weight) was significantly higher than for uninfected specimens ($0.22\,\mu W \cdot mg^{-1}$ wet weight). Becker [1980] concluded that "infected snails restrict their movements to compensate for the higher basal metabolism". The contradictory results between Becker and Lamprecht [1977] and Becker [1980], therefore, are probably caused by a sample of specimens in Becker and Lamprecht [1977] that were not as active as the specimens from Becker [1980]. The comparison of uninfected individuals revealed that the activity of *B. glabrata* requires approximately 80 % of the total energy expenditure.

A similar impact of movement on the calorimetric output has been reported by Pamatmat [1983] in the mussel *Ischadium demissum demissum*, which revealed extreme fluctuations of metabolic rates with time and between individuals as well. The author showed that these variations declined if the movement of the mussels' shell valves was blocked. Furthermore, the orientation of the animal resulted in a measurable difference in heat output. Long-term measurements indicated that metabolic rates became cyclic after a certain period of adaptation inside the chamber of the calorimeter. Interruptions of this state immediately resulted in unpredictable fluctuations again.

Lamprecht and Becker [1988] presented calorimetric measurements in combination with endoscopic observations of a snail (species not mentioned). They further raised the discussion as to whether temporarily observed phases of high calorimetric output correspond to high metabolic activity or if this was just a consequence of the snail's movement. The authors clearly demonstrated that small ripples in the calorimetric signal indicate locomotion of the snail, whereas phases of a "quick increase and a rather slow and nearly-linear decrease" are the result of metabolic responses that happen periodically. This is in contrast to the findings of Becker [1980] where locomotion only resulted in small ripples and activity was not responsible for 80 % of overall energy turnover.

Pamatmat [1978] reported measurements of heat production and simultaneous oxygen consumption for the sea snail *Littorina irrorata* and the fiddler crab *Uca pugnax*. During 16 h of measurements an unproportional decrease of oxygen uptake and heat production of both species was observed resulting in an increased oxy-calorific coefficient, which has been used as an indicator for the onset of anaerobic metabolism. Above a given level of oxygen consumption,

however, the commonly used coefficient was obtained.

A similar disproportion between heat production and oxygen consumption has been reported for some marine bivalve mollusks showing too little oxygen consumption to represent total metabolism, whereas others revealed ratios that were in close accordance to the theoretical values proposed for the turnover of common food substances [Hammen, 1979]. Hammen [1980] additionally showed that for at least four species of bivalves the rate of heat production exceeded the equivalent one for oxygen consumption even at periods of maximum respiration.

The involvement of possible anaerobic metabolic pathways before and during a short period of estivation of the land snail *Oreohelix* has been investigated by Rees and Hand [1990]. Heat production during the non-estivating phase revealed two distinct metabolic states, the "standard" and "active" metabolism, which differed by a factor of 2–3 from one another. By simultaneous measurements of gas exchange *Oreohelix* was found to have a fully aerobic metabolism in both states which depends primary on the turnover of carbohydrate. Rapid transition into estivation took place within 4 days resulting in six fold reduced respiration rates, which is believed to be an "adaptation to survival in desiccating environments".

In order to establish a model (as presented in Chapter 5) that enables narrowing down additional physiological parameters needed for a comprehensive description of *X. derbentina*'s metabolism the current study investigates the metabolic rate of *X. derbentina* at different ambient temperatures. The resulting information is then used in combination with the measurements of oxygen consumption and the geometrical data of *X. derbentina* (as presented in chapter 4). Therefore, the data on energy metabolism is indispensable to draw up an integrative model on the complex physiology taking place in this snail species.

A particular challenge for this analysis of metabolic rates is the rather small size of the animal, which hampered the use of standard calorimeters and, therefore, required a very precise measurement system. This, in turn, facilitated the analysis of recurring and stable frequency patterns that were observed for individuals in their metabolically "inactive" state. The high precision system could be used to analyze these fluctuations as well as alternating phases of activity

and inactivity of this species in a very detailed way. Additionally, long-term measurements were performed to examine the physiological reactions of the animals when their metabolism passes into estivation.

Thus, using individuals of different sizes exposed to different temperatures, the present calorimetric study aims at answering the following questions:

1. How large are the differences between standard/"inactive" and "active" metabolic states and what is the energetic ratio between them?

2. To what extent is the total metabolic energy turnover as well as its division into "active" and "inactive" phases influenced by the animals' size and by ambient temperature?

3. How much time do individuals spend in standard and "active" metabolic states and does this alternation follow a regular cycle?

4. How is the frequency of thermal output for individuals at different metabolic states influenced by the animals' size and by ambient temperature?

3.2 Material and methods

3.2.1 Test organism

All specimens of *X. derbentina* were collected from the same meadow as the ones from the oxygen consumption study in Chapter 2. The collected snails were transferred to Germany and kept well hydrated and fed at ambient temperature and humidity in a terrarium. In this study only white shelled individuals were used (in accordance with the coloration classification patterns used by Köhler et al. [2009]). Due to geometrical limitations of the calorimeter chamber snails larger than 10 mm could not be analyzed. Therefore, two size groups were tested, called "small" and "large" snails. In the two groups the size range from 5.3–5.8 mm and 8.5–8.8 mm in diameter, respectively, measured at their largest cross-section. Additionally, the wet weight of all specimens was determined at the beginning of each measurement.

From both size groups n=3 distinct individuals were tested for a period of 7 days at 20 °C and 30 °C, respectively. To allow for the observation of complete estivation of *X. derbentina* two additional long-term measurements

of n=1 large individual for each temperature were conducted which lasted for 24 days each. The accomplishment of all measurements was, therefore, rather time-consuming and resulted in approximately 5 continuous months of measurements.

3.2.2 Calorimetry

Measurements of heat dissipation due to metabolic energy turnover were accomplished with a "Thermal Activity Monitor" (TAM) 2277 manufactured by Thermometric AB (Jarfalla, Sweden), a micro calorimeter based on the principle of isothermal titration calorimetry. The apparatus consisted of two identical, highly conductive and adiabatically coated cells. The first cell served as the sample cell whereas the second one was used as a reference cell to compensate outer thermal disturbances and thereby increasing the accuracy of the device. For calorimetry measurements it was important to use a reference medium with a heat capacity of maximum similarity to the measured animals. In the present study water has been used as reference medium. For the calculation of the required water mass the specific heat capacities of the shell and the soft tissue of *X. derbentina* at different temperatures have been used and were obtained in preceding studies. Additionally, previous measurements of the water content and mass distribution of shell und soft tissue of the snails delivered a proportion of approximately 2.3 for the mass of soft tissue to the mass of the shell. These results have been used to account for the different heat capacities of shell and soft tissue material. Therefore, each individual snail was weighed and the masses of shell and soft tissue were calculated subsequently. Based on this ratio and the heat capacity of each component a capacity of the mixture was calculated and the equivalent amount of water with the same capacity was used as a reference for each measurement.

The amount of diffusive water loss for the snails during the time of each measurement has not been considered since diffusion out of the measurement cell was negligible and, therefore, a saturated atmosphere can be assumed. Furthermore, the evaporation and condensation processes were taking place in both cells, resulting in effectively no influence on the overall heat signal of the measurement due to water loss. The resolution of the calorimeter was approximately 0.4 µW, and noise was in the range of about 40 nW.

3.2.3 Separation of active and inactive energy turnover

To distinguish between "active" and "inactive" states of metabolism thresholds have been defined for each measurement separating these two states. Since most of the recorded data followed an asymptotical course in the first days, the definition of a constant threshold was found inappropriate. Therefore, "active" phases/peaks were identified and separated block by block and the corresponding starting and end points were connected by a straight line. The integral below this resulting "baseline" energy course was defined to be "constitutive" and thus part of the "inactive" state. Subsequently, "active" and basal metabolic energy turnover were related to the overall energy turnover using the software package MATLAB R2013b (Mathworks, Natick, MA, U.S.A.).

3.2.4 Statistics

Due to the long duration of measurements required for each individual only a small sample size could be realized. Therefore, statistical tests are not applicable to evaluate significances. Whenever statistical data are presented for a particular time series of a measurement, the values are indicated as boxplots showing 25 %, medians and 75 % quartiles.

3.3 Results of 7-days-measurements

3.3.1 Time course of measurements

Figure 3.1 exemplarily shows the results of the 7-days-measurements for one specimen of each size group and temperature. All results displayed in Figure 3.1 show two characteristic levels of thermal output that will be referred to as "active" and "inactive" states of snails. During measurements A, C and D the snails were "active" from the beginning of each measurement and show a much higher initial output than in measurement B, where the snail was "inactive" at most of the time.

The median values and the distribution of the selected "active" and "inactive" time intervals from Figure 3.1 (numbered arrows) are given in Figure 3.2. The time intervals were chosen in such a way that they accurately represent the levels of "active" and "inactive" thermal output. Intervals that were too

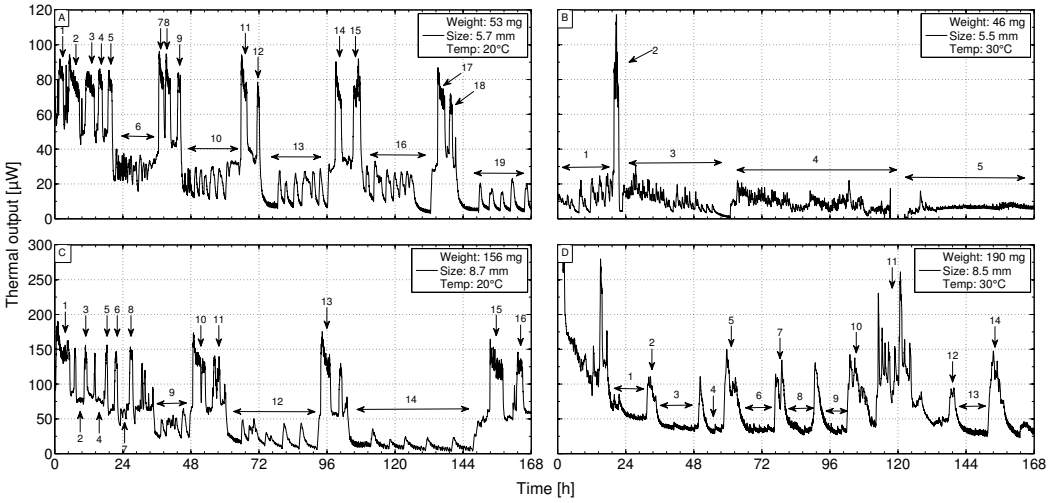

Figure 3.1: Thermal output of an exemplary selection of 7-days-measurements for one specimen of each size group and temperature. Presented measurements are "small2" at 20 °C (A), "small1" at 30 °C (B), "large2" at 20 °C (C), and "large3" at 30 °C (D).

short or rather noisy were excluded. For small snails (A, B) the "active" state results in approximately 4–5 times the thermal output compared to the "inactive" state regardless of the temperature. For larger specimens (C, D) however, the ratio between "active" and 'inactive" thermal output differs for 20 °C and 30 °C, showing maximum ratios of 6–7 at the lower temperature but only a maximum ratio of 5 at the higher temperature.

At 20 °C mean values for the "active" metabolic state vary between 70–85 µW and 120–145 µW for small and large animals, respectively, and 15–25 µW and 15–75 µW in the "inactive" state for small and large animals, respectively. At 30 °C the mean values for the "active" state of the large animals range from 85–110 µW. A comparison with the small specimen is inappropriate since measurement B revealed only a single "active" phase with a mean value of 80 µW. For the "inactive" state values between 8–15 µW and 30–55 µW were reached for small and large animals, respectively.

Figure 3.1 and Figure 3.2 additionally show that the median values of the "inactive" states are asymptotically decreasing over time. For measurements A and C a similar, yet smaller, decline can be seen for the "active" phases. It was

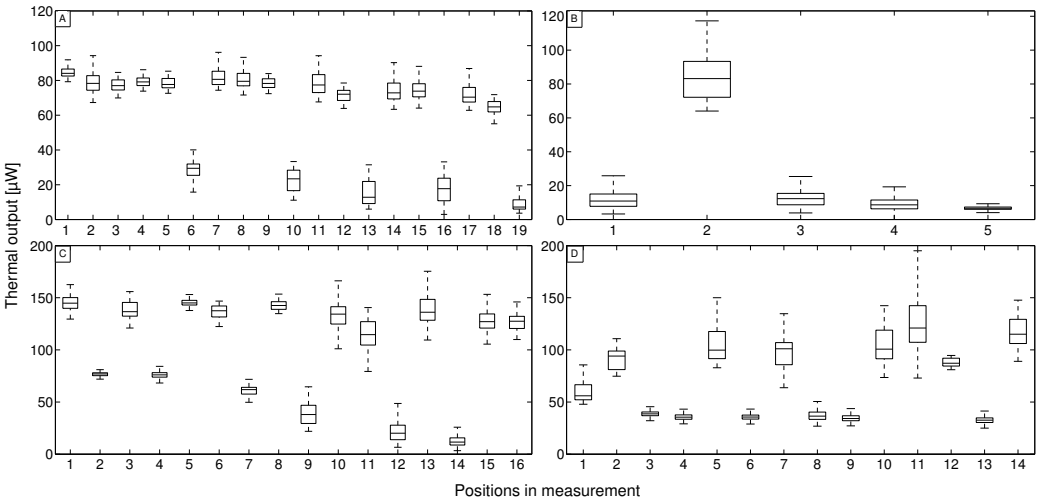

Figure 3.2: Boxplots of the highlighted phases in Figure 3.1

generally observed that the measurements at 20 °C clearly show this kind of behavior, whereas it could not be seen that clearly for measurements at 30 °C.

Particularly for the larger specimens (Figure 3.1, C and D) the overall time courses of all measurements generally show lower "active" levels at higher temperatures. In contrast to this, after 2–3 days, when the asymptotical decrease has settled, the "inactive" metabolic level was higher at the higher temperature.

3.3.2 Total energy turnover and the division into active and inactive states

The power output of the calorimeter was integrated numerically by the trapezoid rule with Excel 2010 (Microsoft Inc., Redmond, WA, U.S.A.) to obtain data for energy turnover of *X. derbentina* measured by its heat production.

The overall energy turnover for all tested snails is given in Figure 3.3 for both temperatures. In measurement "small3" at 20 °C the snail had only three "active" phases, which is one reason for the lower total energy consumption. Furthermore the calorimeter needed to be readjusted by 10 µW, which is another small source of uncertainty in this measurement. Measurements "small1" and "small2" at 30 °C also showed only very little phases of activity, resulting in the similar low total energy turnover. Additionally, measurement "small3"

at 30 °C produced an asymptotical decrease in thermal output during the first day, which was not present in the other measurements for small specimens. Hence, the smaller specimens show a rather high variance in the data.

The mean values at both temperatures for each size group show that energy consumption is similar for large snails but seems to decrease for small snails when temperature is raised from 20 °C to 30 °C. The total energy consumed was 2.7 and 4.9 times higher in large animals compared to small ones at 20 °C and 30 °C, respectively. To account for the mentioned asymptotical decrease in

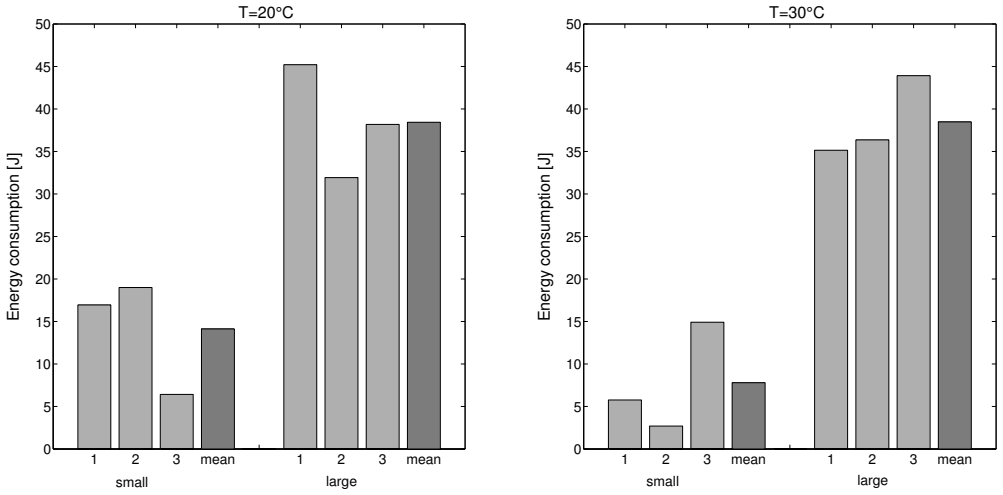

Figure 3.3: Total energy turnover for all tested snails calculated by integration for the temperatures 20 °C and 30 °C. The darkened bar represents the mean value of each block.

thermal output within the first day of measurement integrals for data recorded at $t > 1d$ were additionally calculated. The resulting mean values, however, were very similar to the ones displayed in Figure 3.3.

The separation of "active" and "inactive" energy turnover is given in Figure 3.4. The mean values on top of every group show that the energy consumption to maintain the "active" state generally decreases for both size groups when temperature is increased from 20 °C to 30 °C. The extent of this decrease is more pronounced for the small specimen. Small snails show a higher fraction of "active" state energy than large snails at 20 °C, whereas at 30 °C large snails have a little higher "active" energy demand than the small snails.

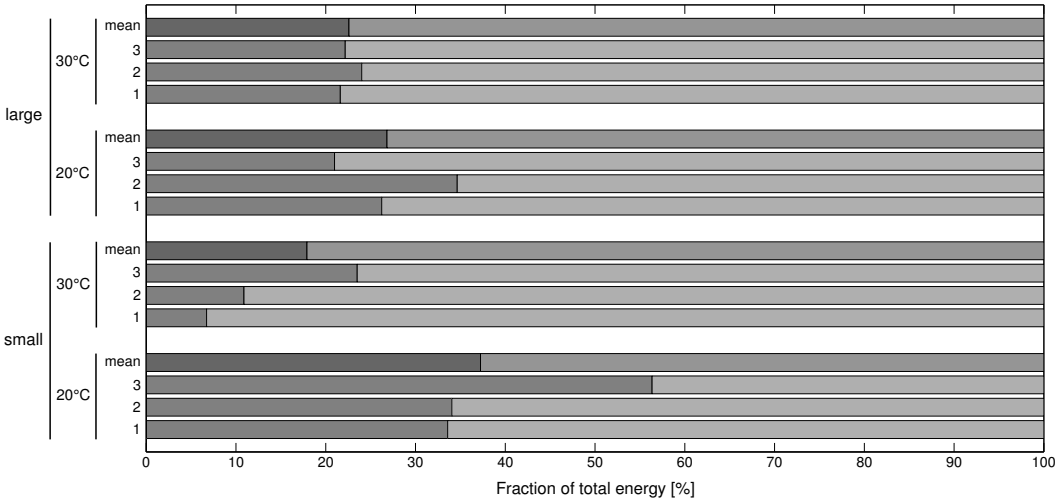

Figure 3.4: Division of "active" and "inactive" energy turnover (standard metabolism) for both size groups and temperatures. Dark bars represent the active parts, pale bars represent the inactive parts. The upper stacked bar shows the mean value of each block.

3.3.3 Phases of active and inactive metabolism over time

On the basis of the aforementioned definition the calculation of the time intervals corresponding to "activity" and "inactivity" was performed. The results on time spent in "activity" and "inactivity" are given in Table 3.1. Number 1, 2 and 3 are the corresponding measurements of each size and each temperature.

Table 3.1: Time fractions of "activity" and "inactivity" for all measurements

[% of total time]		**20 °C**			**30 °C**		
		1	**2**	**3**	**1**	**2**	**3**
small	active	22.4	34.4	26.5	1.2	1.0	39.1
	inactive	77.6	65.6	73.5	98.8	99.0	60.9
large	active	34.4	36.9	27.7	30.7	23.1	31.7
	inactive	65.6	63.1	72.3	69.3	76.9	68.3

With reference to total measurement time larger specimens showed longer times of activity at 20 °C. From an energetic point of view the aforementioned results followed a contrary pattern, namely a lower "active" metabolic fraction of total energy demand for larger animals at 20 °C. There can be two reasons for this: a baseline shift towards a higher metabolic level and, secondly, a real decrease of the "active" metabolic energy level fraction.

The "active time" fractions for 30 °C basically show the same relation but, due to measurements 1 and 2 of the small animals, in which almost no activity at all could be observed, no comparison is drawn. Comparing the time of activity for the large specimens at 20 °C to 30 °C it is obvious that this trend declined again for higher temperatures.

Table 3.2: Mean values of each parameter combination and relative change of the time spent in "activity" and "inactivity"

[% of total time]		**20 °C average**	**30 °C average**	**change %**
small	active	27.8	13.8	−50.4
	inactive	72.2	86.2	19.4
large	active	33.0	28.5	−13.6
	inactive	67.0	71.5	6.7

A comparison of the mean values of each set and the corresponding relative change of the time spent in "activity" and "inactivity" is given in Table 3.2. The overview shows that small animals approximately halve their time spent in "activity" and, therefore, react more sensitive to an increasing temperature. The large individuals are only reducing their "activity" by roughly 14 %.

3.3.4 Frequency patterns

In order to closer investigate the observed frequency patterns of all measurements in more detail the signals were transformed and decomposed into their frequency components (discrete Fourier transformation, DFT) by a fast Fourier transformation (FFT) algorithm using the software package MATLAB R2013b (Mathworks, Natick, MA, U.S.A.). The analysis concentrated on one measure-

ment for each size and temperature. The course of metabolic heat output for every measurement was largely characterized by two patterns: a regular oscillation in the "inactive" state and a much lower frequency of recurring "active" phases. Therefore, the frequency analysis had to be carried out separately for these two regions (Figure 3.5 and 3.6).

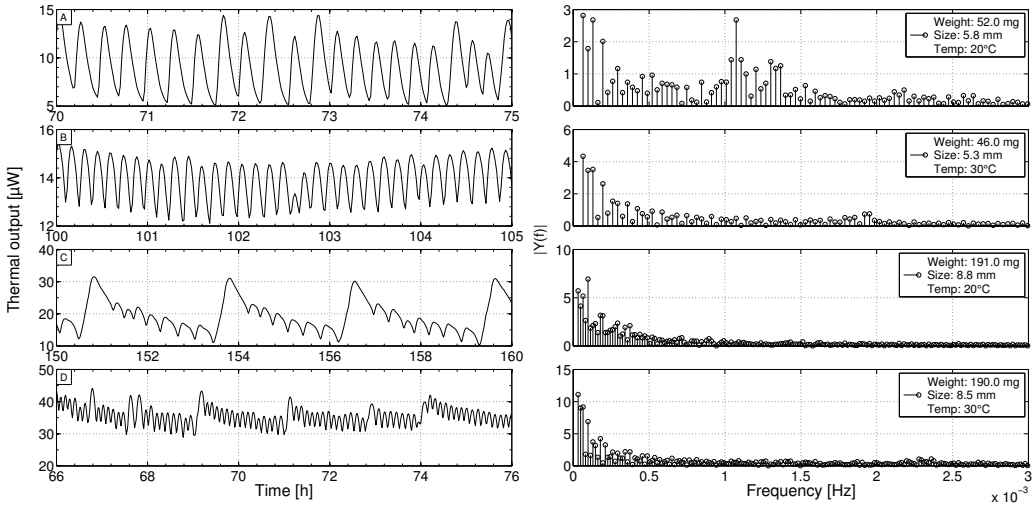

Figure 3.5: Frequency analysis of an "inactive" phase for one specimen of each size group and temperature. Corresponding to the naming in Figure 3.1 and 3.3, presented measurements are "small1" at 20 °C (A), "small3" at 30 °C (B), "large1" at 20 °C (C), and "large3" at 30 °C (D).

Figure 3.5 shows the thermal output of a selection of four individuals in time sections corresponding to "inactivity". The number of peaks for the "inactive" state are 22 (A), 35 (B), 25 (C), and 63 (D) ranging time-wise between 0.17–0.28 h (A), 0.1–0.17 h (B), 0.23–0.65 h (C), and 0.1–0.23 h (D). The mean distance between the peaks was 0.235 h, 0.145 h, 0.394 h, and 0.127 h for measurements A, B, C, and D, respectively. The frequency analysis showed the existence of larger frequency components for higher temperatures. For specimen A ("small", 20 °C) dominant frequency components at about 1.1–1.4×10^{-3} Hz with peak-to-peak amplitudes of 2.5–5.3 µW could be detected, whereas for specimen B ("small", 30 °C) the major frequency increased to about 1.9×10^{-3} Hz with lower amplitudes of 1.5 µW. Measurement C ("large", 20 °C) shows the superposition of two frequencies, a lower one with 1×10^{-4} Hz and a

higher component of 7.2–8.9 $\times 10^{-4}$ Hz. A similar overlay is found for specimen D ("large", 30 °C), with frequencies of 1.3–1.7 $\times 10^{-4}$ Hz and 2.2–2.4 $\times 10^{-3}$ Hz, both being higher than the ones found for the equally sized animal at the lower temperature. Figure 3.6 shows the thermal output of the previous examples

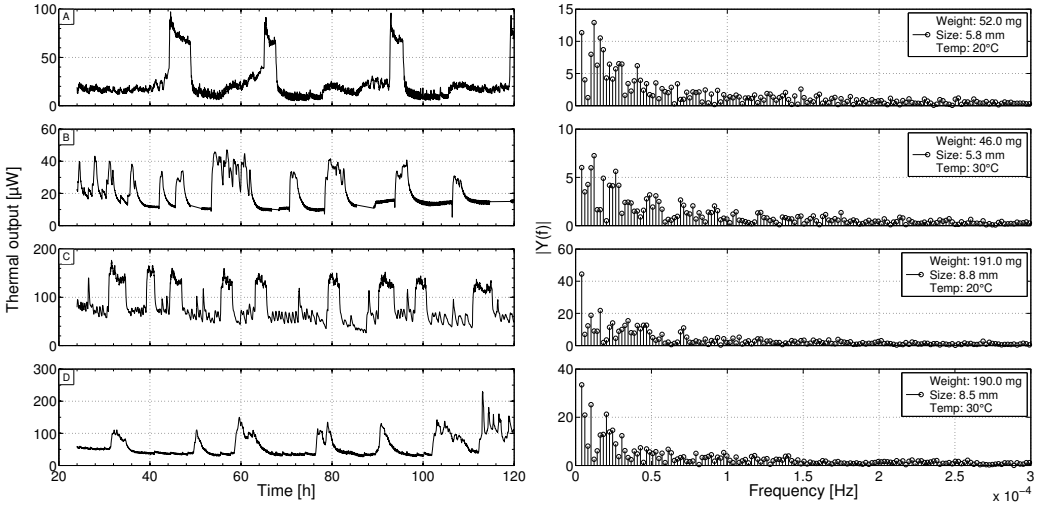

Figure 3.6: Frequency analysis of recurring "active" phases for one specimen of each size group and temperature. Presented data sets are the same as in Figure 3.5.

for a longer time span of 24–120 h (day 2 to end of day 5) with their corresponding frequencies. The repeating phases of high metabolic activity are clearly visualized occurring with frequencies in the range of 1–1.2 $\times 10^{-5}$ Hz, 1.8–7.7 $\times 10^{-5}$ Hz, 1.6–4.7 $\times 10^{-5}$ Hz, and 1.6–3.1 $\times 10^{-5}$ Hz for measurement A, B, C, and D, respectively. There were even lower components, which were, however, related to a very slow oscillation over time and not related to recurring "active" phases. Measurement B was corrected in a way to straighten negative values that were probably linked to fast condensation processes inside the chamber.

No clear pattern in the arrangement of "active" phases could be found with regard to different temperatures and snail sizes.

3.4 Results of long-term measurements

Figure 3.7 shows the results of the long-term measurements for two single large individuals at 20 °C and 30 °C, respectively. At 20 °C (A) the individual showed a very regular pattern of "inactive" phases followed by shorter "active" metabolic peaks that were 2.5–5.5 times higher than standard metabolism. The snail investigated at 30 °C (B) showed a very distinct activity pattern in the first two days. After day 2, even in these very "inactive" phases, a distinct oscillating behavior in heat output can be seen with an amplitude of approximately 20 µW ranging from 20–40 µW. As in Figure 3.1 (A, C, D) both long-term data sets displayed a very slow decrease of thermal output with time, converging asymptotically towards a minimum that was reached at approximately 8–9 days for A and at about 2–4 days for B when the snails may enter estivation.

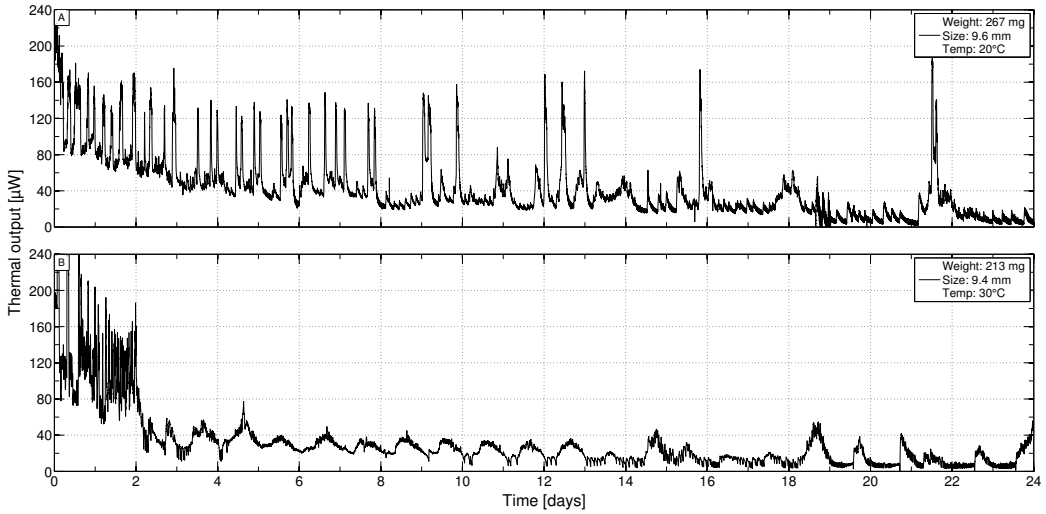

Figure 3.7: Thermal output of the two long-term measurements of 24 days for one large specimen at both temperatures 20 °C and 30 °C

3.5 Discussion

All measurements presented in Figure 3.1 clearly showed two distinct levels of metabolism, an "inactive" and an "active" state, corresponding to the ones

mentioned by Rees and Hand [1990]. The "active" state is probably also related to locomotion [Lamprecht and Becker, 1988, Rees and Hand, 1990], whereas in "inactive" states the snail remains withdrawn in its shell.

The work of Blazka [1955] showed that oxygen consumption only decreases very slowly for starving individuals kept under high humidity conditions. This goes along with the findings of a very slow decrease of thermal output in the long-term measurements (Figure 3.7) where snails were most probably entering estivation. The large difference in the onset of this low level of metabolism between these two individuals is probably due to their different physiological fitness, which is related to the current food and reproduction status as well as humidity level. Beyond these unknown factors *X. derbentina* tends to approach estivation earlier when the ambient temperature rises, which may represent a basic strategy to avoid costly energy expenses when ambient conditions are unfavorable.

Concerning the occurrence of regular patterns the results of Figure 3.1A ("small", 20 °C) showed a slightly shifted daily rhythm of one pronounced activity phase that the snail is still following despite the lack of any light source in the chamber specifying daily phases of brightness and darkness. Phases of inactivity lasted about 15–20 h and were constantly followed by "active" phases. The shift results from increasing phases of inactivity of specimen A, which indicates that the animal saves more and more energy the longer the period of food and water deprivation takes during the measurement. A similar course was found in measurement A ("small", 20 °C) and D ("large", 20 °C) of Figure 3.6, whereas specimens B ("small", 30 °C) and C ("large", 20 °C) clearly showed more times of activity.

Comparing the larger individual C with the small individual A at 20 °C in Figure 3.1 clearly shows that the prolongation of "inactive" phases occurs even earlier for the larger specimen, which may be due to its older age and the higher necessity of saving its resources. Dieterich et al. [2013] have shown older individuals of *X. derbentina* to save resources when down regulating stress protein expression. At the upper temperature of 30 °C only the larger individual (D) showed a daily rhythm with approximately two phases of activity per day.

With reference to the total energy consumption (Figure 3.3) it became obvious that for small individuals a regulation is taking place resulting in lower

values as the temperature transitions from 20 °C to 30 °C. Smaller individuals, therefore, seem to be more "aware" of the higher temperature, which makes it necessary for them to adjust their metabolism towards a lower level. The reason for this observation may be the higher specific surface (surface to volume ratio) of smaller individuals. Since the heat transfer rate is depending on the corresponding surface the heat flux for smaller specific surfaces is higher and, therefore, smaller snails are more affected by an increasing temperature that approaches a critical limit. Larger individuals, however, have shown a notable reduction in "active" metabolic level (Figure 3.1, C and D) at 30 °C, which indicates the presence of adaptation processes for larger specimens as well.

The division of "active" and "inactive" energy fractions (Figure 3.4) showed that "active" energy fractions of both size groups decrease for a transition towards a higher ambient temperature, which may be indicative of the animals' basic mechanism of preserving metabolic energy at more difficult thermal conditions. This effect is especially pronounced for the small specimen. Additionally, at 20 °C a significant decrease of "active" energy fraction was observed for larger specimen compared to the small individuals. This trend could not be found for the higher test temperature, where the "active" fraction only non-significantly differed for larger individuals. The reason for this may be the existence of a lower limit of activity phases. If temperature increases, "active" metabolic energy will be saved. But this decrease may, however, have a lower limit before *X. derbentina* passes into estivation, which could be connected to fixed activity cycles, such as feeding times and liquid intake that individuals are still trying to follow inside the measurement chamber. This limit may have, therefore, already been reached for both size groups at the higher test temperature in a way that no further reduction was possible. The findings of Becker [1980] stating that activity is responsible for 80 % of total energy turnover cannot be confirmed.

The results from the fractions of time spent in the "active" metabolic state (Table 3.1) revealed an increasing time fraction for larger individuals at 20 °C, which at first glance seemed to disagree with the findings from Figure 3.4. However, agreement is still possible as larger individuals reduce their "active" metabolic energy consumption and are, thus, able to spend longer periods in the "active" state. Unfortunately this result was not reproduced by the speci-

men kept at 30 °C. As the energy fractions showed a largely constant "active" demand for both size groups it can be assumed that both size groups spend an approximately equal time in "activity". Poikilothermic animals usually become more active at high temperatures and less active at low temperatures [Mellanby, 1939]. In this respect, *X. derbentina* shows an anomalous response as the time share of "activity" for large individuals subsequently decreases again as temperature rises. However, this is not unknown to happen [Kerkut and Taylor, 1958] but found to be transient until the "normal" behavior adjusts again. Therefore, the reduced time of "activity" as well as the observed lower "active" thermal output level during "activity" (Figure 3.1, C and D) is interpreted as a deliberate action to counteract difficult thermal conditions.

For both size categories a characteristic difference exists between their body weight. Approaching their surfaces by a sphere the ratio of their mean masses can be written as:

$$\left(\frac{\text{large}}{\text{small}}\right)_{\text{mass}} = \frac{m_{\text{large}}}{m_{\text{small}}} = \frac{D^3_{\text{large}}}{D^3_{\text{small}}} = \frac{8.65^3}{5.55^3} = 3.79 \tag{3.1}$$

According to Table 3.2 the ratio of the change of time spent in "activity" (subscript "act") is:

$$\left(\frac{\text{large}}{\text{small}}\right)_{\text{activity change}} = \frac{\Delta t_{\text{act, large}}}{\Delta t_{\text{act, small}}} = \frac{13.6}{50.4} = 0.27 \tag{3.2}$$

Despite the fact that the data for "small" individuals is rather critical it seems that the ratio of change in "activity" for the transition from 20 °C to 30 °C is inversely proportional to the ratio of their masses for large and small individuals:

$$0.27 \approx 3.79^{-1} = 0.26 \tag{3.3}$$

Based on this experimental result the following connection can be made:

$$\frac{(dt_{\text{act}}/dT)_{\text{small}}}{(dt_{\text{act}}/dT)_{\text{large}}} \propto \frac{m_{\text{large}}}{m_{\text{small}}} \tag{3.4}$$

and, thus,

$$\frac{dt_{\text{act}}}{dT} \propto -\frac{1}{m} \tag{3.5}$$

which is the change of activity per degree of temperature increase being proportional to the inverse of the mass. The minus sign results from the fact that activity generally decreases for increasing temperatures. The measured

relationship in Equations 3.1 – 3.3 follows from this since both size categories were subjected to the same temperature increase ΔT. Rearranging Equation 3.5 and integrating over the time spent in activity and temperature yields:

$$\begin{aligned} \int_{t_{\text{act (T=20 °C)}}}^{t_{\text{act (T)}}} dt &\propto -\frac{C}{m} \cdot \int_{20\,^{\circ}\text{C}}^{T} dT \\ t_{\text{act (T)}} &= t_{\text{act (T=20 °C)}} - \frac{C}{m} \cdot (T - 20\,^{\circ}\text{C}) \end{aligned} \tag{3.6}$$

with C as an empirical constant. The time spent in activity, therefore, decreases depending on the temperature change and the mass of the animals. This highlights the fact that the behavior of *X. derbentina* is directly influenced by their exposure to ambient temperature. Based on this simple linear relationship a theoretical temperature maximum can be obtained at which the snails have no activity anymore:

$$T_{\text{max (m)}} = t_{\text{act (T=20 °C)}} \cdot \frac{m}{C} + 20\,^{\circ}\text{C} \tag{3.7}$$

However, this linear trend of T_{max} leads to an unphysical approximation as a global maximum temperature for individuals with high masses is believed to exist. A non-linear asymptotic trend of T_{max} for increasing masses m is more realistic but requires further measurements.

The frequency analysis for the "inactive" state presented in Figure 3.5 revealed a clear dependency on the investigated temperature for both sizes of *X. derbentina*, namely the existence of increased frequency components for the higher test temperature. In a broader sense this result resembles the findings of Kerkut and Ridge [1962], who reported a proportionality of ambient temperature and the frequency of neuronal activity in *Helix aspersa*. Although the thermal output of *X. derbentina* is only weakly linked to the activity of its brain, this accordance is rather unexpected. The calorimetric system monitors the thermal output of the complete organism and, therefore, the identified oscillations most probably represent muscular activity of *X. derbentina* in phases of inactivity since these energetic processes give the largest contribution to thermal output. Crozier and Stier [1925] as well as Bailey and Lazaridou-Dimitriadou [1991] found an increasing heart rate for higher temperatures in *Limax maximus*, *Helix aspersa*, and *Helix lucorum*. With increased heart rate

the metabolic expenditure rises, which explains the higher "inactive" levels found at higher temperatures for the large specimens (Figure 3.1, C and D). A reasonable heart rate in land snails, however, is in the range of 5×10^{-1} Hz [Schwartzkopff, 1954] and, therefore, the results on energetic frequencies do not directly reflect the heartbeat. The consequences of this increased effort at higher temperatures, however, may likely be expressed by the observed frequency increase and may represent indices for thermal stress.

Comparing the courses of thermal output in Figure 3.5 A/C (20 °C) and Figure 3.5 B/D (30 °C) one can see that the pattern changes from a single major component to a superposition of two frequencies for larger animals. The reason for this change remains unclear but this effect is most probably related to their older age and corresponding physiological processes, which demand energy and take place at lower frequencies.

Therefore, the "features with a relatively quick increase and a rather slow and nearly-linear decrease" mentioned by Lamprecht and Becker [1988] that were clearly connected to inactivity can be confirmed by the finding of regular oscillations in the "inactive" state. For *X. derbentina*, however, activity usually resulted in a much higher thermal output level compared to Lamprecht and Becker's unmentioned snail species. After all, the regular and distinct oscillations found in the present study show that *X. derbentina* can undergo remarkable changes in heat production although being a poikilothermic animal without a distinct temperature regulation system. These changes happen within a few minutes. The observed phases of metabolic change could not be associated with phases of locomotion since the latter are most probably connected to the much higher "active" levels found, similar to the results from Rees and Hand [1990]. In contrast, the observed fluctuations in heat output likely represent internal activity changes.

Chapter 4

NMR measurements of *X. derbentina*

Because of the high water content and the disadvantages of drying processes, like the collapse of fragile tissue structures, computer tomography (CT) was not applicable to gain information about the snail's inner and outer proportions. Nuclear magnetic resonance (NMR) is a method that is frequently used in human medicine, where it is commonly called magnetic resonance imaging (MRI) and is primarily used to detect the presence of hydrogen in the human body. Therefore, NMR is very suitable to provide a maximum richness of detail of *X. derbentina*'s inner organs to create a model that serves as a basis for further investigations.

The basic method of NMR provides a wide range of investigation fields. NMR spectroscopy is often used in the field of biochemistry as an analytical method for the identification of substances, the tracing of coupling partners or the identification of concentrations [Hausser and Kalbitzer, 1989]. It is also utilized for the description of dynamic processes in molecules as well as the measurement of interatomic distances.

Another facet of NMR is imaging, which is most commonly called as magnetic resonance tomography or NMR tomography. Depending on the composition of the measured tissue the magnetization is influenced resulting in a map of regions with different contrasts. This effect is measured in a defined number of slices inside the volume element resulting in a three-dimensionally formed pattern.

4.1 Basics of nuclear magnetic resonance

4.1.1 Magnetic moment and nuclear spin

Atomic nuclei are electrically charged and possess an intrinsic angular momentum (spin) that is characterized by a spin quantum number I. Out of theoretical reasons the value of I can only take integer multiples of $\frac{1}{2}$. If the number of protons and/or neutrons of an isotope is odd it has an intrinsic magnetic moment μ and an angular momentum, i.e. a spin quantum number of $I \neq 0$. Because of this property they are similar to a compass with their needles statistically pointing in every possible direction [Hanson, 2008]. However,

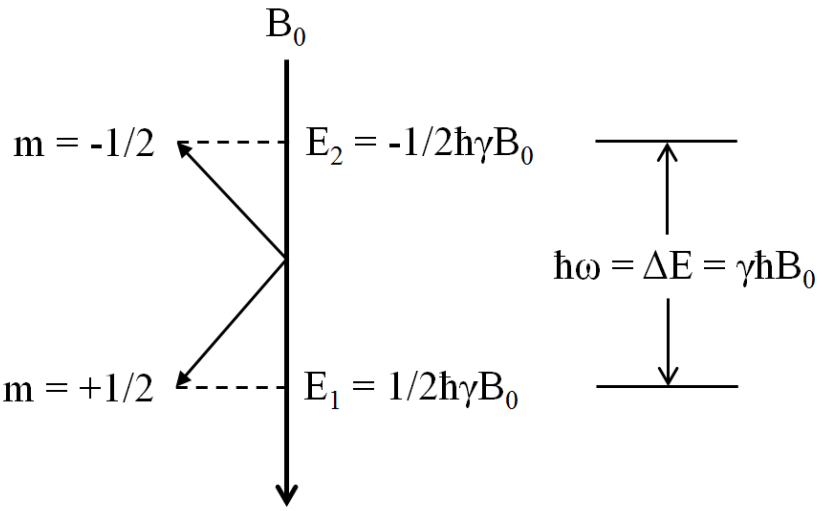

Figure 4.1: Energetic levels and quantization of direction of a nuclear dipole

if these nuclei are subjected to a magnetic field the nuclear dipoles will try to align with and point in the direction of this external field. Quantum physics states that the intrinsic angular momentum can only take defined directions with respect to the preferred direction of the external field (quantization of direction), i.e. for particles with $I = \frac{1}{2}$ one parallel ($+B_0$, spin-up) and one antiparallel ($-B_0$, spin-down) direction corresponding to values of the magnetic quantum number of $m = +\frac{1}{2}$ and $m = -\frac{1}{2}$ (Figure 4.1). The energy of these levels is $E_1 = -\frac{1}{2} \cdot \hbar \cdot \gamma \cdot B_0$ and $E_2 = \frac{1}{2} \cdot \hbar \cdot \gamma \cdot B_0$ [Hornak, 1996]. Analogously to the mechanics of a gyroscope a turning moment $T = \mu \cdot B$ is

exerting on the nucleus when it gets exposed to an external field B that is causing the spin axis to precess with the Larmor frequency $\omega_{\text{Larmor}} = \gamma \cdot B_0$ around the field direction, with γ being a constant called the gyromagnetic ratio that is characteristic for each nucleus. Therefore, if an external field acts on the atomic nuclei the compass needles (visualizing the spin) are also taking the directions specified by the quantization of direction and are precessing on canonical shells around the B_0 direction.

4.1.2 The Bloch equations and spin-lattice relaxation

The precession around the magnetic field direction when magnetization and magnetic field do not have the same direction was first described with differential equations by Bloch [1946].

The energetic level for the nuclei that are pointing in the antiparallel direction (spin-down) is higher because energy needs to be expended to turn these spins against the external field. Shortly after the field acts on the nuclei equal numbers of spins are in the spin-up and spin-down condition. However, Felix Bloch also discovered that a certain time after such a disturbance of the nuclei an equilibrium magnetization in z direction (the direction of the external field B_0, compare Figure 4.2) with a value of M_0 is found.

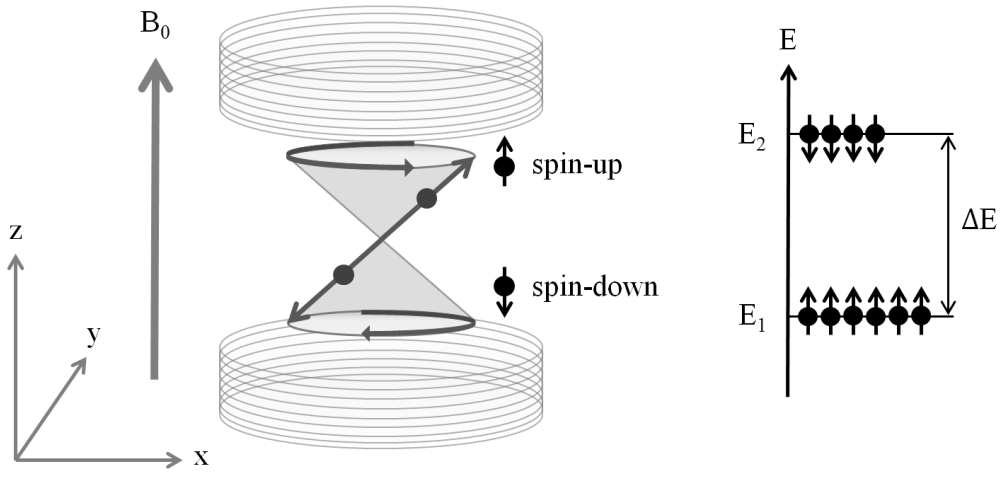

Figure 4.2: Nuclei in spin-up and spin-down state after thermal equilibration in the direction of the external field B_0

The reason for this observation is the thermal energy that is present during the process of thermal equilibration with the environment. This disturbs the initially uniform orientation resulting in more nuclei being in the more favorable state of spin-up when the system reaches its temperature equilibrium. As a consequence the sample exhibits a measurable macroscopic magnetization parallel to the direction of B_0 (Figure 4.2) [Hausser and Kalbitzer, 1989]. It is important to notice that even though all of the individual spins are precessing around the external magnetic field axis, the net magnetization does not precess [Hashemi et al., 2010]. The reason for this is that all spins are out of phase with each other. Therefore, the sum of all spins will have a component along the z direction but due to their phase cancelation they will have no component in the x or y direction.

This phenomenon of establishing the thermal equilibrium of the spin system with its environment is known as spin-lattice relaxation or longitudinal relaxation because the equilibrated magnetization is parallel (longitudinal) to the external field B_0.

4.1.3 Spin flip

If the static field is superimposed with another, yet smaller, transversal orientated and alternating magnetic field B_1 with frequency $\omega = \omega_{\text{Larmor}}$ a strong interaction can be observed. The distributed spins that were previously dephased and, therefore, had no net component in x or y direction now try to align with the additional field which causes them to be in phase and a resulting oscillating magnetization M_{xy} in the $x-y$ plane is built up. The external field now exactly promotes the precession of the spins, which is representing the resonance condition. The spins precess about the B_0 field and the B_1 field at the same time resulting in a spiral motion of the entire magnetization distribution (represented by the net magnetization vector) from the z axis into the $x-y$ plane [Hashemi et al., 2010]. In a coordinate system moving with the main rotation about B_0 this motion is perceived as a so-called flip.

It is also well-known that transitions between the two states of spin-up and spin-down can be induced if the energy of the electromagnetic quanta $\hbar \cdot \omega$ is equal to the energy difference between the two states: $\hbar \cdot \omega_0 = E_2 - E_1 = \hbar \cdot \gamma \cdot B_0$. Therefore, the transversal field B_1, which is oscillating with the exact resonance

frequency $\omega = \omega_{\text{Larmor}} = \omega_0$, stimulates a transition from the lower energy level E_1 (spin-up) to the higher energy level E_2 (spin-down) causing more and more spins to point towards the spin-down direction.

The resulting position of the spins, however, depends on the length of the transversal pulse. A pulse length that will turn the spins exactly into the $x-y$ plane is called a 90° pulse or $\pi/2$ pulse causing both energy levels (spin-up and spin-down) to be equally occupied, the magnetization M_z to vanish and a resulting magnetization in the $x-y$ plane to be built up (Figure 4.3).

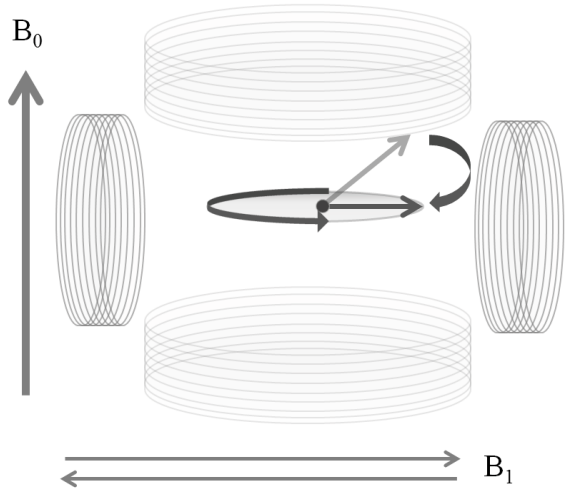

Figure 4.3: Spin flip

4.1.4 Relaxation processes (free induction decay, decay of transversal magnetization and spin-spin interaction)

The transversal coil first operates as a transmitter and causes the flip of the spins. Once the spins are turned into a transversal direction they will oscillate with the frequency ω_0 in the $x-y$ plane. This also causes the magnetization in the transversal coil to oscillate, which in turn induces an alternating current visualizing the nuclear magnetization. Immediately after the current in the coil is turned off, it operates as a receiver and an alternating current with a subsequent decay as the spins turn to the direction of the static field B_0 again

can be observed (Figure 4.4). In order to fully capture this decay two different relaxation processes need to be discussed that are occurring simultaneously.

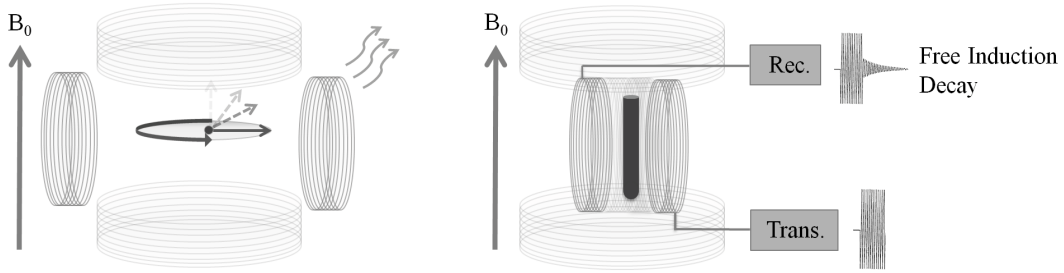

Figure 4.4: Free Induction Decay (FID) after $\pi/2$ pulse

Immediately after the 90° pulse spins are flipped into the $x-y$ plane and oscillate around the z axis with all spins in phase with each other. After the transversal coil is turned off spins will recover again and try to align with the external magnetic field B_0 since this represents their lowest energy level. This is the process of spin-lattice relaxation described before and is characterized by the time constant T_1. Additionally, the magnetization M_{xy} decays as observed in the recorded signal of the transversal coil, which occurrs at a different rate characterized by the time constant T_2. It is important to notice that the recovery of M_z and the decay of M_{xy} are independent processes with the time constant T_2 being 5 to 10 times smaller than T_1 and, therefore, the involved process happens much faster than spin-lattice relaxation does [Hashemi et al., 2010]. The reason for the faster decay of M_{xy} is the dephasing of the spins in the $x-y$ plane after the spins flipped causing the net magnetization to further decrease in addition to the already lowered component in the $x-y$ plane as magnetization in z direction is built up again along the main magnetic field.

The dephasing of spins has two reasons: spin-spin interaction and field inhomogeneities [Hausser and Kalbitzer, 1989, Hornak, 1996]. Due to spins that are spatially close to each other but pointing in different directions the strength of the effective magnetic field acting on their neighbors is modified resulting in slightly higher, and respectively lower Larmor frequencies. The second reason is inhomogeneities in the external field causing the spins at different locations to precess at different frequencies. This influence is due to

the imperfection of the external magnetic field itself and cannot be completely avoided. Consequently, the spins will slowly dephase inside the sample causing the net magnetization M_{xy} to decay. Therefore, the NMR signal immediately after the impulse shows the free precession of the spins that decays with time and induces a current in the receiver coil and is, therefore, called Free Induction Decay (FID). The characteristic time for the overall process is T_2^*, which depends on the external field (including its inhomogeneities) and the spin-spin interactions, whereas T_2 primarily depends on spin-spin interactions and, therefore, T_2^* is always less than T_2.

4.1.5 Spin echo pulse sequence

External field inhomogeneities can be prevented by a pulse sequence called Spin Echo (SE) that was discovered by Hahn [1950]. After the 90° pulse spins are flipped into the $x-y$ plane and, due to field inhomogeneities, these spins eventually become out of phase. By applying a 180° pulse after a time τ spins are flipped and precess in the opposite direction. This will cause the spins to rephase again at the time 2τ and will induce a signal in the receiving transversal coil. However, spin-spin interaction is still present, which results in decaying maximum echo amplitudes if this process is repeated several times. Since field inhomogeneities have now been eliminated the characteristic time constant for the repeated series is T_2, whereas each decaying echo signal is characterized by T_2^*.

4.1.6 Repetition time T_R and echo time T_E

T_1 and T_2 are inherently fixed for the tissue under investigation, T_2^* is more or less fixed and only depends on the uniformity of the magnet. T_R and T_E, however, are adjustable to gain control of the resulting contrast of the image [Hashemi et al., 2010]. The repetition time T_R is defined as the time between successive 90° pulses. If T_R is less than the time T_1 it takes for full recovery of the longitudinal magnetization M_z the next 90° flip will result in a lower magnetization value of the projection of M_z onto the $x-y$ plane M_{xy}. The received signal after the second flip will, therefore, be a FID with a slightly lower amplitude. The echo time T_E is defined as the time of the maximum

amplitudes in the echos of the sample, corresponding to the spin echo pulse sequence described above. The 180° pulse is applied at time $T_E/2$.

The choice of T_R and T_E becomes especially important when dealing with different tissues that have different characteristic times T_1 and T_2. If T_R is too long the difference in their T_1 recovery is reduced since both tissues have enough time for a recovery of their longitudinal magnetization, and the contrast between them will vanish. Therefore, short T_R accentuates the T_1 contrast inside a sample of multiple tissues. However, a too short repetition time will result in no signal at all [Hashemi et al., 2010].

Contrary to this, a short echo time T_E will result in a reduced T_2^* effect. The longer T_E is the more pronounced will be the differences inside two tissues due to their different decay curves of their echos resulting from the remaining spin-spin interactions that cannot be eliminated in the spin echo pulse sequence. Therefore, large T_E enhances the T_2^* effect [Hashemi et al., 2010].

4.2 Basics of imaging

The more spins that exist inside a sample the higher is the magnetization and the initial amplitude of the FID. This, in turn, shows that the intensity of the signal depends upon the concentration of specific nuclei, which is of great importance for the quality when NMR is used in the process of imaging.

By the application of the aforementioned procedures only an integral signal of a sample will be acquired without any spatial information since all regions experience the same magnetic field strength. To assign the different regions of spin to corresponding positions in x, y, and z direction these spin regions need to experience a unique field that relates the spins to their spatial position. This is accomplished by linear gradient fields G_x, G_y, and G_z that are superimposed upon the external field and influence the resulting resonance frequency [Hornak, 1996]. By this technique more than one region containing spin is resolved indicated by additional frequency components in the NMR spectrum.

An image is finally generated by a method called phase encoding and Fourier transformation imaging. Therefore, the volume of interest is investigated by the successive measurements of slices in z direction. The slice selection hereby is achieved by a one-dimensional, linear magnetic field gradient that is applied

during the time of the 90° flip pulse. This will only cause those spins to rotate that are located in a plane through the object [Hornak, 1996].

For this imaging process a typical sequence contains a 90° slice selective pulse, a slice selection gradient pulse, a phase encoding gradient pulse, a frequency encoding gradient pulse, and a signal [Hornak, 1996]. After the slice selection gradient G_s is turned off a phase encoding gradient G_ϕ is applied in x direction, which results in different Larmor frequencies along the gradient for the whole slice. After the gradient G_ϕ is turned off again each spin packet will have the same frequency again but they now have a phase shift relative to each other along the x axis. Subsequently a frequency encoding gradient G_f is applied along the y direction. Thereby, spin packets will precess in the $x-y$ plane with a frequency along the y direction according to the gradient G_f. Now each location in the $x-y$ plane has spin packets precessing with a unique phase shift and frequency and they can now be analyzed by a two-dimensional Fourier transformation.

4.3 Experimental setup

The NMR measurements on *X. derbentina* were performed at the facilities of Bruker BioSpin GmbH in Rheinstetten. For the NMR experiments an Avance II 400 MHz Wide Bore System, 9.4 T, equipped with a Micro2.5 Gradient System and a 10 mm 1H resonator was used. A live snail with an outer shell diameter of approximately 9.0–9.5 mm was fixed in a 10 mm NMR tube and kept at a temperature of 25 °C. To improve the contrast the snail was fed with the contrast agent Magnevist® (Bayer Pharma AG) dissolved in water which resulted in a strong signal of the snail's gastro-intestinal system.

A T_1 and T_2 weighted Spin Echo 3D (SE3D) experiment was performed on the snail 19 h after it was fed the contrast agent with the following parameters:

- Repetition time T_R: 50 ms
- Echo time T_E: 4.43 ms
- Field of View (FOV): $12 \times 12 \times 12\,\mathrm{mm}^3$
- Matrix: $256 \times 192 \times 192$ voxels

- Resolution: $47 \times 62 \times 62\,\mu m$
- Averages: 4
- Time for experiment: 2 h 2 min

4.4 Imaging data and reconstructed systems

Figure 4.5 shows 16 slices of the resulting SE3D dataset of *X. derbentina*. It is particularly notable how the addition of the contrast agent highlights the snail's gastro-intestinal system (brightest structure on slice 2–8, in the vertical center slightly right, highlighted on slice number 2) that forms a loop after the first whorl of the snail's shell (compare Figure 4.6 and Figure 4.7).

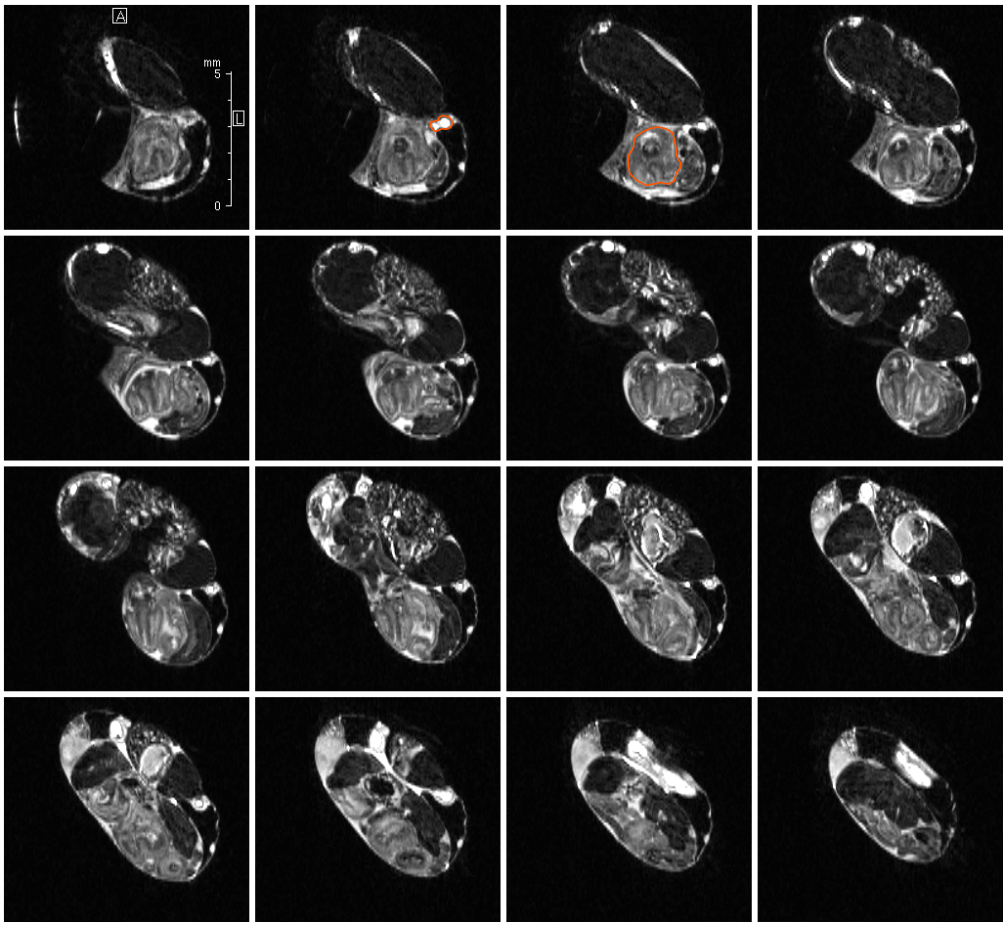

Figure 4.5: 16 slices through *X. derbentina* from the resulting spin echo dataset

Additionally the retracted foot of *X. derbentina* can clearly be seen in the

first 12 slices forming a complex folded structure (highlighted in Figure 4.5 on slice number 3).

The spin echo experiment resulted in a detailed resolution of the inner organic structures of *X. derbentina* and provided a solid basis for the reconstruction of the main organs. A volume rendering of the complete dataset obtained with the software package Amira 5.4.3 (FEI Visualization Sciences Group, Bordeaux, France) is shown in Figure 4.6. At the aperture of the snail's shell the main vein with its branched capillaries can be seen that is located next to the shell and covers the snail's lung. Additionally, the aforementioned loop of the intestine can be well observed. In the last whorls of the snail's shell the hepatopancreas is located that is part of its digestive tract and provides the functions of the liver and pancreas in mammals [Storch et al., 2006]. The hepatopancreas is half encircled by a bright structure and, therefore, contains a high amount of water that most probably represents mucus.

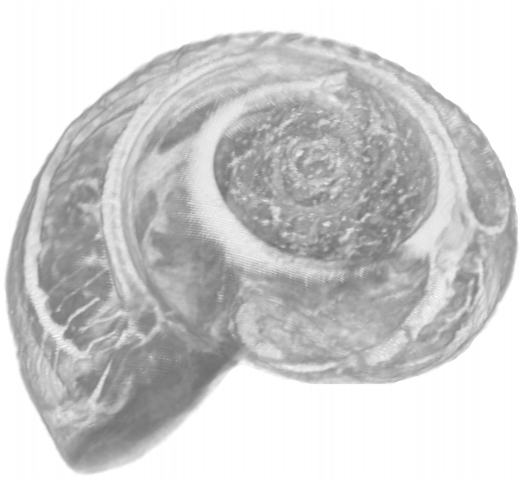

Figure 4.6: Volume rendering of the complete spin echo dataset

On the basis of this measurement a reconstruction of the inner organs of *X. derbentina* was accomplished using the software package Mimics (Materialise, Leuven, Belgium). Within the limits of the obtained resolution the hepatopancreas, the kidney, the intestine, the heart, and the lung with its overlying vein system could be partitioned and are presented in Figure 4.7 together with the volume rendering of the measurement. Unfortunately, a re-

construction of further organs was not possible due to an insufficient resolution and the poorly distinguishable parts especially in the inner shell regions of *X. derbentina*. However, the results provided reliable values for the size of the heart ($V_{\text{heart}} = 8.5\,\text{mm}^3$) and the size of the lung ($V_{\text{lung}} = 35.1\,\text{mm}^3$), which was gathered by smoothing and exporting the corresponding regions in Mimics and the subsequent volume meshing and computation of the volume with the software package ANSA v15 (BETA CAE Systems, Thessaloniki, Greece).

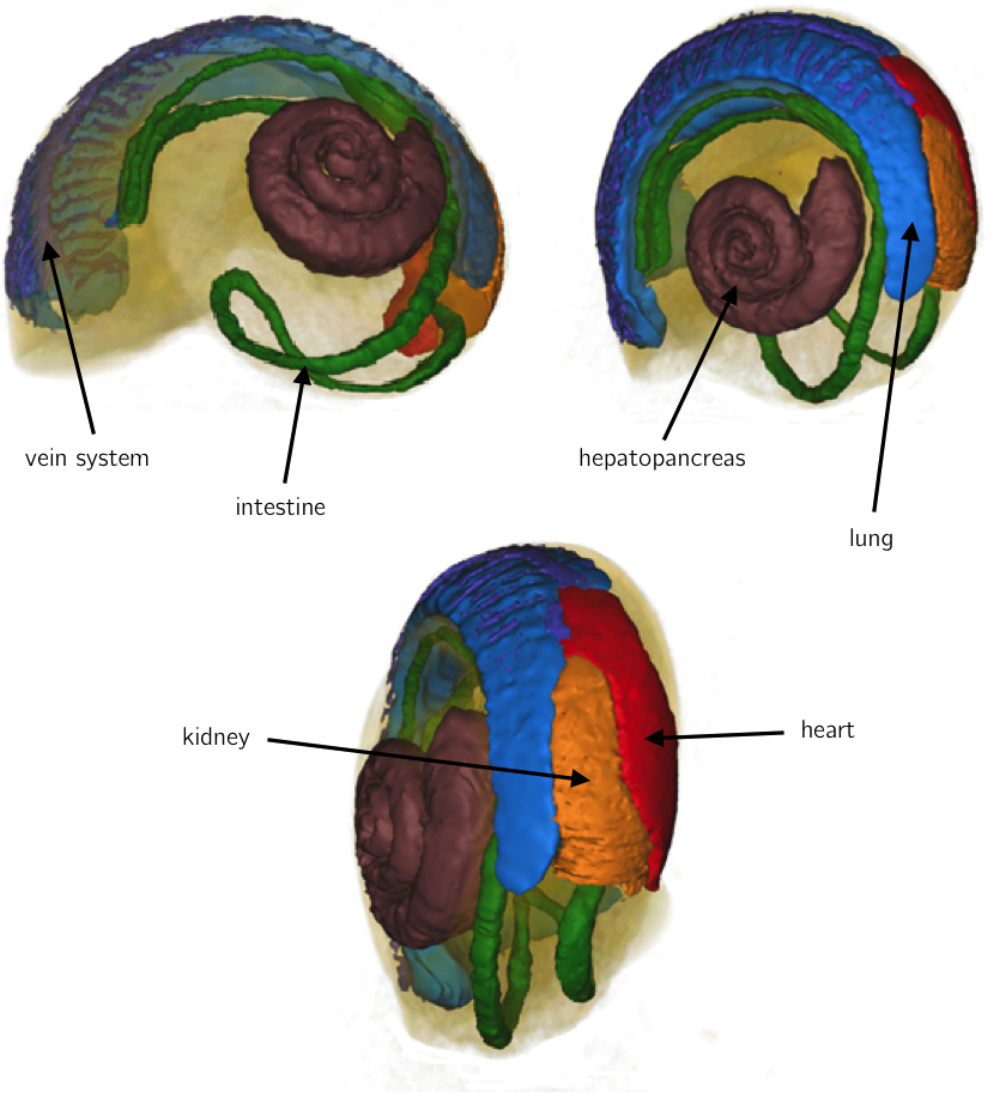

Figure 4.7: Reconstructed organs of *X. derbentina* and volume rendering

The volume of the heart and the volume of the lung are two very important

values for an integral analysis of the snails' metabolism that complement the previously measured parameters of oxygen consumption (compare Chapter 2) and energy turnover (compare Chapter 3) of the animal.

In the following Chapter an approach is presented, which shows that both datasets are quantitatively consistent with each other. Combining this information with the geometrical data presented in this chapter helps to gain further physiological details. Later on, a strong emphasize will be put on the snails' lung by investigating arterial and venous oxygen concentrations as well as the distribution of concentration along the capillaries and the main vein. Therefore, the geometrical data obtained from the NMR measurements presented define key elements for all further investigations discussed in this work.

Chapter 5

Approach to an integrative physiological model

From the basics of physiology it is clear that oxygen consumption, blood flow and metabolism are directly linked to each other and depend on the instantaneous needs of an organism. Air is inhaled and the oxygen is passed to the hemolymph which is transported by the beating heart. Despite the snail having an open cardiovascular system that is very different to human circulation, the same basic principles must still be applicable [Müller, 2001].

With the help of physical modelling reasonable statements concerning the physiological state of X. derbentina can be made. Therefore, a physiological model will be presented that makes use of the quantitative consistency of direct calorimetry and respirometry data and, by combining it with the information obtained from the NMR measurements, reveals further physiological parameters of this species, such as breathing frequency and the reduction of oxygen concentration per breath of air. This approach helps to further characterize the physiological state of the animal without measuring the corresponding parameters. The size of the animal's lung was gained from the NMR measurements presented in the previous Chapter 4 and corresponds to the "non-movement state" of the snail, i.e. when it is withdrawn in its shell.

The oxygen consumption $\dot{V}_{O_2}$, depicted as a volume flow in the units of $[\mathrm{m}^3 \cdot \mathrm{s}^{-1}]$, can be calculated by the product of the breathing volume per minute $\dot{V}_b$ and the oxygen reduction per breath $\Delta O_{2_{\mathrm{breath}}}$, given as a dimensionless fraction resulting from the difference in oxygen mass fraction between inhalation

and exhalation (Equation 5.1):

$$\dot{V}_{O_2} = \dot{V}_b \cdot \Delta O_{2_{\text{breath}}} \tag{5.1}$$

Using the definition of the molar volume V_m the oxygen consumption $\dot{V}_{O_2}$ can be converted to $\dot{n}_{O_2}$ and expressed in the units of $[\text{mol} \cdot \text{s}^{-1}]$:

$$\dot{n}_{O_2} = \frac{\dot{V}_{O_2}}{V_m} = \frac{1}{V_m} \cdot \dot{V}_b \cdot \Delta O_{2_{\text{breath}}} \tag{5.2}$$

with $V_m = 22.41 \times 10^{-3}\,\text{m}^3 \cdot \text{mol}^{-1}$. The breathing volume V_b is defined by the following relationship:

$$V_b = \frac{\dot{V}_b}{f_b} \tag{5.3}$$

with f_b as the breathing frequency of the animal. For a lung volume V_l the ratio

$$r = \frac{V_l}{V_b} \tag{5.4}$$

is defined as a characteristic physiological ratio of lung to breathing volume. For human beings this ratio is in the range of 10 [Müller, 2001], i.e. only 10 % of our complete lung volume is in- and exhaled during a regular breath.

Based solely on the consumption of glucose, the measured thermal output P_{th} from Chapter 3 is calculated using the caloric value CV of glucose and the amount m of mol O_2 to oxidize 1 mol of glucose:

$$P_{\text{th}} = \frac{CV \cdot \dot{n}_{O_2}}{m} \tag{5.5}$$

Equation 5.1 to 5.5 can be combined to express the unknown oxygen reduction per breath $\Delta O_{2_{\text{breath}}}$ by the other two unknown variables breathing frequency f_b and ratio of lung volume to breathing volume $r = V_l/V_b$:

$$\Delta O_{2_{\text{breath}}} = \frac{P_{\text{th}} \cdot m \cdot V_m \cdot r}{V_l \cdot f_b \cdot CV} \tag{5.6}$$

The stoichiometry for the oxidation of glucose reveals 6 mol of oxygen are needed per mol glucose. Expressing the breathing frequency f_b in the units of $[\text{min}^{-1}]$, the lung volume V_l in the units of $[\text{mm}^3]$, the thermal output in the units of [W], the oxygen reduction per breath $\Delta O_{2_{\text{breath}}}$ in the units of [%] and using the caloric value CV of glucose of $2826\,\text{kJ} \cdot \text{mol}^{-1}$ Equation 5.6 can be written as:

$$\Delta O_{2_{\text{breath}}} = \frac{P_{\text{th}} \cdot 6 \cdot 22.41 \cdot r}{V_l \cdot f_b \cdot 2826} \cdot 6 \times 10^6 \tag{5.7}$$

Using Equation 5.7, containing three unknowns, a surface plot was created that shows oxygen reduction per breath $\Delta O_{2_{\text{breath}}}$ as a function of breathing frequency f_b and the ratio of lung volume to breathing volume $r = V_l/V_b$. With the measured values of thermal output P_{th} and lung volume V_l this surface shows possible combinations of the three unknown properties that would all be consistent with the results of the experimental methods, oxygen consumption (compare Chapter 2), direct calorimetry (compare Chapter 3) and, the geometrical data of the lung by NMR measurements (compare Chapter 4).

This equation only holds true if the metabolism of *X. derbentina* is aerobic, as was checked before. Data for oxygen consumption in *X. derbentina* was presented in Chapter 2 for three different size groups in their "inactive" state for the temperatures 25 °C, 30 °C and 38 °C. However, the size of the measurement chamber inside the calorimeter limited the range of these measurements. Size group 2 from the oxygen consumption measurements with an average diameter of 0.9–1.0 cm closely matched the investigated "large snails" in the calorimetric investigations and, therefore, oxygen consumption values at 30 °C of this group will be used to check for aerobic metabolism. The division of "caloric value of glucose / amount of mol O_2 to turn over 1 mol of glucose" in Equation 5.5 is the "calorimetric equivalent" *CE* and varies between 19.63–21.13 $\text{kJ} \cdot \text{l}^{-1} O_2$ (neglecting the influence of temperature) depending on the composition of the nutrients [Lusk, 1924]. Calculating the theoretical thermal output for *X. derbentina* individuals with a diameter of 0.9–1.0 cm with their average oxygen consumption of $1.56 \times 10^{-10}\,\text{mol} \cdot \text{s}^{-1}$ at 30 °C (compare Chapter 2) results in a heat output of 73.7 µW, 68.5 µW and 70.3 µW, for the consumption of carbohydrates, lipids, and proteins, respectively. This is in good agreement with the data recorded for the "inactive" state of *X. derbentina* presented in Chapter 3 considering that the individuals in this case were slightly smaller than the ones from the oxygen consumption study and therefore values of approximately 70 µW fit very well to slightly upwards corrected values from the "inactive" levels in Figure 3.6. This shows that the "inactive" metabolic state of *X. derbentina* is aerobic. The NMR measurement to obtain the geometrical volume of the lung ($V_l = 35.1\,\text{mm}^3$) has been performed with an individual of 0.95 cm size and, therefore, fits the "large" group of snails in the calorimetric study and "group 2" of the oxygen consumption study. Thus, the value of

70 µW is used for the calculation of the response surface at 30 °C for "inactive" individuals sized between 0.9–1.0 cm. Assuming that *X. derbentina* is also aerobic at a slightly lower temperature, an additional dataset was calculated for 25 °C using the value of oxygen consumption of 1.04×10^{-10} mol · s^{-1} (compare Chapter 2) measured for equally sized snails and the caloric equivalent resulting in approximately 49 µW.

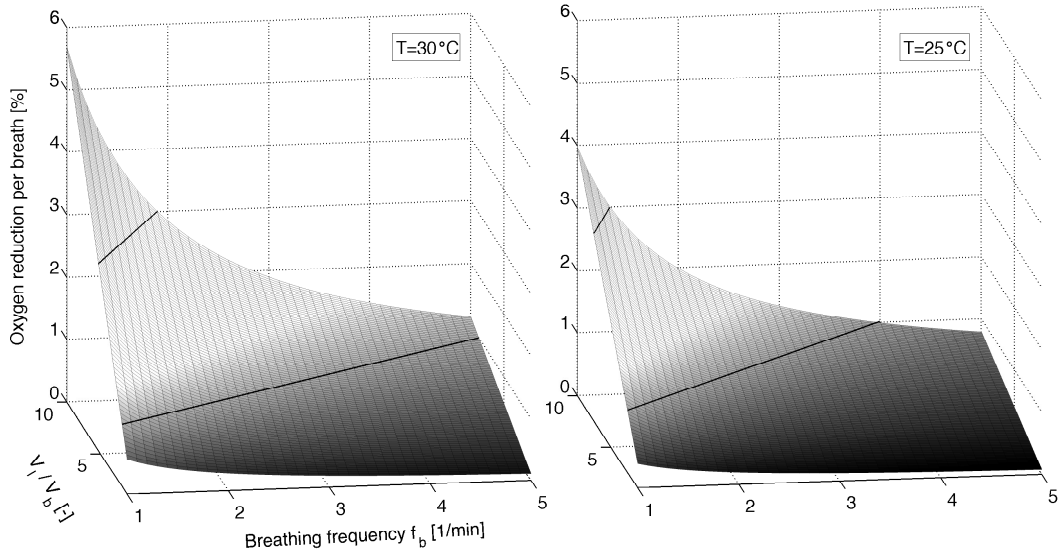

Figure 5.1: Response surfaces calculated for oxygen reduction per breath vs. breathing frequency and ratio of lung volume to breathing volume (medium sized snail of 0.9–1 cm, aerobic state, heat output of approximately 70 µW (30 °C) and 49 µW (25 °C), lung volume 35.1 mm^3)

Figure 5.1 shows the resulting surfaces of oxygen reduction per breath $\Delta O_{2_{\text{breath}}}$ vs. the ratio of lung volume to breathing volume V_l/V_b and breathing frequency f_b for both temperatures. It can be seen that $\Delta O_{2_{\text{breath}}}$ needs to be increased in order to maintain the metabolic state when either the breathing frequency decreases or when the volume ratio increases, which is clearly plausible. The range for breathing frequency is very reasonable compared to values of about 3.5 breath cycles per minute found for *Helix pomatia* [Maas, 1939].

It is known that an average human being reduces the oxygen concentration per breath by approximately 5 %, from a concentration of 21 % to 16 % in air [Schmidt et al., 2005]. In this regard the highly efficient alveolar design of

mammalian lungs is considered to be much more efficient than the rather basic respiratory system of pulmonate snails and, therefore, an upper reasonable limit of oxygen reduction may be defined by a value of 3 %. In combination with the assumption of a lower limit of 1 % (black lines in Figure 5.1) the delimited remaining area in the 3D plot describes all possible physiological states of *X. derbentina* based on the measurements and on the assumptions of the model. Due to the lower level of oxygen consumption at 25 °C this area is smaller than the one calculated for 30 °C.

In the following chapters additional physiological parameters, like the heartbeat frequency and cardiac output of *X. derbentina*, will be derived. But as these parameters rely partly on certain additional assumptions and therefore are error-prone, they are presented separately. Nevertheless all presented insights complement the available values and add to the overall picture of the physiological state of the animal.

Chapter 6

Diffusive and convective transport of oxygen through the venous system

The transport of oxygen in the snail's blood, the hemolymph, relies upon two mechanisms: physically dissolved in the aqueous blood plasma and chemically bound to hemocyanin, a protein found in the blood of some invertebrates.

Every O_2 molecule inhaled into the lung passes the state of physical solubility after it has diffused through the venous membrane and comes into contact with the transportation fluid (hemolymph). Only in this solute phase the oxygen is able to reach its reaction partner hemocyanin and to form a chemical bond with it depending on the remaining capacity of the protein. In order to do so the O_2 molecule leaves the state of physical solubility. After the oxygen has been transported to the tissue the molecule dissociates from this bond again and reenters the phase of physical solubility to perform the exchange between blood and tissue [Larsen and Ziegenfuß, 2009].

The absorption in the chemical bond takes place simultaneously with the transport in the solute phase making the hemocyanin act like a buffer. While this buffer is filled up additional oxygen can pass from the gaseous into the dissolved phase until both systems are saturated. However, the amount of oxygen that is transported by hemocyanin is much higher than the amount of dissolved O_2.

Following this introduction the physical principles and basic calculation

methods are presented that are used to obtain values for the concentration of oxygen in the vein and artery of *Xeropicta derbentina* as well as the heart beat frequency and the average thickness of venous membrane through which the diffusion takes place. This gives further insights into the structure of the venous system and reveals additional physiological parameters of *X. derbentina*. Finally, the results serve as boundary conditions for the diffusive transport of oxygen through the venous system as well as the distribution of oxygen concentration along the main vein and capillaries. The latter is achieved by an application of the Colburn analogy that is used to calculate oxygen concentrations based on local shear stress.

6.1 Henry's law

The solubility behavior of volatile substances is described by Henry's law. It states that an equilibrium exists between the concentration of a solute gas and the partial pressure of the gas above the liquid surface while volatiles are constantly exchanged between gaseous (subscript "gas") and the aqueous (subscript "aq") phase. For a constant temperature the solubility (i.e. the concentration c inside the solution) of a gas is, therefore, proportional to its partial pressure with the constant of proportionality $k_{\mathrm{H,cp}}$ $[\mathrm{mol} \cdot \mathrm{l}^{-1} \cdot \mathrm{atm}^{-1}]$ being the Henry constant specified for each liquid-gas combination:

$$c_{\mathrm{aq}} = k_{\mathrm{H,cp}} \cdot p_{\mathrm{gas}} \tag{6.1}$$

The Henry constant depends on the temperature resulting in a generally decreasing solubility for increasing temperatures. Henry's law can be written differently corresponding to the conversion that is needed and, therefore, different constants for the equation exist. The subscript "cp" in Equation 6.1 indicates the connection between the value of the concentration c in the solution and the value of the partial pressure p of the gas. Henry's law can also be written in order to link the value of concentration on both sides. In this case the constant holds the index "cc" indicating that it represents a value for the conversion between two concentrations. A comprehensive list of Henry's law constants and the corresponding conversion factors can be found in Sander [1999] and Sander [2015].

Throughout the further work a quantity with reference to a certain volume, for example $[\mathrm{mol} \cdot \mathrm{m}^{-3}]$ or $[\mathrm{ml} \cdot 100\,\mathrm{ml}^{-1}]$, will be called a concentration and denoted with the symbol c.

6.2 Oxygen concentration in vein and artery

Oxygen partial pressures for vein and artery have been investigated for the pulmonate land snail *Helix pomatia* by Mikkelsen and Weber [1992]. Unfortunately, for *X. derbentina* no values are reported. However, as the respiration apparatus of both species is basically built in a similar way the values of *H. pomatia* may very well be equal to the oxygen pressures in *X. derbentina*'s vein and artery. Therefore, the following calculations are based upon the assumption of this similarity. Additionally, it will be assumed that the physical properties of the snail's blood are very similar to water, and, therefore, values for the Henry constants $k_{\mathrm{H,cp}}$ and $k_{\mathrm{H,cc}}$ will be used for the solubility of oxygen in water found at Sander [2015].

Mikkelsen and Weber [1992] report values for *H. pomatia* of $p_{O_2} = 2399.8\,\mathrm{Pa}$ and $p_{O_2} = 12\,132.3\,\mathrm{Pa}$ for venous and arterial blood, respectively. With Henry's law an oxygen concentration in the vein can be calculated that is based on the physical solubility of oxygen in the snail's blood.[1] Therefore, the constant $k_{\mathrm{H,cp}} = 1.3 \times 10^{-3}\,\mathrm{mol} \cdot \mathrm{l}^{-1} \cdot \mathrm{atm}^{-1}$ is used to convert the partial pressures into molar concentrations. Applying Equation 6.1 and multiplying with the molar mass of oxygen $M_{O_2} = 31.9988\,\mathrm{g} \cdot \mathrm{mol}^{-1}$ divided by the density of gaseous oxygen at 25 °C $\rho_{O_2} = 1.308\,\mathrm{g} \cdot \mathrm{l}^{-1}$ one obtains:

$$\begin{aligned} c_{O_2,\mathrm{vein,phys.sol.}} &= k_{\mathrm{H,cp}} \cdot p_{O_2} \cdot \frac{M_{O_2}}{\rho_{O_2}} \\ &= 1.3 \times 10^{-3}\,\mathrm{mol} \cdot \mathrm{l}^{-1} \cdot \mathrm{atm}^{-1} \cdot 2399.8\,\mathrm{Pa} \cdot \frac{31.998\,\mathrm{g} \cdot \mathrm{mol}^{-1}}{1.308\,\mathrm{g} \cdot \mathrm{l}^{-1}} \\ &= 0.0753\,\mathrm{ml} \cdot 100\,\mathrm{ml}^{-1} \end{aligned} \tag{6.2}$$

[1] A blood gas analysis carried out on human beings primarily measures the partial pressure of oxygen that is due solely to the physical solubility of oxygen in the blood. However, the additional acquisition of oxygen saturation and hemoglobin concentration facilitates the determination of the share of hemoglobin/hemocyanin concentration in the total oxygen concentration.

The resulting concentration is interpreted as the volume of dissolved oxygen per 100 ml of blood/water. Analogously, a theoretical concentration in the artery representing the maximum uptake of oxygen by physical solubility alone can be calculated using the oxygen partial pressure given for the artery:

$$c_{O_2,\text{artery,phys.sol.}} = 0.381\,\text{ml} \cdot 100\,\text{ml}^{-1} \tag{6.3}$$

The theoretical concentration in the artery resulting from the presence of the complete 20.95 % of the ambient oxygen concentration in the snail's lung reveals:

$$\begin{aligned} c_{O_2,\text{artery,ambient,phys.sol.}} &= k_{\text{H,cc}} \cdot c_{O_2,\text{ambient}} \\ &= 3.18 \times 10^{-2}\,\text{ml} \cdot 100\,\text{ml}^{-1} \cdot 0.2095 \\ &= 0.666\,\text{ml} \cdot 100\,\text{ml}^{-1} \end{aligned} \tag{6.4}$$

This result is in good accordance with the value of $0.652\,\text{ml} \cdot 100\,\text{ml}^{-1}$ for the solubility of ambient O_2 (20.95 %) in water at 25 °C given in Lide [2004][2] and confirms the chosen values of $k_{\text{H,cp}}$ and $k_{\text{H,cc}}$. Comparing the results of Equation 6.3 and Equation 6.4 shows that the maximal physical solubility cannot be reached with an oxygen pressure of 12 132.3 Pa resulting in a value of approximately half of the theoretically possible amount. This is most probably due to a reduced oxygen pressure compared to ambient conditions in *X. derbentina*'s lung that effectively lowers the dissolved oxygen in the artery. According to Krämer [2005], who describes this effect on a human lung, the reasons for this decreased oxygen pressure abutting in the snail's lung are mainly the humidification and the addition of CO_2 as the breathing air is inhaled into the lung.

However, as discussed above, this concentration only results from the physical solubility of the oxygen and the chemical bonding to hemocyanin has so far been ignored. It is well known that due to this bonding the resulting concentration is substantially raised. If humans were purely dependent on the solubility of oxygen in water our heart would need to beat 1200 times min^{-1} requiring a blood flow of $85\,\text{l} \cdot \text{min}^{-1}$ [Müller, 2001]. Markl [1996] states that

[2]The values in Lide [2004] are given as mole fraction solubilities for a pressure of 1 atm above the solution and, therefore, need to be multiplied with the molar mass fraction $M_{O_2}/M_{\text{solvent}} = M_{O_2}/M_{H_2O}$ and the fraction of ambient oxygen concentration 20.95/100 to obtain the presented value.

hemocyanin raises the concentration of solute oxygen by a factor of $\Phi = 2 - 4$ due to chemical bonding. A final result for the concentration in the artery of *X. derbentina* can be obtained that is based on the previously calculated physical solubility (Equation 6.3) and the additional raise by hemocyanin:

$$c_{O_2,\text{artery}} = \Phi \cdot 0.381\,\text{ml} \cdot 100\,\text{ml}^{-1} \tag{6.5}$$

This yields a minimum and maximum value for the concentration in the artery $c_{O_2,\text{artery,min}}$ and $c_{O_2,\text{artery,max}}$ by evaluating Equation 6.5 at the minimum and maximum value of the factor Φ:

$$c_{O_2,\text{artery,min}} = 0.762\,\text{ml} \cdot 100\,\text{ml}^{-1} \tag{6.6}$$

$$c_{O_2,\text{artery,max}} = 1.523\,\text{ml} \cdot 100\,\text{ml}^{-1} \tag{6.7}$$

Assuming that the hemocyanin of the venous blood has completely dissociated its oxygen molecules and the remaining concentration in the vein is completely due to the physical solubility, the previously calculated value of $c_{O_2,\text{vein}} = 0.0753\,\text{ml} \cdot 100\,\text{ml}^{-1}$ may hold true for a final value. Otherwise the minimum and maximum values $c_{O_2,\text{vein,min}}$ and $c_{O_2,\text{vein,max}}$ result in:

$$c_{O_2,\text{vein,min}} = 2 \cdot 0.0753\,\text{ml} \cdot 100\,\text{ml}^{-1} = 0.151\,\text{ml} \cdot 100\,\text{ml}^{-1} \tag{6.8}$$

$$c_{O_2,\text{vein,max}} = 4 \cdot 0.0753\,\text{ml} \cdot 100\,\text{ml}^{-1} = 0.301\,\text{ml} \cdot 100\,\text{ml}^{-1} \tag{6.9}$$

The amount of oxygen concentration that is absorbed in the snail's lung is the difference between arterial and venous concentration. Taking the minimum and maximum values of the arterial concentration into account and assuming no complete hemocyanin dissociation of the venous blood the minimum ($\Phi = 2$) and maximum ($\Phi = 4$) values for the absorbed concentration result in:

$$c_{\text{absorbed,min}} = c_{O_2,\text{artery,min}} - c_{O_2,\text{vein,min}} = 0.611\,\text{ml} \cdot 100\,\text{ml}^{-1} \tag{6.10}$$

$$c_{\text{absorbed,max}} = c_{O_2,\text{artery,max}} - c_{O_2,\text{vein,max}} = 1.222\,\text{ml} \cdot 100\,\text{ml}^{-1} \tag{6.11}$$

6.3 Heartbeat frequency

The heartbeat frequency f and the resulting transported volume flow of blood are closely connected to the amount of consumed oxygen. The amount of consumed oxygen is exactly the amount that is absorbed by the blood and transported to the organs. Therefore, the amount of absorbed oxygen per volume of blood can also be written as:

$$c_{\text{absorbed}} = \frac{\dot{V}_{\text{consumed } O_2}}{\dot{V}_{\text{blood flow}}} \tag{6.12}$$

Based on the previous NMR measurements of *X. derbentina* and the subsequent segmentation of specific organs (compare Chapter 4) the inner geometrical volume of the heart is known to be $V_{\text{heart}} = 8.5\,\text{mm}^3$. Furthermore the volume of blood flow per second follows from the size of the corresponding ventricle (heart chamber) that fills up and empties again with each heartbeat and thereby defines the stroke volume. According to Müller [2001] the size of a human ventricle is about 35 % of the size of the complete heart. Unlike the human heart, which provides a systemic circulation and a pulmonary circulation with two auricles (atriums) and ventricles, most snail species possess a bilocular heart consisting of only a single auricle and a single ventricle that are arranged in a linear sequence [Hill and Welsh, 2013, Jones, 1971, Saleuddin and Wilbur, 2012]. Due to this less complex arrangement of the molluscan heart the size of one ventricle is larger than the aforementioned fraction for human beings. To account for the incomplete emptying of the ventricle during a systole DeFur and Mangum [1979] used a conservative value of 50 % of the heart volume in order to obtain the stroke volume for *Busycon*. Depledge and Phillips [1986] used a less conservative value of 70 %.[3] The uncertainty involved in the segmentation of *X. derbentina*'s heart in the corresponding periphery results in an underestimated value of the heart volume so that a value of 50 % of the heart volume may very well represent the volume of the ventricle including an incomplete emptying of it. This assumption leads to the volume of one ventricle of about $4.25 \times 10^{-6}\,\text{l}$ and, therefore, the volume flow of blood results in:

$$\dot{V}_{\text{blood flow}} = V_{\text{ventricle}} \cdot f = 4.25 \times 10^{-6}\,\text{l} \cdot f \tag{6.13}$$

[3] The heart volume defined by the authors equals the inner volume of the ventricle.

With the calculated range for the absorbed amount of oxygen c_{absorbed} (Equation 6.10 and Equation 6.11) and the oxygen consumption $\dot{V}_{\text{consumed } O_2} = 1.395 \times 10^{-7}\,\text{l} \cdot \text{min}^{-1}$ at 25 °C (compare Chapter 2) the resulting heartbeat frequency range is:

$$f = 2.7 - 5.4\,\text{min}^{-1} \tag{6.14}$$

for "inactive" specimens of 0.9–0.95 cm diameter at 25 °C ambient temperature. Schwartzkopff [1954] reported values for the heartbeat frequency of *H. Pomatia* in the range of $f = 23.7 - 30\,\text{min}^{-1}$ measured in an artificial circulatory.[4] However, as these values represent the maximum frequency corresponding to an "active" state of the animal the range calculated above is very reasonable for "inactive" specimens of *X. derbentina*.

6.4 Amount of active diffusive surface

The diffusion flux j is defined as the amount of a substance passing through the cross section A per unit time t and, thus, has the units of $[\text{mol} \cdot \text{m}^{-2} \cdot \text{s}^{-1}]$. In our problem it presents a connection between the oxygen consumption of *X. derbentina* and the diffusive surface A, provided by its vein system, over which the diffusion process takes place. The diffusion flux can be calculated by the following equation:

$$j = \frac{\dot{n}}{A} \tag{6.15}$$

Additionally, Fick's first law of diffusion states that the diffusion flux j is proportional to the negative local concentration gradient. For a one-dimensional diffusion process this results into:

$$j = -D \cdot \frac{\partial c}{\partial x} \tag{6.16}$$

with D $[\text{m}^2 \cdot \text{s}^{-1}]$ being the diffusion coefficient and c $[\text{mol} \cdot \text{m}^{-3}]$ being the molar concentration.

The partitioned vein system extracted from the NMR measurements (Figure 4.7) is rather coarse due to the limited resolution of the NMR experiment and the very small dimension of the capillaries but it still provides a reasonable

[4] The author dissected the heart of shell-free live animals and connected their artery and vein to a conduit system. Pressure vessels facilitated the regulation of venous and arterial blood supply to adjust the desired pressure conditions.

starting point for a computer aided optimization. This was realized with the CAD tool CREO Parametric 2.0 (PTC, Needham, MA, U.S.A) by constructing a set of closed surfaces of the vein system that consists of the main vein and the individual capillaries that guide the hemolymph towards the former which subsequently empties into the snail's heart. A mean diameter of all constructed capillaries and of the main vein was calculated and used as a surrogate model with constant diameters at all sections. The final model consists of 37 capillaries with a diameter of 0.15 mm and the main vein with a diameter of 0.35 mm and is presented in Figure 6.1. The blood flow in Figure 6.1 is from the lower left to the upper right of the picture where the heart of *X. derbentina* is located. At first always two opposing capillaries where created. Based on the NMR data this duality is interrupted further downstream of the main vein which is most probably due to the asymmetrical structure of the snail.

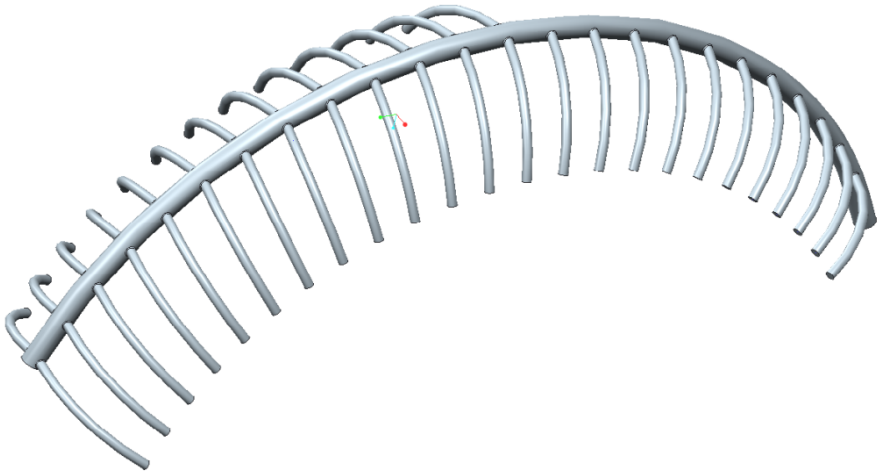

Figure 6.1: Surrogate model of *X. derbentina*'s vein system

By writing Fick's first law as a difference equation, setting $\Delta x = d$, and combining it with Equation 6.15 on can calculate the active diffusive surface A. In order to do so the distance d over which diffusion takes place has to be known. For the present problem this distance is the thickness of the capillaries and the main vein. These values were measured graphically in Figure 6.2 using an image from a dissection of *X. derbentina*'s lung that was achieved by

removing the first whorls of the shell from the snail. The dissected snail was then placed above a squared paper with 1×1 mm unit in order to calculate a scale between measured value and real value (compare Figure 6.2). The thickness of a capillary wall (membrane) results in approximately 0.06 mm. The membrane thickness of the main vein was found to be approximately twice as thick with a value of 0.12 mm. The values of capillary and main vein diameter used in the surrogate model above can also be verified by the graphical measurement, which yields approximately 0.1–0.15 mm and 0.3–0.38 mm for capillary and main vein diameter, respectively.

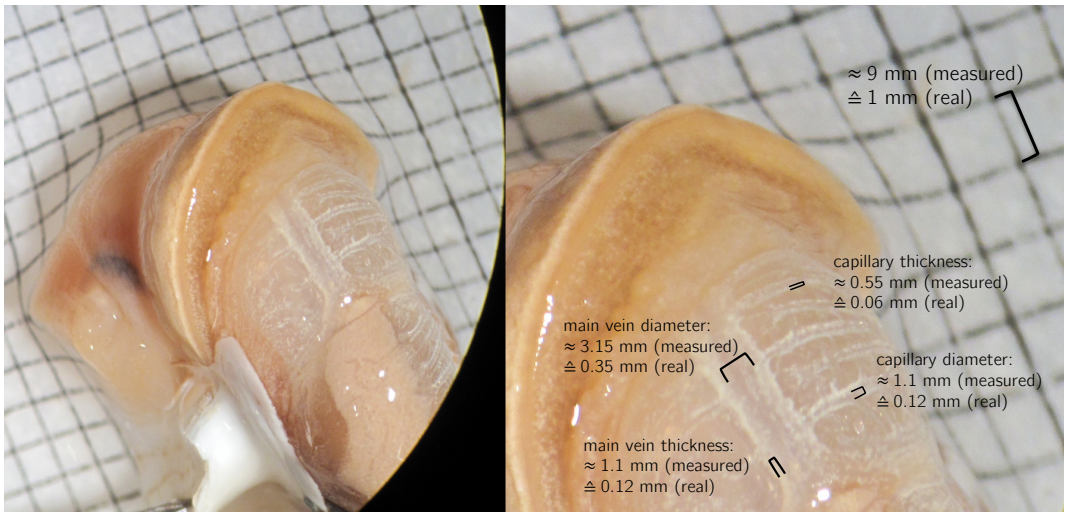

Figure 6.2: Outer view of the dissected lung and measurement of the membrane thicknesses and diameters

Murray's law states that the cube of the radius of the parental vessel equals the sum of the cubes of the radii of the daughter vessels [Murray, 1926]. In order to satisfy this law the capillaries would need to have an average radius of 0.11 mm, which is in close accordance to the value of 0.15 mm. Although the graphically measured values of the diameters differ slightly from the ones chosen in the surrogate model the preparation of the original NMR data has shown that the selected diameters very well represent the mean diameters inside *X. derbentina*'s vein system especially when considering that main vein and capillaries may form irregularly protruded shapes towards the inner lung surface that are not visible from the outer view in Figure 6.2.

From Figure 6.2 it can be seen that capillaries and main vein are merged with the inner surface of the lung resulting in approximately half-cylindrical shapes of capillaries and main vein (compare Figure 6.3). By exemplarily choosing a perimeter fraction of 0.5 for capillaries and main vein that actually participates in the diffusive exchange of oxygen between the lung and the blood and using the lengths gathered from the surrogate model from Figure 6.1 a resulting active diffusive surface of 53.9 mm^2 can be computed from the CAD model in CREO Parametric 2.0.

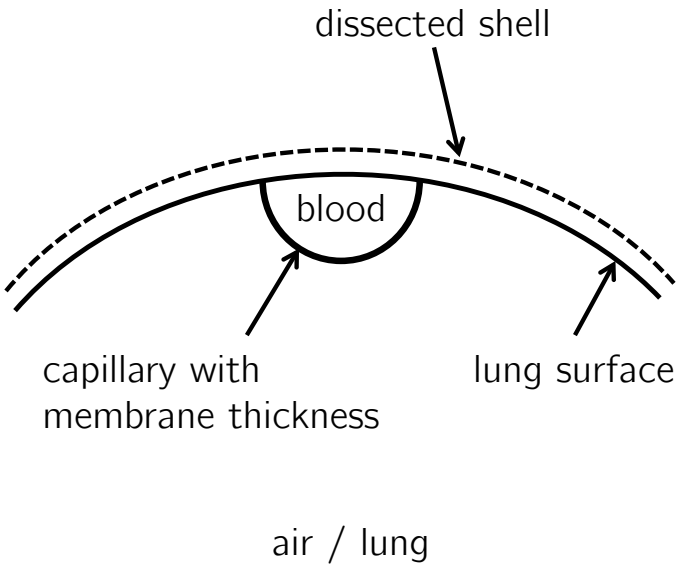

Figure 6.3: Geometrical shape of capillaries

Considering the reported values of oxygen partial pressure $p_{O_2} = 2399.8\,\mathrm{Pa}$ and $p_{O_2} = 12\,132.3\,\mathrm{Pa}$ for venous and arterial blood [Mikkelsen and Weber, 1992] and the measured oxygen consumption of $1.04 \times 10^{-10}\,\mathrm{mol} \cdot \mathrm{s}^{-1}$ for medium sized specimens at 25 °C (compare Chapter 2) a diffusive surface is calculated using Henry's law with the constant $k_{\mathrm{H,cp}} = 1.3 \times 10^{-3}\,\mathrm{mol} \cdot \mathrm{l}^{-1} \cdot \mathrm{atm}^{-1}$

and the definition of the diffusion flux j from Equation 6.15 and 6.16:

$$\begin{aligned} A &= \frac{\dot{n}}{j} = \frac{\dot{n} \cdot \Delta x}{D \cdot \Delta c} = \frac{\dot{n} \cdot d_{\text{membrane,av}}}{D \cdot k_{\text{H,cp}} \cdot \Delta p} \\ &= \frac{1.04 \times 10^{-10}\,\text{mol} \cdot \text{s}^{-1} \cdot 0.078 \times 10^{-3}\,\text{m}}{2.3 \times 10^{-9}\,\text{m}^2 \cdot \text{s}^{-1} \cdot 1.3 \times 10^{-3}\,\text{mol} \cdot \text{l}^{-1} \cdot \text{atm}^{-1} \cdot (12132.3 - 7266)\text{Pa}} \\ &= 56.2\,\text{mm}^2 \end{aligned} \tag{6.17}$$

In the calculation of Equation 6.17 the following assumptions were made:

- The diffusive length is the mean thickness $d_{\text{membrane,av}}$ of capillaries and main vein weighted by their corresponding surface area to account for the presence of both diffusive lengths.
- The venous oxygen partial pressure is the mean value of the ones of artery and vein. The reason for this is the continually increasing p_{O_2} in the snail's vein that merely has a value of $p_{O_2} = 2399.8\,\text{Pa}$ at the very beginning of the vein.
- The diffusion coefficient D is the one for diffusion of O_2 in pulmonary tissue that is reported by Grote [1967] to be $D = 2.3 \times 10^{-9}\,\text{m}^2 \cdot \text{s}^{-1}$.

The active diffusive surface resulting from geometrical data ($53.9\,\text{mm}^2$) is found to be in good agreement with the one obtained by Fick's law ($56.2\,\text{mm}^2$)that is based on the measured value for oxygen consumption and the oxygen partial pressures reported in the literature as well as on the assumptions stated above.

For the sake of completeness and as an additional comparison the complete dissection of *X. derbentina*'s lung allows a graphical measurement of its surface size and is presented in Figure 6.4. Therefore, the lung was again placed on top of a squared paper with $1 \times 1\,\text{mm}$ unit. This measurement reveals a total surface size of approximately 50–55 mm^2.

Due to the relatively large thickness of capillary and main vein membrane the active diffusive surface increases so that the resulting size approximates the total surface size of the animal's lung. This result is plausible and can easily be visualized by the unrolling of the half cylindrical vein surfaces in Figure 6.2 that span a significantly increased surface. Therefore, the value found by this procedure complements the previous results and confirms the correctness of the surrogate model and the calculation based on Fick's law.

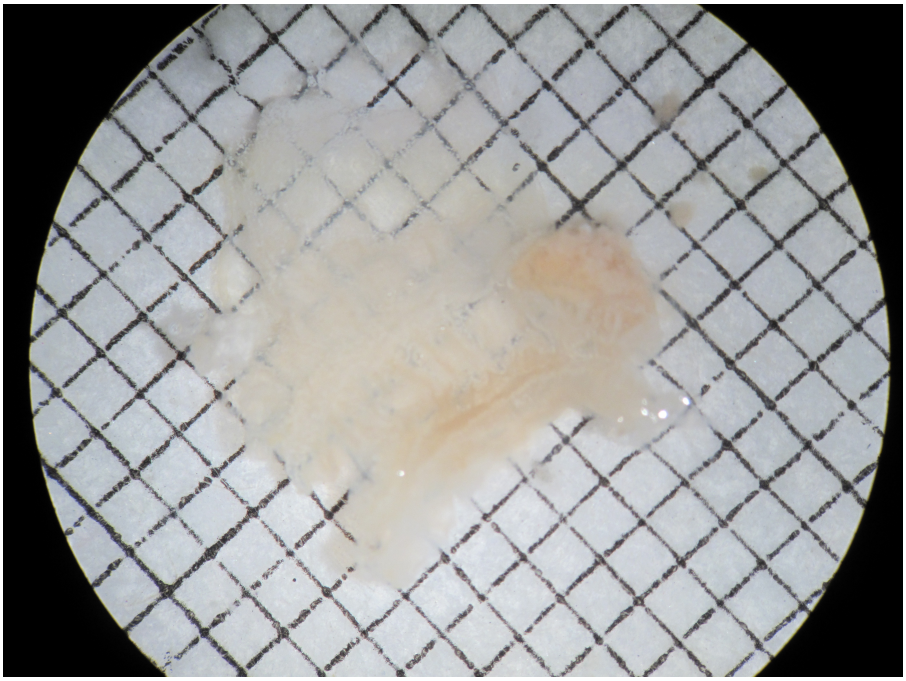

Figure 6.4: Dissection of *X. derbentina*'s lung surface

6.5 Derivation of dimensionless numbers

In the following sections 6.6 and 6.7 much use of dimensionless quantities is made. In order to develop a better understanding of their physical meaning, the derivation of some exemplary numbers is presented in this section.

Dimensionless numbers are obtained by non-dimensionalizing the governing equations of heat, mass and momentum transfer. Additionally, for some special cases, non-dimensionalizing the boundary conditions of these partial differential equations reveal dimensionless numbers as well. The numbers derived this way provide a physical insight into the importance of various terms in the system of governing equations. By a dimensionless approach a problem is generalized in such a way that a dimensionless solution can be used to describe many dimensional solutions. However, the dimensionless solution depends on a set of dimensionless parameters. These dimensionless numbers provide information about how a physical system behaves. Moreover, many solution techniques require a non-dimensional problem in order to be solved effectively.

6.5.1 The Reynolds number *Re*

The Reynolds number *Re* is a fundamental number that helps to characterize the state of a flow and is very often used to predict the onset of turbulence in a system. By the use of this number the geometry of model test geometries can be scaled in a way that the characteristic state of the flow matches the one of the real geometry that is investigated. It can be obtained by non-dimenzionalizing the momentum equation in the Navier-Stokes equations. The momentum equation for an incompressible flow is:

$$\rho\left(\frac{\partial\vec{v}}{\partial t}+(\vec{v}\cdot\nabla)\vec{v}\right)=-\nabla p+\mu\Delta\vec{v}+\vec{f} \tag{6.18}$$

with the dynamic viscosity μ. By just taking the x-direction into account and assuming a two-dimensional flow (x and y direction with velocity components u and v) without any volume forces $\vec{f}$ Equation 6.18 simplifies to:

$$\frac{\partial u}{\partial t}+u\frac{\partial u}{\partial x}+v\frac{\partial u}{\partial y}=-\frac{1}{\rho}\frac{\partial p}{\partial x}+\nu\left(\frac{\partial^2 u}{\partial x^2}+\frac{\partial^2 u}{\partial y^2}\right) \tag{6.19}$$

with the kinematic viscosity $\nu=\mu/\rho$. By the introduction of the dimensionless variables

$$\begin{aligned} t^*&=t\frac{u_\infty}{L} \qquad x^*=\frac{x}{L} \qquad y^*=\frac{y}{L} \qquad u^*=\frac{u}{u_\infty}\\ v^*&=\frac{v}{u_\infty} \qquad \rho^*=\frac{\rho}{\rho_\infty} \qquad p^*=\frac{p}{\rho_\infty\cdot u_\infty^2} \end{aligned}$$

with L being a characteristic length, the subscript ∞ denoting conditions in the undisturbed upstream flow, and inserting into Equation 6.19 one obtains:

$$\begin{aligned} &\frac{\partial u^* u_\infty}{\partial t^*\frac{L}{u_\infty}}+u^* u_\infty\frac{\partial u^* u_\infty}{\partial x^* L}+v^* u_\infty\frac{\partial u^* u_\infty}{\partial y^* L}=\\ &-\frac{1}{\rho^*\rho_\infty}\frac{\partial p^*\rho_\infty u_\infty^2}{\partial x^* L}+\nu\left(\frac{\partial^2 u^* u_\infty}{\partial x^{*2}L^2}+\frac{\partial^2 u^* u_\infty}{\partial y^{*2}L^2}\right) \end{aligned} \tag{6.20}$$

After collecting terms and dividing by u_∞^2/L Equation 6.20 can be written as:

$$\frac{\partial u^*}{\partial t^*}+u^*\frac{\partial u^*}{\partial x^*}+v^*\frac{\partial u^*}{\partial y^*}=-\frac{1}{\rho^*}\frac{\partial p^*}{\partial x^*}+\frac{\nu}{L\cdot u_\infty}\left(\frac{\partial^2 u^*}{\partial x^{*2}}+\frac{\partial^2 u^*}{\partial y^{*2}}\right) \tag{6.21}$$

The expression $\nu/(L\cdot u_\infty)$ in front of the viscous term is known as the inverse of the Reynolds number *Re*. Examing Equation 6.21 it becomes clear that the Reynolds number defines the influence of the viscous term. As $Re\rightarrow 0$

the magnitude of the viscous forces increases. As $Re \to \infty$ the inertial terms on the left side of Equation 6.21 dominate the flow. Therefore, its physical interpretation is the ratio of inertial to viscous forces [Jischa, 1982].

6.5.2 The Prandtl number Pr

The Prandtl number is only based on the thermodynamic material properties and generally depends on the temperature T and the pressure p, in reality it mostly depends on the temperature T. The Prandtl number describes the ratio of momentum diffusivity to thermal diffusivity [Jischa, 1982]. It can also be interpreted as the ratio of the thicknesses of the laminar flow boundary layer to the temperature boundary layer. Gases have a Prandtl number Pr of about 0.7, whereas it varies over a larger range for liquids [Böckh and Wetzel, 2014]. The Prandtl number can be obtained by non-dimensionalizing the heat conduction equation that is based on the energy equation of the Navier-Stokes equations. The energy equation for the case of a stationary fluid ($\vec{v} = 0$) without any volumetric heat addition is:

$$\rho \frac{\partial e}{\partial t} = \frac{\partial}{\partial x}\left(\lambda \frac{\partial T}{\partial x}\right) + \frac{\partial}{\partial y}\left(\lambda \frac{\partial T}{\partial y}\right) + \frac{\partial}{\partial z}\left(\lambda \frac{\partial T}{\partial z}\right) \tag{6.22}$$

with λ as the thermal conductivity. Inserting the state relation for the internal energy $e = c_v \cdot T$, with c_v as the specific heat capacity, and assuming λ is constant Equation 6.22 is written as:

$$\frac{\partial T}{\partial t} = a\left(\frac{\partial^2 T}{\partial x^2} + \frac{\partial^2 T}{\partial y^2} + \frac{\partial^2 T}{\partial z^2}\right) \tag{6.23}$$

The expression $a = \lambda/(\rho \cdot c_v)$ is called the thermal diffusivity and indicates the fluid's ability to "conduct energy due to thermal conduction compared to its ability to retain this energy, i.e. its capacity to absorb heat" [Anderson, 2012]. The higher a is the faster a temperature change will spread and propagate inside a fluid/liquid. By inserting the dimensionless variables from Chapter 6.5.1 and additionally introducing the following variables

$$z^* = \frac{z}{L} \qquad T^* = \frac{T}{\Delta T_0}$$

with ΔT_0 being a constant temperature difference (e.g. difference between free stream temperature and wall temperature) Equation 6.23 results into:

$$\frac{\partial T^* \Delta T_0}{\partial t^* \frac{L}{u_\infty}} = a\left(\frac{\partial^2 T^* \Delta T_0}{\partial x^{*2} L^2} + \frac{\partial^2 T^* \Delta T_0}{\partial y^{*2} L^2} + \frac{\partial^2 T^* \Delta T_0}{\partial z^{*2} L^2}\right) \tag{6.24}$$

Collecting terms again and dividing by $u_\infty \cdot \Delta T_0/L$ yields the dimensionless heat conduction equation:

$$\frac{\partial T^*}{\partial t^*} = \frac{a}{u_\infty \cdot L}\left(\frac{\partial^2 T^*}{\partial x^{*2}} + \frac{\partial^2 T^*}{\partial y^{*2}} + \frac{\partial^2 T^*}{\partial z^{*2}}\right) \tag{6.25}$$

The term in front of the right side must be dimensionless by definition and can be written as:

$$\frac{a}{u_\infty \cdot L} = \frac{1}{Re} \cdot \frac{a}{\nu} \tag{6.26}$$

The remaining expression a/ν is the inverse of the Prandtl number Pr. Therefore, its physical interpretation is the ratio of diffusion by momentum, expressed by the kinematic viscosity ν, to the thermal diffusion, expressed by a, i.e. the capacity to absorb heat.

6.5.3 The Nusselt number Nu

The Nusselt number Nu is a dimensionless number that describes the convective heat transfer between a surface and a moving fluid. Convective heat transfer is, in contrast to conduction, linked to the motion of particles that carry energy and is almost always present in fluids. In order to be solved the heat conduction equation (Equation 6.23) requires a starting condition ($t = 0$) and boundary conditions at the outside (walls) of the body of investigation. In general three different types of boundary conditions are possible that differ in whether they directly specify a value for the temperature or the derivative of the temperature:

1. Dirichlet: T_0 specified
2. Neumann: $\frac{\partial T}{\partial x}\Big|_w$, i.e. heat flux $q_0 = -\lambda \frac{\partial T}{\partial x}\Big|_w$ (Fourier) specified
3. Cauchy: convective heat transfer, i.e. $-\lambda \frac{\partial T}{\partial x}\Big|_w = \alpha \cdot (T_\infty - T_w)$

The third boundary condition is also called a mixed boundary condition as it specifies a mixture of T and its spatial derivative at the position of the wall (denoted by the subscript w). It results from the balance of heat flux at this position, which is illustrated in Figure 6.5. It shows the course of temperature inside a solid body (conduction) with a convective heat transfer at the left boundary where a fluid flow is present. Due to the no-slip condition the direct

vicinity of the wall is also characterized by conduction, which will continuously pass into a non-linear course described by the heat transfer coefficient α.

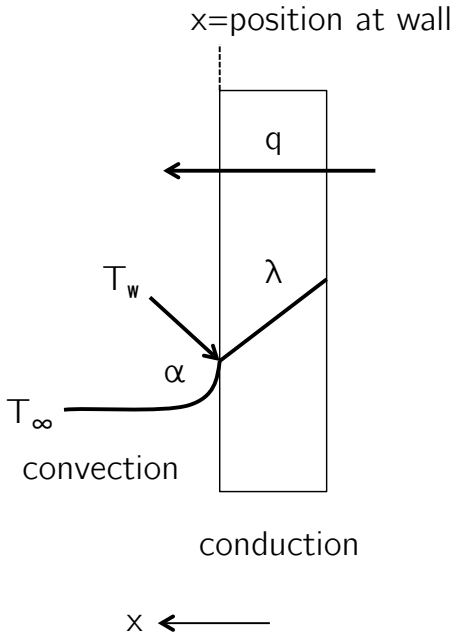

Figure 6.5: Convective heat transfer

The right side of the third boundary condition is known as Newton's law of cooling, which states that the heat flux between a body and its surrounding (denoted by the subscript ∞) is proportional to the temperature difference between them. The Nusselt number can finally be obtained by non-dimensionalizing the third boundary condition. Inserting the dimensionless variable x^* and introducing a dimensionless temperature difference

$$T^* = \frac{T - T_\infty}{T_w - T_\infty}$$

the boundary condition can be written as:

$$\begin{aligned} -\lambda \cdot \frac{\partial T^* \cdot (T_w - T_\infty) + T_\infty}{\partial x^* \cdot L} &= \alpha \cdot (T_w - T_\infty) \\ -\lambda \cdot \left(\frac{\partial T_\infty}{\partial x^* \cdot L} + \frac{\partial T^* \cdot (T_w - T_\infty)}{\partial x^* \cdot L} \right) &= \alpha \cdot (T_w - T_\infty) \\ -\frac{\partial T^*}{\partial x^*} &= \frac{\alpha \cdot L}{\lambda} = Nu \end{aligned} \tag{6.27}$$

Equation 6.27 shows that the Nusselt number Nu is the dimensionless temperature gradient at the wall. Its physical interpretation is the ratio of convective

heat transfer to heat conduction through a stationary fluid. The Nusselt number expresses by which ratio the convective heat transfer is higher compared to pure conduction. It is also called the dimensionless heat transfer coefficient.

6.6 Analogy of heat, mass and momentum transfer

The exchange of heat, mass and momentum are transport phenomena that share an identical mathematical foundation. As neither energy, mass nor momentum can be destroyed all of these quantities must be conserved. Mathematically this is achieved by the conservation laws for the respective quantity. Furthermore heat, mass and momentum transfer are physical quantities that are specific to a material, e.g. the amount of energy passing through a certain material, or the momentum of a solid body with mass m and velocity $\vec{v}$. The response of this specific material to an external field/force is described by constitutive equations. The comparison of one-dimensional conservation laws and constitutive equations of these transport phenomena reveals their physical analogy to each other as it is shown in the following Table 6.1.

Table 6.1: Conservation laws and constitutive equations of transport phenomena

transport	conservation law	constitutive equation
heat	$\frac{\partial T}{\partial t} = a \cdot \frac{\partial^2 T}{\partial x^2}$	$q = -a \cdot \frac{\partial \rho c_v T}{\partial x} = -\lambda \cdot \frac{\partial T}{\partial x}$
mass	$\frac{\partial c}{\partial t} = D \cdot \frac{\partial^2 c}{\partial x^2}$	$j = -D \cdot \frac{\partial c}{\partial x}$
momentum	$\frac{\partial u}{\partial t} + u \cdot \frac{\partial u}{\partial x} = -\frac{1}{\rho} \cdot \frac{\partial p}{\partial x} + \nu \cdot \frac{\partial^2 u}{\partial x^2}$	$\tau_{yx} = -\nu \cdot \frac{\partial \rho u}{\partial y}$

The conservation law of momentum and energy (the heat conduction equation) have been introduced before. The conservation law of mass transfer is mathematically identical to the one for energy conservation and is known as Fick's 2. law.

The left side of all constitutive equations contains a flux, i.e. the quantity that is transported per unit time per unit area. These are the heat flux q [$\mathrm{J \cdot m^{-2} \cdot s^{-1}}$=$\mathrm{W \cdot m^{-2}}$], the diffusion flux j [$\mathrm{mol \cdot m^{-2} \cdot s^{-1}}$], and the momentum flux τ_{yx} [momentum $\cdot\ \mathrm{m^{-2} \cdot s^{-1}}$], for heat, mass, and momentum transfer, respectively. The right side always contains a constant factor times a concentration gradient. The constants are called transport properties, or diffusivities, and are the thermal diffusivity a, the molecular diffusivity (diffusion coefficient) D, and the momentum diffusivity (kinematic viscosity) ν. These are all in the units of [$\mathrm{m^2 \cdot s^{-1}}$]. The concentrations are $\rho c_v T$ [$\mathrm{J \cdot m^{-3}}$] (similar to an energy density), the molar concentration c [$\mathrm{mol \cdot m^{-3}}$], and the momentum concentration ρu [momentum $\cdot\ \mathrm{m^{-3}}$].

The constitutive equation for heat transfer is known as Fourier's law of heat conduction, the one for mass transfer is known as Fick's 1. law of diffusion. The one for momentum transfer is based on Newton, who stated that the flux of x-directed momentum towards the y direction, the shear stress τ_{yx}, is proportional to the gradient of the momentum concentration ρu in the y-direction. The gradient in y direction necessary for this momentum flux can either stem from a fluid's no-slip condition at a wall or from random diffusion of molecules.

The following Table 6.2 summarizes concentrations, fluxes and diffusivities for heat, mass and momentum transfer:

Table 6.2: Concentration, flux and diffusivity for transport phenomena

	heat	mass	momentum
concentration	$\rho c_v T$	c	ρu
flux	q	j	τ
diffusivity	a	D	ν

The present section illustrates that the basic mechanisms of heat, mass and momentum transfer are essentially the same. Under certain conditions this mathematical and physical similarity facilitates the use of a direct relation between heat transfer coefficient, diffusion coefficient and the friction factor (the dimensionless representation of the momentum flux). In the following chapter the Reynolds analogy and the Colburn analogy are presented which are based upon the similarities between heat and momentum transfer. The transition to the analogy between mass and momentum transfer is then easily achieved by the interchangeability of the dimensionless number that is characteristic for each transport phenomena.

6.7 Analysis of wall shear stress and the Colburn analogy

In the present chapter the results of the oxygen consumption measurements are compared with a pragmatic model. In this model the capillaries and main vein are divided into segments of defined length and the spatial variation of concentration within both systems is calculated by successively passing the values for each segment to the next one. This is first done for all isolated capillaries, which subsequently empty into and mix with the main vein at the corresponding downstream positions resulting in a final concentration that develops along the aorta towards the snail's heart. The necessary input parameters for this procedure only rely on a simple flow simulation through the venous system yielding the velocity and wall shear stress distribution along capillaries and main vein. The presented approach then utilizes an analogy between wall shear stress and mass transfer, which is known as the Colburn analogy [Incropera, 2007, Jischa, 1982, Subramanian, 2014]. In contrast to this, a complex CFD simulation that directly takes the diffusive processes of oxygen in water into account requires a much higher computational effort. Therefore, this method represents an elegant way to calculate the concentration distribution with only minimal costs of computation time. An evaluation of analytical solutions and correlations based on the Reynolds analogy (upon which the Colburn analogy is based) for heat transfer in turbulent tube flow is presented by Webb [1971]. Successful applications of the Colburn analogy

have been reported among others by Dalkilic et al. [2013] for the prediction of heat transfer coefficient of the cryogen R134a under a forced convection laminar condensation process. Astolfi-Filho et al. [2012] used the Colburn analogy to verify experimental data of friction factors and heat transfer coefficients of sugarcane juices in order to accurately design its industrial processing.

The Colburn analogy represents a modified and improved version of the very famous Reynolds analogy, that is used to predict the heat transfer from momentum transfer. It can be derived by examining the classical problem of convective heat transfer of laminar flow over a flat plate. By non-dimensionalizing the boundary layer conservation equations for momentum and energy it can be shown that for Prandtl number $Pr = 1$ both equations are identical. As the solutions for u^* and T^* are the same a relation between the friction coefficient c_f and the heat transfer coefficient α is expected. The friction coefficient is defined by:

$$\begin{aligned} \frac{c_f}{2} &= \frac{\tau_w}{\rho \cdot u_\infty^2} = \frac{\nu \frac{\partial u}{\partial y}}{u_\infty^2} \\ &= \frac{\nu \cdot \frac{\partial u^* \cdot u_\infty}{\partial y^* \cdot L}}{u_\infty^2} = \frac{\nu \cdot \frac{\partial u^*}{\partial y^*}}{u_\infty \cdot L} \\ &= \frac{\frac{\partial u^*}{\partial y^*}}{Re} \end{aligned} \tag{6.28}$$

with x in streamwise direction and y perpendicular to the flat plate. By using the definition of the Nusselt number Nu from Equation 6.27 and taking into account that

$$\frac{\partial T^*}{\partial y^*} = \frac{\partial u^*}{\partial y^*} \tag{6.29}$$

Equation 6.28 results into:

$$\frac{c_f}{2} = \frac{\frac{\partial u^*}{\partial y^*}}{Re} = \frac{\frac{\partial T^*}{\partial y^*}}{Re} = \frac{Nu}{Re} \tag{6.30}$$

Equation 6.30 is known as the Reynolds analogy that relates momentum flux with heat flux and is only valid for Prandtl number $Pr = 1$ and constant wall temperature T_w. The limitation of $Pr = 1$ of Equation 6.30 can be suppressed by modifying it with a proportionality of $Pr^{-1/3}$ to be valid for Prandtl numbers $Pr > 0.6$ [Jischa, 1982]. This yields the following relationship that is known as the Colburn analogy between momentum flux and heat flux:

$$\frac{c_f}{2} = \frac{Nu}{Re} \cdot Pr^{-1/3} = \frac{\tau_w}{\rho \cdot u_\infty^2} \tag{6.31}$$

For $Pr = 1$ the Colburn analogy merges into the Reynolds analogy.

In Chapter 6.6 the physical and mathematical similarities between heat and mass transfer were discussed. As both processes are described by a similar set of equations, it is now possible to transfer the depicted relationships onto the process of diffusion by replacing the thermal diffusivity a of the Prandtl number Pr by the diffusion coefficient D. As a result the Schmidt number Sc number is obtained that is the characteristic mass transfer analogue to the heat transfer. It describes the ratio of momentum transfer to diffusive mass transfer. The Schmidt number Sc can be derived by non-dimensionalizing the conservation equation for mass transfer (Table 6.1) and is defined as:

$$Sc = \frac{\nu}{D} \tag{6.32}$$

Schmidt number and Prandtl number do not contain any length scale and only depend upon the fluid and the fluid state. They are usually of the same order of magnitude.

Analogously to the definition of the heat flux from a wall to a fluid for convective heat transfer (compare Chapter 6.5.3)

$$q_w = \alpha \cdot \Delta T = -\lambda \cdot \frac{\partial T}{\partial y}\Big|_w \tag{6.33}$$

one can define a diffusion flux for mass transfer by

$$j_w = \beta \cdot \rho_w \cdot \Delta\omega = -\rho_w \cdot D \cdot \frac{\partial \omega}{\partial y}\Big|_w \tag{6.34}$$

with the mass transfer coefficient β and the concentration difference $\Delta\omega$ given as mass fractions. The diffusion flux defined in Equation 6.34 is basically the constitutive equation for mass transfer (Fick's 1. law of diffusion) that has been introduced earlier but written for mass fractions ω, i.e. with reference to mass instead of molar or volume concentrations c, i.e. with reference to volume. The mass fraction is defined as the mass ratio of one substance (here oxygen) to the total mass of the mixture. Despite the fact that its units do not really cancel it will be written dimensionlessly throughout the further work. As a consequence of choosing mass fractions the units of j_w are $[\mathrm{kg} \cdot \mathrm{m}^{-2} \cdot \mathrm{s}^{-1}]$, whereas it was $[\mathrm{mol} \cdot \mathrm{m}^{-2} \cdot \mathrm{s}^{-1}]$ before (compare Chapter 6.4).

The dimensionless notation of the mass transfer coefficient β is analogous to Equation 6.27 defined as the Sherwood number Sh

$$Sh = \frac{\beta \cdot L}{D} = \frac{j_w \cdot L}{\rho \cdot D \cdot \Delta\omega} \tag{6.35}$$

with L being the characteristic length of the mass transfer. The Sherwood number Sh is the formal analogue of the Nusselt number Nu. It is, therefore, possible to apply the Colburn analogy between momentum flux and heat flux (Equation 6.31) to the diffusive mass transfer by replacing the Nusselt number Nu by the Sherwood number Sh and the Prandtl number Pr by the Schmidt number Sc, which yields the Colburn analogy between momentum flux and mass flux:

$$\frac{c_f}{2} = \frac{Sh}{Re} \cdot Sc^{-1/3} = \frac{\tau_w}{\rho \cdot u_\infty^2} \tag{6.36}$$

Inserting the definition of the Sherwood number Sh (Equation 6.35) into the Colburn analogy for mass transfer yields the transfered diffusion flux at a wall boundary:

$$j_w = D \cdot \Delta\omega \cdot \frac{1}{L} \cdot Re \cdot Sc^{1/3} \cdot \frac{\tau_w}{u_\infty^2} \tag{6.37}$$

Considering the venous system of *X. derbentina* the characteristic length L of the Sherwood number Sh is the length of the corresponding segment of the capillary and main vein, respectively, over which the diffusive mass transfer takes place (x direction in Figure 6.6). Due to the fine segmentation of the venous system the problem approaches the case of an overflowed flat plate instead of a tube flow. Therefore, the Reynolds number Re is also calculated with this characteristic length L (otherwise the diameter of the tube would need to be used) and Equation 6.37 simplifies to:

$$j_w = \left(\frac{D_1}{\nu}\right)^{2/3} \cdot \Delta\omega \cdot \frac{\tau_w}{u_\infty} \tag{6.38}$$

with $\Delta\omega = \omega_w - \omega_2$ as the difference of oxygen mass fraction between the inner membrane wall ω_w and the snails' hemolymph ω_2. It is important to mention that the diffusion coefficient D_1 in Equation 6.38 is that of oxygen in hemolymph, which will be approximated by that of oxygen in water, which is $D_1 = 2.1 \times 10^{-9}\,\mathrm{m^2 \cdot s^{-1}}$ [Cussler, 2009]. Furthermore, the corresponding area over which diffusion takes place is the inner membrane wall A_{inner}.

The diffusion flux transferred into *X. derbentina*'s hemolymph is the same that passes through the membrane of the capillaries and main vein. Due to the curved shape of the membrane the area over which diffusion takes place depends on the radius which results in a nonlinear trend of diffusion flow along the radius of the membrane. According to Specht [2008] the equation for the

diffusion across a plate is still sufficiently valid if the area given by the mean of the inner and outer radius of the capillary/main vein tube is used for the calculation. The error made by this simplification is less than 3 % for the capillaries and less than 5 % for the main vein. Therefore, the diffusion flux through the membrane tissue can be written:

$$j = \rho \cdot D_2 \cdot \frac{\Delta\omega_{\text{memb}}}{\Delta y_{\text{memb}}} = \rho \cdot D_2 \cdot \frac{\omega_{\max} - \omega_w}{\Delta y_{\text{memb}}} \tag{6.39}$$

with D_2 as the diffusion coefficient for oxygen in pulmonary tissue [Grote, 1967], $\Delta\omega_{\text{memb}}$ as the difference of the constant oxygen mass fraction between the lung $\omega_{\max}$ and the one at the inner membrane wall ω_w, and Δy_{memb} being the membrane thickness. Furthermore, the corresponding area over which diffusion takes place is the area given by the mean of the inner and outer radius of the capillary/main vein tube A_{mean}. By taking the corresponding areas of diffusion into account this implication yields the relationship between ω_w and ω_2:

$$\omega_w = \frac{A_{\text{inner}} \cdot \omega_2 \cdot \left(\frac{D_1}{\nu}\right)^{2/3} \cdot \frac{\tau_w}{u_\infty} + A_{\text{mean}} \cdot \rho \cdot D_2 \cdot \frac{\omega_{\max}}{\Delta y_{\text{memb}}}}{A_{\text{inner}} \cdot \left(\frac{D_1}{\nu}\right)^{2/3} \cdot \frac{\tau_w}{u_\infty} + A_{\text{mean}} \cdot \rho \cdot D_2 \cdot \frac{1}{\Delta y_{\text{memb}}}} \tag{6.40}$$

Figure 6.6 illustrates the convective mass transfer model that is used for *X. derbentina*'s vein system. At the bottom of Figure 6.6 the lung volume is located with its oxygen mass fraction $\omega_{\max}$ resulting from ambient conditions. Adjacent to it is the membrane wall through which oxygen diffuses into the snail's blood. Additionally the course of mass fraction is schematically depicted. Through the membrane wall a linear decrease of mass fraction is present that transitions into a non-linear course as soon as the convective transport of oxygen into the blood begins. This is evaluated in every segment of each capillary and main vein based on the momentum flux at the wall (shear stress).

Taking the previously mentioned increase of oxygen concentration by a factor of $\Phi = 2 - 4$ due to chemical bonding into account it is practical to define a ratio X of concentration that passes from the physical solution into the state of chemical bonding. The following statement can then be made about the physically dissolved mass fraction ω_2 before and after chemical bonding:

$$\omega_{2,\text{after chem. bond.}} = (1 - X) \cdot \omega_{2,\text{before chem. bond.}} \tag{6.41}$$

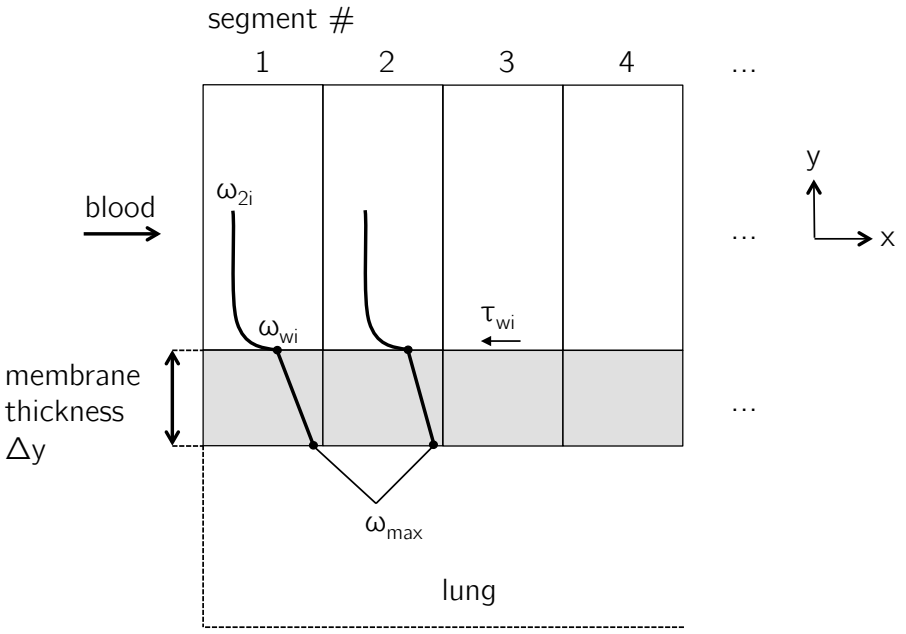

Figure 6.6: Convective mass transfer model for *X. derbentina*'s vein system

Therefore, the ratio X is directly connected to the increase of oxygen mass fraction due to chemical bonding Φ from the relationship:

$$X = \frac{\Phi - 1}{\Phi} \tag{6.42}$$

It has already been discussed that the ambient oxygen concentration of 20.9 % is significantly reduced during the process of inhalation [Krämer, 2005]. Thus, the gradient $\omega_{\max} - \omega_w$ has to be calculated with a reduced mass fraction $\omega_{\max}$ inside the snail's lung. Krämer [2005] reports a decrease of 0.625 of the initial ambient oxygen concentration for human beings. As described before, the author states that the reasons for this decreased oxygen pressure are mainly the humidification of the breathing air and the addition of considerable amounts of CO_2 during inhalation. For *X. derbentina* this decrease may very well be less pronounced than for human beings since the breathing apparatus is far less complex and mitigates these influences. To account for this decrease the oxygen mass fraction $\omega_{\max}$ that is present in the snail's lung needs to be multiplied by a factor ξ that by definition should lie in the range of $0.625 - 0.75$. Therefore, $\omega_{\max}$ is calculated in the following way using the

Henry constant $k_{\mathrm{H,cp}}$, the molar mass of oxygen $M_{O_2} = 31.99\,\mathrm{g \cdot mol^{-1}}$, and the density of water $\rho_{H_2O} = 997\,\mathrm{kg \cdot m^{-3}}$:

$$\begin{aligned}\omega_{\max} &= \xi \cdot k_{\mathrm{H,cp}} \cdot p_{O_2,\mathrm{atm}} \cdot \frac{M_{O_2}}{\rho_{H_2O}} \\ &= \xi \cdot 1.3 \times 10^{-3}\,\mathrm{mol \cdot l^{-1} \cdot atm^{-1}} \cdot 0.2095\,\mathrm{atm} \cdot \frac{3.199 \times 10^{-2}\,\mathrm{kg \cdot mol^{-1}}}{0.997\,\mathrm{kg \cdot l^{-1}}}\end{aligned} \tag{6.43}$$

As an intermediate summary the following variable values have been introduced that need to be adjusted to the actual geometrical and physiological setup of *X. derbentina*:

- The surface area fraction of the capillary and main vein tube that is available for diffusion to take place. This surface fraction is an unknown parameter but it should be in the range of 40–60 % of the complete inner tube area resulting in approximately half of the cylindrical surface of capillaries and main vein to participate in the diffusion process (compare Figure 6.3).

- The ratio X of mass fraction that passes from the physical solution into the state of chemical bonding. This ratio should be chosen in a way that the increase of concentration due to chemical bonding Φ results in a range of 2–4 [Markl, 1996].

- The decrease ξ of the initial ambient oxygen concentration that yields the actual concentration in the snail's lung. According to Krämer [2005] this decrease is 0.625 for human beings but it is very likely higher for *X. derbentina*.

Some additional remarks have to be made concerning the chosen method of the Colburn analogy. Numerous textbooks cover the topic of heat transfer in a laminar tube flow with either constant heat flux q_w or constant wall temperature T_w [Baehr and Stephan, 2013, Fournier, 2007, Incropera, 2007, Kraume, 2012, Subramanian, 2014]. Both cases can easily be transformed to mass transfer by replacing the Nusselt number Nu with the Sherwood number Sh in the same way as it has been done in this chapter. These solutions correspond to an integral view of a tube of considerable length. However, the

method presented above utilizes the segmentation of the system. Due to its short axial length each segment much more resembles the shape of a flat plate than that of a tube and each mass transfer calculation is only applied for a single segment as well. The method presented calculates the mass transfer for a small segment and adds the sum of all transferred masses into the next segment. Therefore, the tube flow solution is not applicable and the use of the analogy on a flat plate is justified.

The Colburn analogy (as well as the Reynolds analogy) are only valid for constant wall mass fractions ω_w. At first appearance it seems that this requirement is not fulfilled as the wall mass fraction constantly changes downstream due to the enrichment of oxygen inside the blood and its feedback to the membrane wall. But keeping in mind that the use of the Colburn analogy only takes place inside a single segment, inside which a constant wall mass fraction is present, the requirement is still fulfilled.

6.7.1 Calculation procedure

In the following section the basic procedure is described for the calculation of the mass fraction course of oxygen along all capillaries and the main vein and the corresponding amounts of oxygen that are transferred over each segment. Additionally, Figure 6.7 gives an overview of the segmentation of capillaries and main vein that provides the basis for the following calculation procedures.

Procedure for each capillary divided into $N = 40$ segments:

1. Define $\omega_{2i} = 0$ for the first segment ($i = 1$)

2. Calculate $\omega_{\mathrm{w}i}$ for the first segment using Equation 6.40

3. Calculate the absolute diffusion mass flow J [$\mathrm{kg \cdot s^{-1}}$] using the mean surface area A_{mean} (between inner and outer radius) and membrane thickness of the corresponding capillary segment by applying Fick's law for mass fractions:

$$J_i = A_{\mathrm{mean,cap}} \cdot \rho \cdot D_2 \cdot \frac{\omega_{\max} - \omega_{\mathrm{w}i}}{\Delta y_{\mathrm{memb,cap}}} \tag{6.44}$$

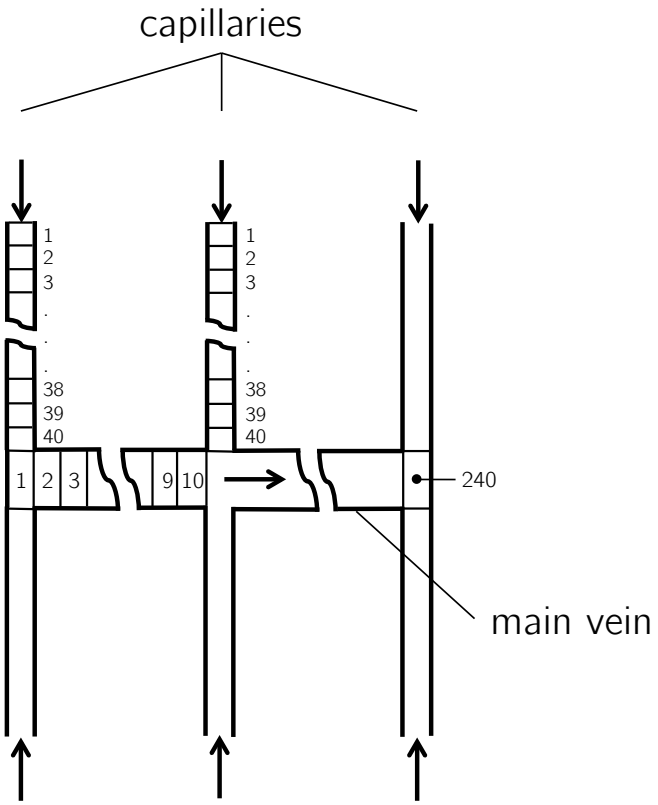

Figure 6.7: Segmentation of capillaries and main vein for the vein system

4. For the following segments ($i = 2 \dots 40$) use the effective physically dissolved mass fraction after chemical bonding, introduced by the ratio X, for the calculation of ω_{2i} by relating the absolute diffusion mass flow up to this position to the mass flow of hemolymph at the current position:

$$\begin{aligned} \omega_{2i} &= (1 - X) \cdot \frac{\sum_{n=1}^{i-1} J_n}{\dot{m}_i} \\ &= (1 - X) \cdot \frac{\sum_{n=1}^{i-1} A \cdot \rho \cdot D_2 \cdot \frac{\omega_{\max} - \omega_{wn}}{\Delta y_{\text{memb,cap}}}}{\rho \cdot A_{\text{cross-section,cap}} \cdot u_{\infty,i,\text{cap}}} \end{aligned} \tag{6.45}$$

5. For the following segments ($i = 2 \dots 40$) calculate ω_{wi} using Equation 6.40 with the effective physically dissolved mass fraction after chemical bonding ω_{2i} obtained from step 4.

6. Calculate the total oxygen mass fraction ω_{ti} inside the capillary segment:

$$\omega_{\mathrm{t}i} = \frac{\sum_{n=1}^{i-1} J_n}{\dot{m}_i} = \frac{\sum_{n=1}^{i-1} A \cdot \rho \cdot D_2 \cdot \frac{\omega_{\max} - \omega_{\mathrm{w}n}}{\Delta y_{\mathrm{memb,cap}}}}{\rho \cdot A_{\text{cross-section,cap}} \cdot u_{\infty,i,\mathrm{cap}}} \tag{6.46}$$

7. Finally calculate the sum of all $N = 40$ diffusion mass flows J [$\mathrm{kg} \cdot \mathrm{s}^{-1}$] yielding the total mass diffusion flow per capillary.

Procedure for the main vein divided into $N = 10$ segments between each capillary inflow resulting in a total number of $N = 240$ segments:

1. For the first main vein segment ($i = 1$) calculate the effective physically dissolved mass fraction after chemical bonding ω_{2i} according to Equation 6.45 based on the summarized diffusion mass flow from the first two capillaries that have entered the main vein until then[5] related to the mass flow of hemolymph.

$$\begin{aligned} \omega_{2i} &= (1 - X) \cdot \frac{\sum_{m=1}^{2} J_{\mathrm{cap},m}}{\dot{m}_i} \\ &= (1 - X) \cdot \frac{J_{\mathrm{cap},1} + J_{\mathrm{cap},2}}{\rho \cdot A_{\text{cross-section,main vein}} \cdot u_{\infty,i,\text{main vein}}} \end{aligned} \tag{6.47}$$

2. Calculate $\omega_{\mathrm{w}i}$ for the first main vein segment ($i = 1$) with Equation 6.40 using ω_{2i} from step 1.

3. Calculate the absolute diffusion mass flow for the first main vein segment ($i = 1$) using the mean surface area A_{mean} (between inner and outer radius) and membrane thickness of the corresponding main vein segment by applying Fick's law for mass fractions:

$$J_i = A_{\text{mean,main vein}} \cdot \rho \cdot D_2 \cdot \frac{\omega_{\max} - \omega_{\mathrm{w}i}}{\Delta y_{\text{memb,main vein}}} \tag{6.48}$$

4. For the following main vein segments ($i = 2 \ldots 240$) calculate ω_{2i} based on the summed diffusion mass flows from all capillaries that have entered

[5] On the left side of Figure 6.7 two capillaries enter the main vein at the front, so that the first main vein segment is already mixed with the diffused oxygen flow of these two capillaries.

the main vein until then related to the mass flow of hemolymph at the current position, and additionally add the diffusion mass flows from the previous main vein segments from step 3.

$$\begin{aligned}\omega_{2i} &= (1-X)\cdot\frac{\sum J_{\text{cap}}+\sum_{n=1}^{i-1}J_n}{\dot{m}_i}\\ &= (1-X)\cdot\frac{\sum J_{\text{cap}}+\sum_{n=1}^{i-1}A\cdot\rho\cdot D_2\cdot\frac{\omega_{\max}-\omega_{wn}}{\Delta y_{\text{memb,main vein}}}}{\rho\cdot A_{\text{cross-section,main vein}}\cdot u_{\infty,i,\text{main vein}}}\end{aligned} \tag{6.49}$$

The value for $u_{\infty,i,\text{main vein}}$ in step 1 and step 4 is obtained by the volume averaged velocities in the capillaries that have entered the main vein until then and the corresponding ratio of the cross-sections between capillary and main vein.

5. Calculate the total oxygen mass fraction $\omega_{\text{t}i}$ inside the main vein segment:

$$\omega_{\text{t}i} = \frac{\sum J_{\text{cap}}+\sum_{n=1}^{i-1}J_n}{\dot{m}_i} = \frac{\sum J_{\text{cap}}+\sum_{n=1}^{i-1}A\cdot\rho\cdot D_2\cdot\frac{\omega_{\max}-\omega_{wn}}{\Delta y_{\text{memb,main vein}}}}{\rho\cdot A_{\text{cross-section,main vein}}\cdot u_{\infty,i,\text{main vein}}} \tag{6.50}$$

6. Finally calculate the sum of all diffusion mass flows J $[\text{kg}\cdot\text{s}^{-1}]$ transferred in the $N = 240$ main vein segments and additionally add the sum of all diffusion mass flows J $[\text{kg}\cdot\text{s}^{-1}]$ from each capillary yielding the total mass diffusion flow.

Additional checks have been implemented for all calculations of the effective physical solute mass fraction after chemical bonding to assure this mass fraction cannot exceed the maximum value $\omega_{\max}$ that represents the physical solubility of oxygen in water for the given conditions inside *X. derbentina*'s lung. Therefore, the calculated values are only used if they are smaller than $\omega_{\max}$, otherwise they are exchanged for $\omega_{\max}$.

6.7.2 Boundary conditions

The analysis was undertaken for an "inactive" specimen of 0.9–0.95 cm diameter at 25 °C ambient temperature with a corresponding heartbeat frequency of $4.8\,\text{min}^{-1}$ representing an arbitrary value that covers the upper range derived in

Chapter 6.3. The chosen heartbeat frequency in conjunction with the volume flow through the snail's heart given by the derived volume of the ventricle yields a velocity of $u_{\text{main vein}} = 0.0035\,\text{m} \cdot \text{s}^{-1}$ that is used as a boundary condition for the main vein outlet of the surrogate model in the CFD simulation. On the inlets of each capillary an ambient pressure boundary condition is applied in order to let velocities in each capillary develop according to the corresponding position along the main vein.

The simulation is performed with the commercial CFD solver Star-CCM+ by CD-adapco (Melville, NY, U.S.A.). The flow is laminar with a Reynolds number of $Re \approx 1.2$. Additionally all hemocyanin flow properties in the simulation are approximated by the selection of water.

The distributions and the final sum of all diffusion mass flows yielding the total amount of transferred oxygen depend on the chosen values for the variables defined at the end of Chapter 6.7. Therefore, reasonable values for these variables were chosen to conduct the calculation presented above.

- The surface area fraction of the capillary and main vein pipe that is available for the diffusion process was chosen to be 60 % of the complete inner pipe area (compare Figure 6.3). This value seems reasonable because the surfaces of the capillaries and the main vein are likely uneven and larger than an ideal half cylindrical surface. Furthermore the NMR measurement was conducted with an insufficient resolution to obtain the correct surface of the animal's vein system and, therefore, is error-prone.

- The ratio X of mass fraction that passes from the physical solution into the state of chemical bonding is 0.553 resulting in a value for $\Phi = 2.24$. This follows from the chosen heartbeat frequency above that depends on the amount of absorbed oxygen and the value of Φ (compare Chapter 6.2 and Chapter 6.3).

- The decrease ξ of the initial ambient oxygen concentration due to inhalation effects was chosen to be $\xi = 0.75$. This results in a value for $\omega_{\text{max}} = 6.56 \times 10^{-5}$.

6.7.3 Wall shear stress distribution

The result of the flow simulation yielding the wall shear stress distribution for the surrogate model is given in the following Figure 6.8.

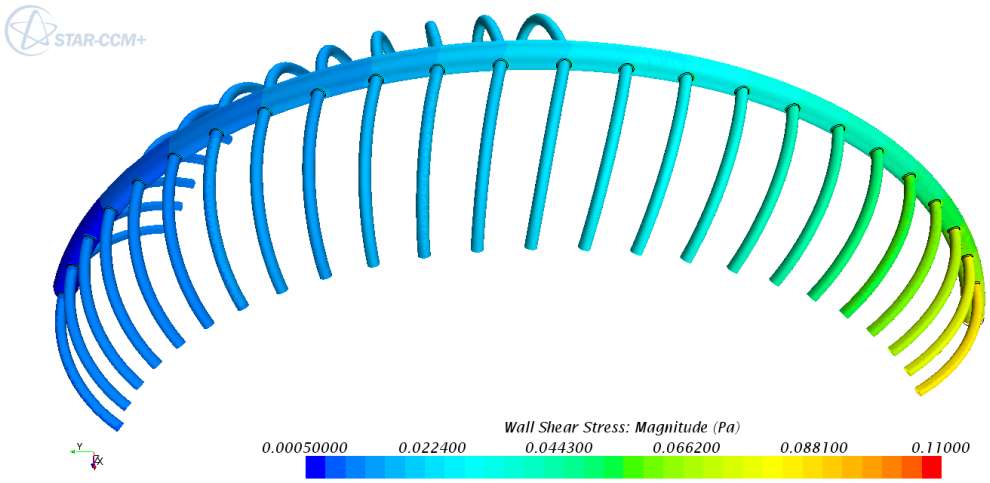

Figure 6.8: Wall shear stress distribution in the vein system

It can be seen that in each capillary the wall shear stresses are approximately constant neglecting the influence of the run-in distance of the laminar flow. Due to the main vein velocity outlet and the capillaries pressure inlet boundary conditions the volume flow generally increases for capillaries further downstream corresponding to higher values of wall shear stress as it can be observed from Figure 6.8.

For further analysis the velocity and wall shear stress for each capillary is assumed to be constant. The distribution for the main vein is evaluated at the inlet, at the outlet, and at a middle position in order to calculate a quadratic fit that will serve as an approximation to the actual distribution.

The theoretical value for the wall shear stress can easily be derived by the velocity distribution for laminar flow in a pipe (Hagen-Poiseuille) and the definition of pressure loss for laminar flow. The velocity distribution along the cross-section for a fully developed laminar flow is:

$$u_{(y)} = \frac{\Delta p}{4 \cdot \mu \cdot l} \cdot (R^2 - y^2) \tag{6.51}$$

with l being the length of the pipe, R being the radius and y being a coordinate originating at the middle of the cross-section with $0 < y < R$. The definition of wall shear stress is:

$$\tau_w = \mu \cdot \frac{\partial u}{\partial y}\Big|_w \tag{6.52}$$

Pressure loss for laminar flow is defined in the following way:

$$\Delta p = \frac{\lambda \cdot l}{d} \cdot \frac{\rho}{2} \cdot u_\infty^2 = \frac{64}{Re} \cdot \frac{l}{d} \cdot \frac{\rho}{2} \cdot u_\infty^2 = \frac{32 \cdot l}{d} \cdot \frac{\nu \cdot \rho}{d} \cdot u_\infty \tag{6.53}$$

The derivative $\partial u/\partial y$, evaluated at the wall position $y = R$, can easily be calculated and yields:

$$\frac{\partial u}{\partial y}\Big|_w = 2 \cdot R \cdot \frac{\Delta p}{4 \cdot \mu \cdot l} \tag{6.54}$$

Combining these results one obtains for the theoretical ratio of wall shear stress to the free-stream velocity:

$$\frac{\tau_w}{u_\infty} = 8 \cdot \frac{\nu \cdot \rho}{d} \tag{6.55}$$

This ratio is easily found by evaluating the wall shear stress for each capillary in Star-CCM+ resulting in values in the range of $46.5 - 47.2$ with a theoretical value of 47.7. The assumption of a quadratic wall shear stress along the main vein results in values in the range of $19.8 - 27.2$ with a theoretical value of 20.3, which is still a reasonable range. Furthermore the error made by this assumption has very little influence on the results presented in the following section.

6.7.4 Distribution of oxygen mass fraction along capillaries and main vein

In the following section results are presented for the distribution of oxygen mass fraction along each capillary and along the main vein.

The development of velocity is shown for all capillaries at the top and along the main vein at the bottom of Figure 6.9. Capillary numbers are counted streamwise of the main vein from the beginning of the snail's lung up to the heart starting with number 1 on the left side, number 2 on the right side in front view. The opposing capillary pairs up to capillary number 26 (compare Figure 6.1) are displayed only once.

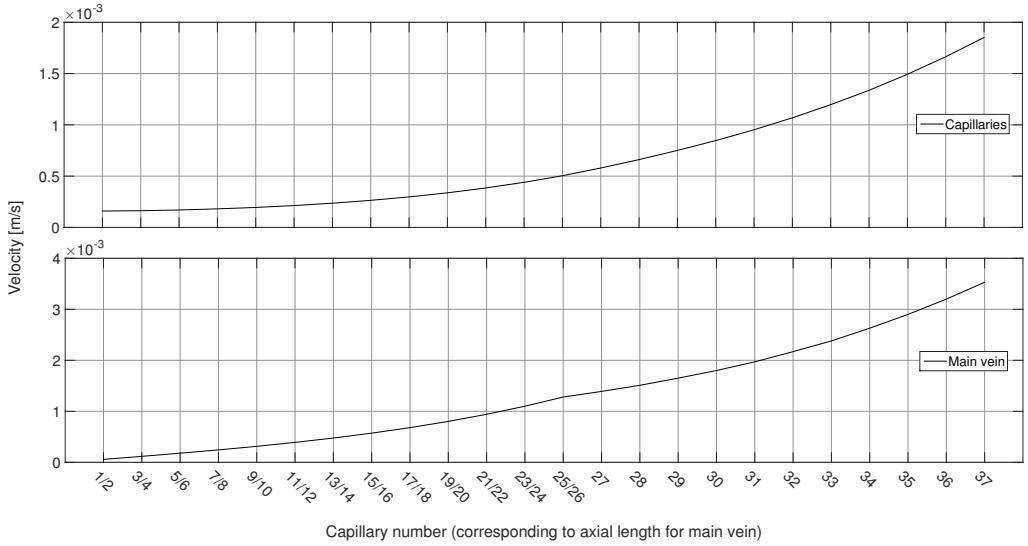

Figure 6.9: Development of velocity in capillaries and main vein

It can be seen that velocity in the capillaries increases non-linearly (Figure 6.9, top), which is a consequence of pressure loss inside the vein system. Due to the pairwise inflow into the main vein up to capillary pair 25/26 velocity inside the main vein increases slower for axial positions corresponding to capillary numbers 27-37 (Figure 6.9, bottom) resulting in the change of slope that can be observed at capillary number 27. At the end of the main vein, corresponding to capillary number 37, the velocity $u_{\text{main vein}} = 0.0035\,\text{m} \cdot \text{s}^{-1}$ is reached according to the boundary condition.

Figure 6.10 shows the physical solute mass fraction of oxygen after chemical

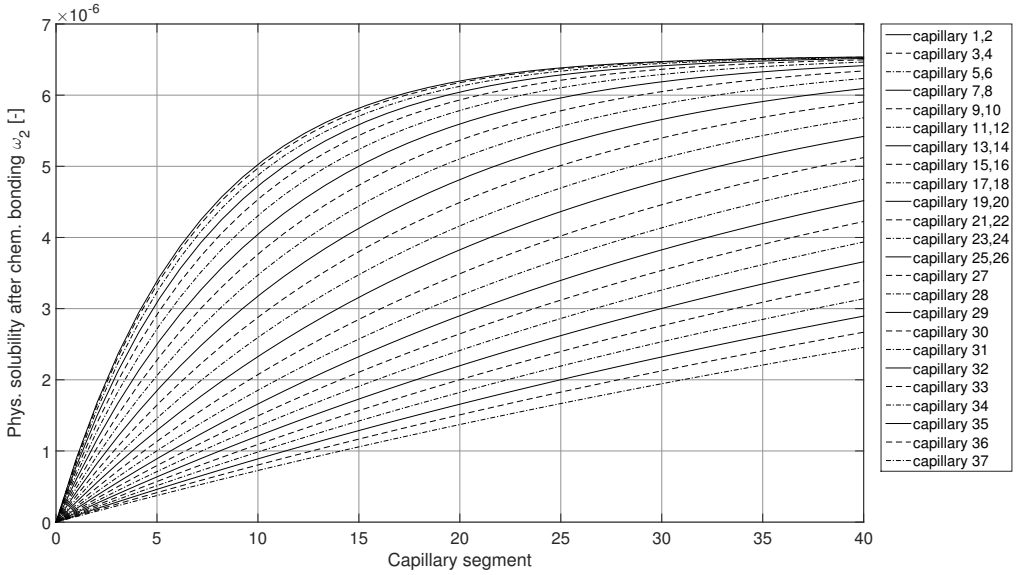

Figure 6.10: Mass fraction of physical solute O_2 in the hemolymph along each capillary

bonding ω_2 in the hemolymph of *X. derbentina* along the $N = 40$ segments of all capillaries according to Equation 6.45. It can be observed that the progression of ω_2 along each capillary proceeds in an asymptotical way and approaches the saturation value $\omega_{\max}$. Values for ω_2 are generally reduced for downstream capillaries. The reason for this behavior can be found in the aforementioned increasing velocity inside the downstream capillaries that results in the concurrent increase of mass flow into which the transferred diffusion mass flow of oxygen has to dissolve. Thereby the mass fraction decreases. Another explanation for this observation is the lower contact time of the snail's hemolymph with the membrane surface that prevents a further rise in oxygen mass fraction.

The physical solute oxygen mass fraction after chemical bonding ω_{w} at the membrane wall is presented in Figure 6.11 for all capillaries along their $N = 40$ segments. The trend of ω_{w} is basically the same as the one found for ω_2 with the absolute values of ω_{w} always being higher than the ones for ω_2. This is reasonable since the concentration gradient always points towards the hemolymph that is continuously enriched with oxygen.

Due to this decrease in oxygen concentration for capillaries in the down-

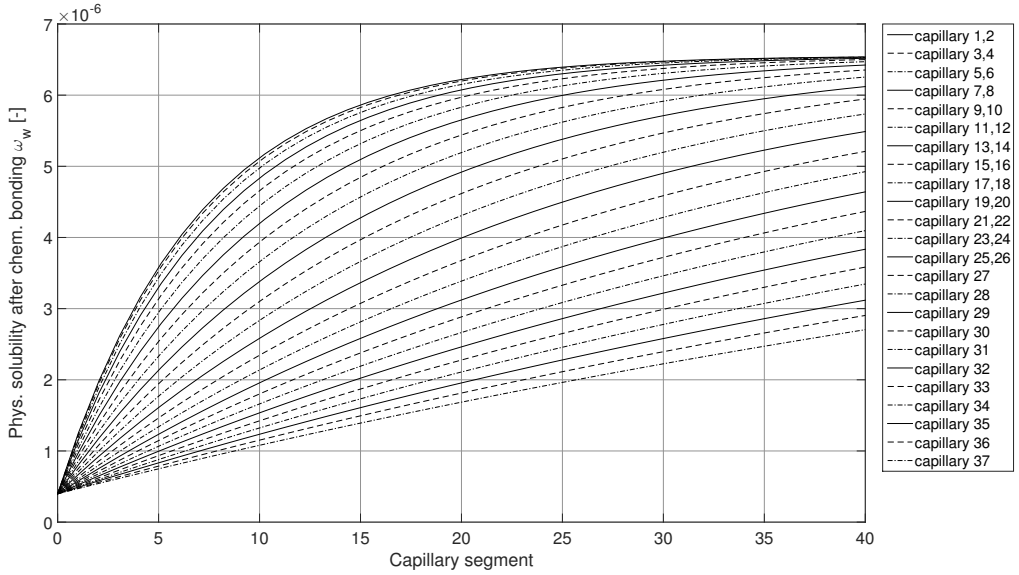

Figure 6.11: Mass fraction of physical solute O_2 at the membrane wall along each capillary

stream direction the overall gradient between the constant mass fraction $\omega_{\max}$ inside *X. derbentina*'s lung and the membrane wall ω_{w} increases. As a consequence this increased gradient results in a higher diffusion mass flow J into the hemolymph for downstream capillaries. This relationship is shown in Figure 6.12. It can clearly be seen that this progression is directly related to the mass fraction ω_{w} at the membrane wall. It shows an asymptotically decreasing diffusion mass flow to the limiting value $J = 0$. The first capillaries that almost reach the saturated value $\omega_{\max}$ at segment 40 only have a small mass fraction capacity left resulting in the lowest diffusion mass flows. However, further downstream capillaries have higher capacities due to the higher gradient resulting in a higher diffusion mass flow.

This relation can be further visualized by examining the integrated diffusion mass flows J for each capillary (Figure 6.13). For this purpose the single mass flows of each segment are summed up for each capillary, which represents a basic integration of every curve presented in Figure 6.12. When plotted over the capillary number it can be seen that the integral mass flow strongly increases for the first capillaries. However, the trend possesses an inflection

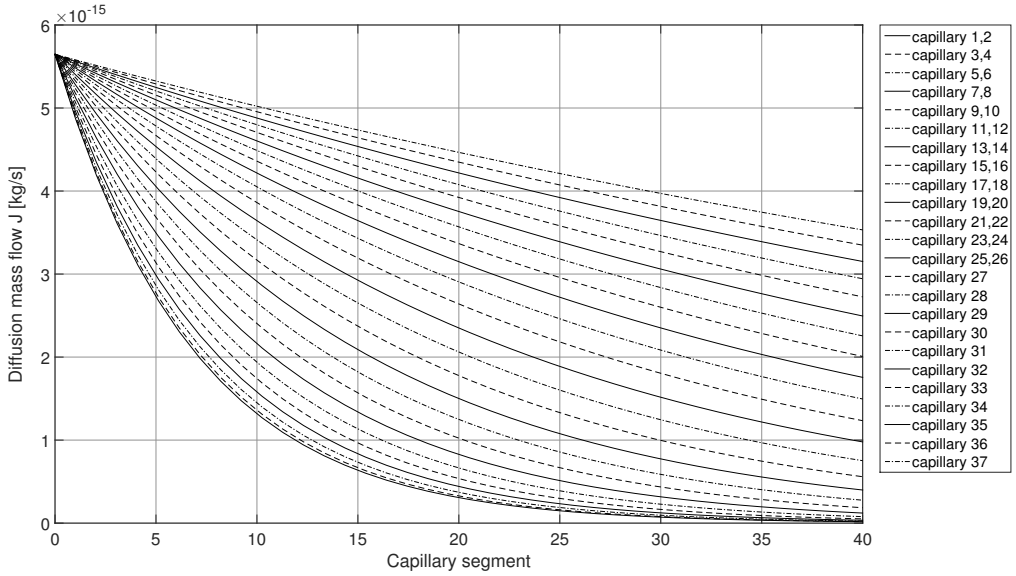

Figure 6.12: Development of diffusion mass flow J along each capillary

point at the position of capillary 25/26 after which the slope decreases again and takes an asymptotical course towards the last capillaries. This behavior

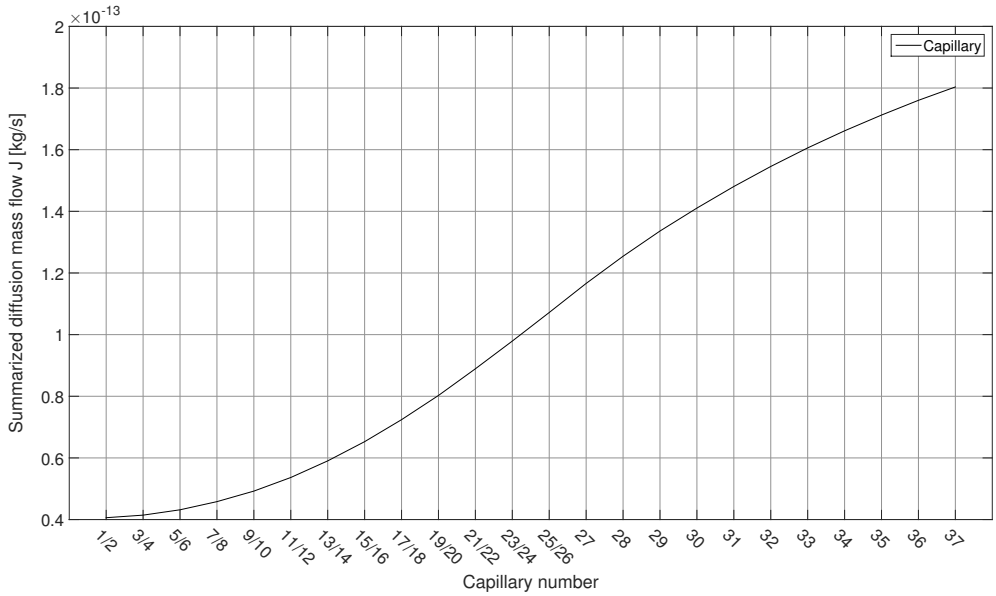

Figure 6.13: Integrated diffusion mass flow J for each capillary

was expected due to the distance between the single curves in Figure 6.12 that similarly increases for downstream capillaries up to number 25/26 and beyond that position decreases again. The reason for this can be found in the progression of mass fractions in Figure 6.10 and Figure 6.11. The existence of an upper and lower limit for those mass fractions ω_2 and ω_w, namely ω_max and 0 or ω_w1 for the first segment, respectively, prohibits concentrations that exceed or fall below these values. However, these limits will not be reached suddenly but in an asymptotical way. Otherwise an implausible discontinuity would exist. As the mass fractions basically have the same trend as the diffusion mass flows the same holds for the latter explaining the observed inflection point in Figure 6.13.

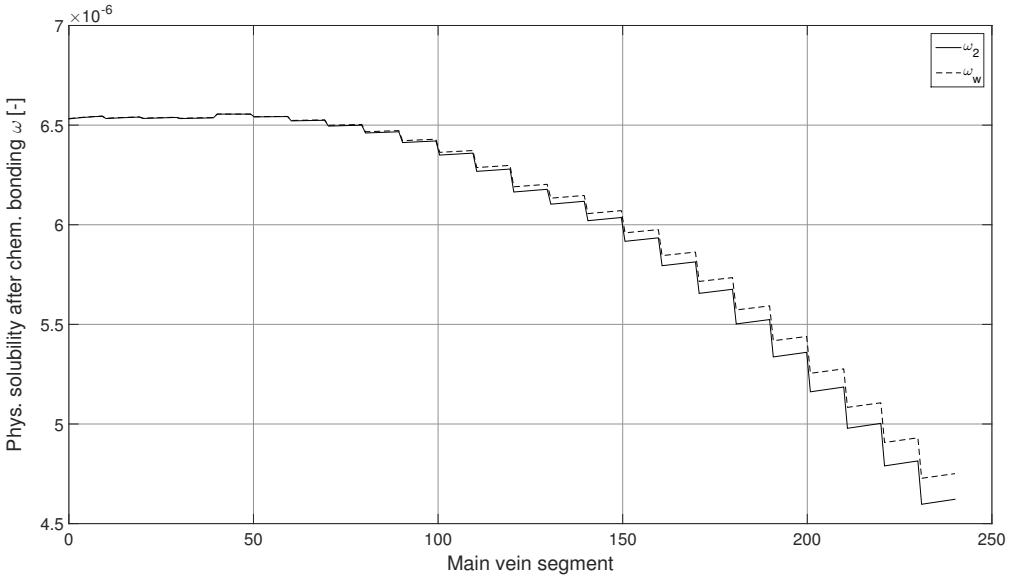

Figure 6.14: Mass fraction of physical solute O_2 in hemolymph and at the membrane wall along the main vein

The mass fraction of physical solute oxygen after chemical bonding, ω_2 and ω_w, along the main vein (Figure 6.14) shows a different progression from the ones of the capillaries. Sharp edges can be seen at the positions of each capillary inflow resulting in sudden decreases of ω_2 and ω_w. The mass fraction ω is defined as the diffusion mass flow of oxygen per mass flow of hemolymph and this will consequently result in a decrease of ω if the hemolymph mass

flow abruptly increases. In between two capillary inflows the mass fraction will always increase as the mass flow remains unchanged but oxygen continues to diffuse over the corresponding main vein segments. Because of the lowered mass fractions for downstream capillaries (Figure 6.10 and Figure 6.11) these sudden decreases of ω_2 and ω_w in the main vein are intensified. Due to this repeated mixing process the overall concentration along the main vein decreases steadily.

Figure 6.15 shows the total oxygen mass fraction ω_t along the main vein. The calculation of this quantity takes the total mass of transferred oxygen into account and is not limited by the value of ω_max and represents, therefore, the total oxygen mass fraction inside the hemolymph that is achieved by the supplemental rise due to chemical bonding onto hemocyanin. With the set definition of Φ the ratio of total mass fraction ω_t due to chemical bonding to the mass fraction of physical solute oxygen after chemical bonding in hemolymph ω_2 is always 2.24. The trends presented in Figure 6.15 are, therefore, similar to the ones in Figure 6.14. The only difference is a slight shift towards higher mass fraction levels.

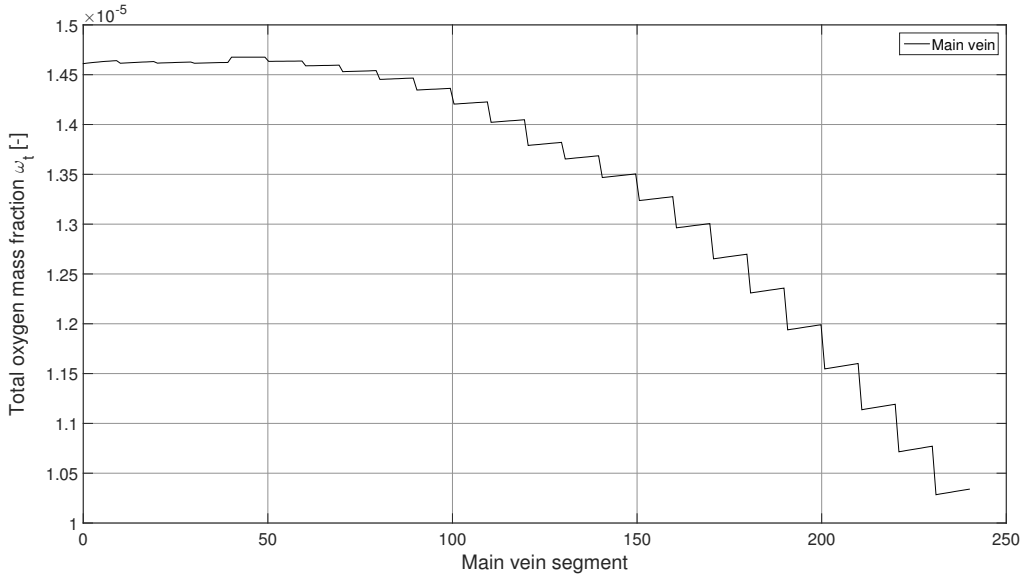

Figure 6.15: Total oxygen mass fraction along main vein

Related to the observations for the capillaries an increasing diffusion mass

flow of oxygen along the main vein (Figure 6.16) can be found corresponding to the decline in mass fraction seen in Figure 6.14. Again, due to the mass fraction decrease inside the main vein in downstream direction the gradient $\omega_{\max} - \omega_{\mathrm{w}}$ increases, which results in a higher diffusion mass flow J into the hemolymph towards the snail's heart. The diffusion mass flow along the main

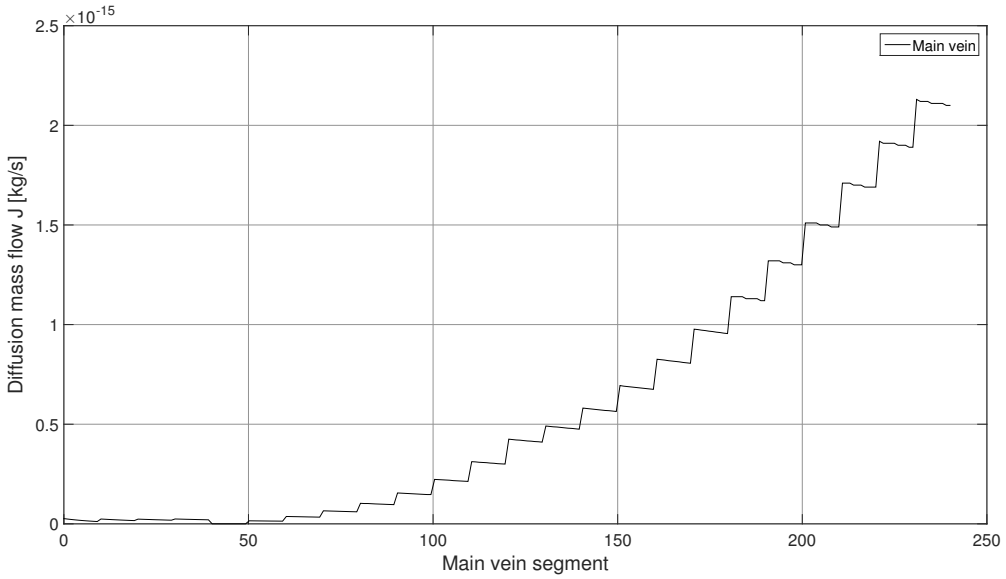

Figure 6.16: Diffusion mass flow along main vein

vein in Figure 6.16 is again used to perform an integration of the $N = 240$ main vein segments to obtain the total mass flow of transferred oxygen for the entire main vein. By the addition of the integrated mass flows for each capillary the diffusion mass flow for the complete vein system of *X. derbentina* is obtained.
Converting this value using the molar mass of oxygen M_{O_2} a final value of

$$\dot{n}_{O_2} = 1.097 \times 10^{-10}\,\mathrm{mol} \cdot \mathrm{s}^{-1} \tag{6.56}$$

is obtained. Comparing this value with the measured oxygen consumption for medium-sized specimens at 25 °C of $(1.04 \pm 0.25) \times 10^{-10}\,\mathrm{mol} \cdot \mathrm{s}^{-1}$ (compare Chapter 2) shows an excellent agreement with the measurements. This suggests that the calculated value of the measured oxygen consumption provides a meaningful proof for the correctness of the chosen values of the variables defined above and for the applied concept of the Colburn analogy as a whole.

6.7.5 Limitations of the procedures and methods

The limitations of the presented methods become clear when examining the actual amount of oxygen dissolved in the hemolymph of *X. derbentina*. Based on the ventricle volume that has been segmented from the NMR measurements and the estimated heartbeat frequency for medium-sized specimens at 25 °C ($f = 4.8\,\mathrm{min}^{-1}$) the volume flow of hemolymph was calculated to be approximately $2 \times 10^{-5}\,\mathrm{l} \cdot \mathrm{min}^{-1}$. This is also the exact volume flow that passes the lung of the animal after oxygen has been transported to the organs. The measured oxygen turnover ($1.04 \times 10^{-10}\,\mathrm{mol} \cdot \mathrm{s}^{-1} = 1.4 \times 10^{-7}\,\mathrm{l} \cdot \mathrm{min}^{-1}$), therefore, is the same amount that dissolves into this amount of hemolymph. The amount of dissolved ml of oxygen per 100 ml of hemolymph, therefore, results in:

$$c_{\text{dissolved } O_2} = \frac{1.4 \times 10^{-7}\,\mathrm{l} \cdot \mathrm{min}^{-1}}{2 \times 10^{-5}\,\mathrm{l} \cdot \mathrm{min}^{-1}} = 0.7\,\mathrm{ml} \cdot 100\,\mathrm{ml}^{-1} \tag{6.57}$$

According to Lide [2004] the physical solubility of oxygen in water at 25 °C is $0.65\,\mathrm{ml} \cdot 100\,\mathrm{ml}^{-1}$. Therefore, the rise of solute oxygen concentration due to chemical bonding onto hemocyanin results into $0.7/0.65 = 1.077$, which is significantly lower than the defined value of $\Phi = 2.24$ used for the theoretical calculation of oxygen consumption based on the Colburn analogy. However, oxygen consumption was measured with an uncertainty of $0.25 \times 10^{-10}\,\mathrm{mol} \cdot \mathrm{s}^{-1}$. Taking the highest value of $\dot{n}_{O_2} = 1.29 \times 10^{-10}\,\mathrm{mol} \cdot \mathrm{s}^{-1}$ into account the rise results in 1.34 and the discrepancy to $\Phi = 2.24$ decreases.

The same considerations can be made for specimens of *X. derbentina* at the higher temperature of 30 °C with a mean oxygen consumption value of $1.56 \times 10^{-10}\,\mathrm{mol} \cdot \mathrm{s}^{-1} = 2.1 \times 10^{-7}\,\mathrm{l} \cdot \mathrm{min}^{-1}$. According to the procedure in Chapter 6.3 a new heartbeat frequency range can be obtained in the range of 4–8 min^{-1} corresponding to values of $\Phi = 4$ and $\Phi = 2$, respectively. This results in an increase in concentration due to chemical bonding of 1.9 for the lower heartbeat frequency and even a decrease of 0.95 for the higher frequency. Both results show a distinct deviation from the theoretical values of $\Phi = 4$ and $\Phi = 2$. Taking the measured uncertainty into account again reduces this error but cannot fully eliminate it.

The reasons for these discrepancies are most likely caused by the calculation of the heartbeat frequency in Chapter 6.3 that is based on the oxygen partial pressures according to the results of Mikkelsen and Weber [1992] for *H. poma-*

tia. As these values are so far unknown for *X. derbentina* this source of error cannot be eliminated. Additionally it is known that stroke volume in mollusks can change considerably during exercise as the heart is not strictly rigid but its shape and volume depends rather on the internal pressures that provide structural stability [Jones, 1970, 1971]. Furthermore the heart adapts to the venous flow (preload) by varying its stroke volume [Smith, 1985, 1987], which is also known as the Frank-Sterling mechanism. Smith and Hill [1987] also reported a decrease of stroke volume by the addition of cardioactive drugs in *Busycon canaliculatum*. All these influences on cardiac output constitute a large source of error that is likely to be the reason for the previously discussed deviations. As the NMR measurements only provide a relatively undefined snapshot of the cardiac system of *X. derbentina* a slight change in heart volume is certainly the case in the present investigation.

Chapter 7

Cardiac performance of *X. derbentina*

The function of the heart of all animals is to circulate blood. In order to achieve a blood flow a pressure difference between the venous side and the arterial side of the heart must be established [Jones, 1971]. It is the function of the heart to produce a pressure gradient high enough to overcome the pressure losses caused by the blood vessels and the flow into and out of the lacunae where the hemolymph is collected after passing the organs. Furthermore, it is necessary to build up a certain surplus in pressure for the sustainment of ultrafiltration by exceeding the colloidal osmotic pressure of the blood [Dale, 1974]. The blood of gastropods serves the additional purpose of a hydrostatic skeleton about which the snail can perform muscular movements. For terrestrial snails it also serves to maintain the posture of the visceral mass and the shell.

In general cardiac performance is characterized by two parameters: the volume flow of blood and the pressure difference generated by the heart. For terrestrial snails little information is available concerning the cardiac output, i.e. the volume flow of blood, under "inactive" conditions. In an early investigation Schwartzkopff [1953] has measured the cardiac output of the heart of *H. pomatia* in an artificial circulatory. The author reports an average pressure difference of $7.7\,\mathrm{cmH_2O}$ and a corresponding volume flow of $0.89\,\mathrm{cm^3 \cdot min^{-1}}$ associated with the cardiac performance maximum with an arterial excess pressure. Herold [1975] measured the mechanical power of an isolated heart of *H. pomatia*, which was perfused with hemolymph. With this technique he was

able to modify the generated pressure rise of the heart and calculate the cardiac performance within the range of 0.76–7.71 W for pressure differences in the range of 2–8 cmH_2O. Based on his data, values for cardiac output can be calculated that are of the same magnitude as the ones from Schwartzkopff [1953]. Estimates of cardiac output for the sea snail *Hemifusus tuba* (Gmelin) are presented in a comprehensive study by Depledge and Phillips [1986] in the range of 0.1–2.22 $cm^3 \cdot min^{-1}$ for individuals of 7.6–13.6 cm shell length. The data in their study additionally provides values of wet weight and blood pressure of all tested specimens. Further investigations of the pressures in the cardiac system of mollusks are conducted by DeFur and Mangum [1979], Smith [1985], Smith and Hill [1987] on *Busycon canaliculatum* and Dale [1974] on *Lymnaea stagnalis*. However, these are all aquatic snails. Though measurement techniques have evolved enormously the small sized species *X. derbentina* still lacks any measured data concerning cardiac output or cardiac performance.

Therefore, an alternative approach has to be used to gather further information about the species under investigation. By reviewing the thesis that the cardiac output of snails correlates in general with body size or body weight another correlation should exist between blood pressure rise and body size or body weight. For this purpose the data provided by Schwartzkopff [1953] for *H. pomatia*, Depledge and Phillips [1986] for *H. tuba*, and DeFur and Mangum [1979] for *B. canaliculatum* will be combined and checked for the proposed assumptions.

Depledge and Phillips [1986] have presented a correlation between shell length and wet weight of the investigated specimens so that total body weight can be calculated easily for six individuals of *H. tuba* corresponding to each estimated cardiac output. Schwartzkopff [1953] and DeFur and Mangum [1979] reported an average weight of 23 g of *H. pomatia* and 49 g of *B. canaliculatum*, respectively, corresponding to the average cardiac output of each species. According to the physiological parameters previously derived for *X. derbentina* (heartbeat frequency of 4.8 min^{-1} and ventricle volume of 4.25×10^{-6} l) a cardiac output of 0.02 $cm^3 \cdot min^{-1}$ is obtained for a total body weight of 0.2 g. The combined data of cardiac output for these four species (including *X. derbentina*) plotted over total body weight is presented in Figure 7.1. Additionally, a linear fit of the data is plotted with $R^2 = 0.866$.

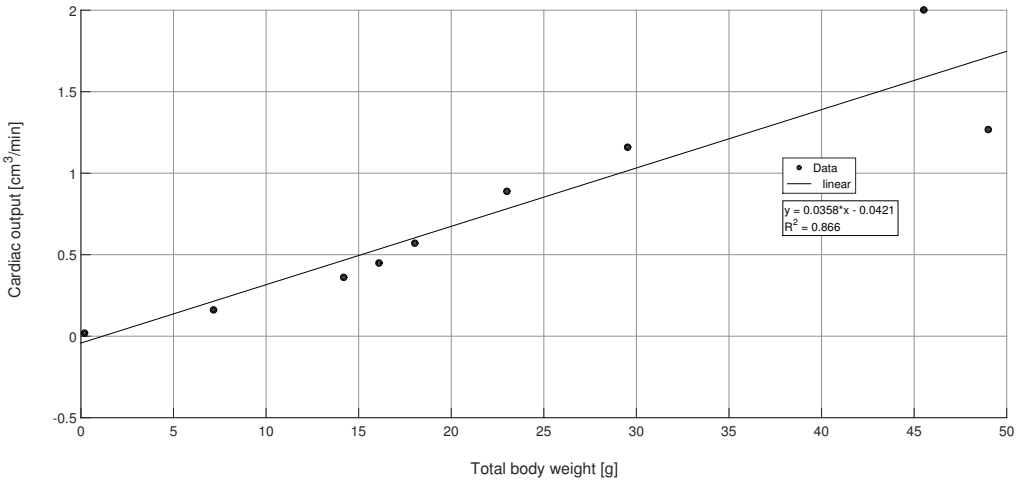

Figure 7.1: Cardiac output vs. total body weight of selected snail species

The interspecific depiction in Figure 7.1 clearly shows the suspected correlation between total body weight and cardiac output. Accordingly, the possible coherence between the pressure gradient produced by the heart and total body weight will be examined in the following Figure 7.2 for the same set of snails.

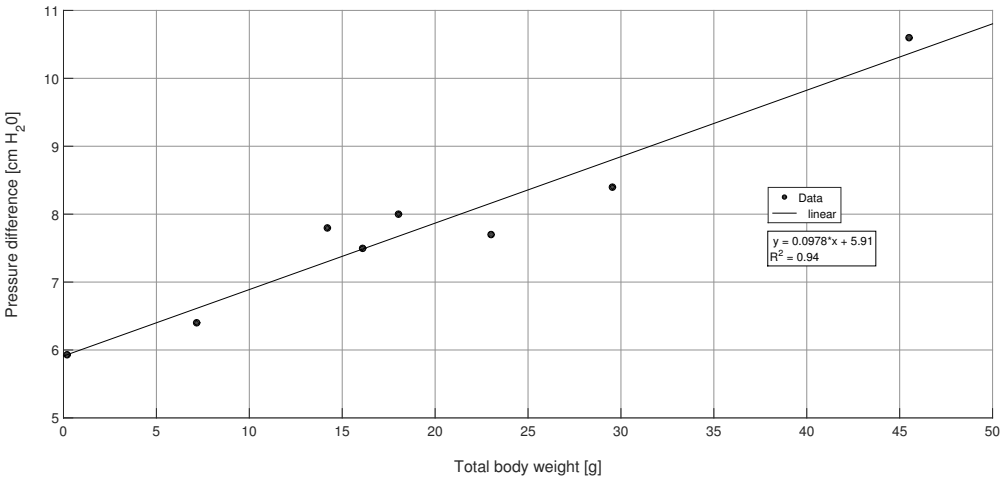

Figure 7.2: Pressure difference produced by the heart vs. total body weight of selected snail species

It is evident that a correlation with $R^2 = 0.94$ exists between these two

physiological parameters. Based on this connection, a pressure difference generated by the heart of *X. derbentina* can be calculated using the correlation equation given in Figure 7.2. Evaluating the pressure rise for a mean total body weight of 0.2 g, corresponding to medium sized specimens, yields a value of approximately 5.9 cmH_2O. The resultant point for *X. derbentina* has been plotted into Figure 7.2 subsequently so that the correlation equation remains unchanged.

The cardiac performance follows from the product of volume flow of blood and pressure increase:

$$\begin{aligned} P &= \dot{V}_{\text{blood}} \cdot \Delta p_{\text{heart}} \\ &= 3.4 \times 10^{-10}\,\text{m}^3 \cdot \text{s}^{-1} \cdot 578.6\,\text{Pa} \\ &= 1.97 \times 10^{-7}\,\text{W} \end{aligned} \tag{7.1}$$

This result of cardiac performance for *X. derbentina* compares with a specific output of 15–30 $\times 10^{-6}\,\text{W} \cdot \text{g}^{-1}$ ventricular tissue for *B. canaliculatum* [Smith, 1985]. Using a mean output of $22.5 \times 10^{-6}\,\text{W} \cdot \text{g}^{-1}$ and a mean ventricular tissue weight of 0.25 g of the investigated specimens of *B. canaliculatum* an absolute cardiac performance of $P = 5.63 \times 10^{-6}\,\text{W}$ can be derived. Taking into account that *B. canaliculatum* grow to a much larger size than *X. derbentina* the lower cardiac performance is reasonable and the difference between these two species appears rather small.

By means of the caloric equivalent for the conversion of carbohydrates (see chapter 5) the calculated cardiac performance can be converted into an equivalent oxygen consumption that is necessary to deliver this performance.

$$\begin{aligned} \dot{m}_{O_2,\text{heart}} &= \frac{P}{CE} \cdot \rho_{O_2} \\ &= \frac{1.97 \times 10^{-7}\,\text{W}}{21\,130\,\text{J} \cdot \text{l}^{-1}} \cdot 1.309\,\text{kg} \cdot \text{m}^{-3} \\ &= 1.218 \times 10^{-14}\,\text{kg} \cdot \text{s}^{-1} \end{aligned} \tag{7.2}$$

The overall oxygen consumption of *X. derbentina* is $1.04 \times 10^{-10}\,\text{mol} \cdot \text{s}^{-1} = 3.33 \times 10^{-12}\,\text{kg} \cdot \text{s}^{-1}$. In relation to this the following percentage is attributable to the sole cardiac performance of the animal:

$$x_{\text{cardiac}} = \frac{1.218 \times 10^{-14}\,\text{kg} \cdot \text{s}^{-1}}{3.33 \times 10^{-12}\,\text{kg} \cdot \text{s}^{-1}} = 0.37\,\% \tag{7.3}$$

At first glance this value seems very low but considering the uncertainties mentioned concerning the correct value of heart volume for *X. derbentina* the calculated fraction for cardiac performance is still in a reasonable range. Although values for the human heart reside around 9 % one has to keep in mind that the life style of an entirely "inactive" terrestrial snail is tremendously slower compared to that of a human being.

Chapter 8

Summary and Outlook

The present work comprises the analysis of heat balance and temperature regulation in the terrestrial snail *X. derbentina* (Gastropoda, Hygromiidae) abundant in southern France. This snail species has to cope with extreme climatic conditions of up to 45 °C air temperatures few centimeters above the soil surface that directly hamper its survival. Due to its high water content of more than 75 % [Reuner et al., 2008] desiccation poses a major threat to the snail, which is further enhanced by these hostile conditions. Climbing vertical objects to reach more favorable conditions is one of the believed survival strategies of the animal [Aubry et al., 2006] as well as the formation of clusters of hundreds of animals. Measurements at a population site in southern France have indicated that this species easily withstands temperatures of over 40 °C for a whole day without damage [Ludwig, 2012]. One proven mechanism to survive these conditions is the production of heat shock proteins that effectively protects the snail's cells from proteotoxic damage [Dieterich et al., 2013]. Next to the molecular response the entire metabolism of *X. derbentina* is investigated, which also needs to be adapted to these high temperature conditions in its habitat.

Oxygen consumption at three different ambient temperatures has been investigated. The additional differentiation between three shell size groups allowed for the study of size- and age-specific influences of temperature on each group.

Neglecting the influence of temperature, an increased shell size could be associated with an increase in oxygen consumption. A temperature influence

on oxygen consumption for shell size group 1, the smallest specimens, could not be found indicating that no thermal regulation is present. The reason for this observation is believed to be the age of the investigated specimens as young individuals may tolerate higher temperatures before metabolic regulation takes place. Individuals belonging to shell size group 2, however, showed a significant trend towards a regulation at the highest test temperature of 38 °C. This result coincides with the investigations of Riddle [1977] and Steigen [1979]. A similar but non-significant trend was found for shell size group 3 snails. The distinct size groups, therefore, revealed different amounts of metabolic regulation capacities at higher temperatures, which are clearly related to their different life stages. This goes along with the results of Köhler [2009] and Mayer and Bukau [2005] who mentioned a reduced Hsp70 level in older individuals of *X. derbentina* into which the stress protein was more difficult to induce. As Dieterich et al. [2013] pointed out this reduced capability is probably related to the accumulation of stress effects at the end of summer as well as the need for maintaining certain capacities in order to ensure a viable reproduction of the animals [Mizrahi et al., 2011]. Yengkokpam et al. [2008] showed that, in general, a relationship between Hsp70 production and oxygen consumption exists. Therefore, their results further support the conclusion that metabolic regulations, expressed by oxygen consumption, may very well be explained by the older life stage and the general "weakening" of older animals that limits their metabolic activity in the heat.

A response surface was calculated that shows the dependence of oxygen consumption upon temperature and shell-free weight. The extrapolation of the measured data matrix revealed upper and lower theoretical temperature "limits" beyond which the oxygen consumption is negative. The lower temperature "limit" could be to associated with conditions triggering arousal and the upper "limit" corresponded very well to the temperature that induces the maximum Hsp70 response after 8h exposure [Troschinski et al., 2014].

The weight-/metabolism relationship was investigated by the analysis of the metabolic scaling exponent α, i.e. the slope in a log-log-diagram of the characteristic curve of oxygen consumption over shell-free weight for each temperature. The results indicated a clear coherence between metabolic scaling exponent and ambient temperature showing a decreasing exponent α for in-

creasing temperatures with α in the range of 0.69–1.22.

The overall metabolic energy turnover was closer investigated by the means of direct calorimetry for two size groups and two temperatures. For each size and temperature combination measurements were conducted over a period of 7 days and a long-term measurement. Two distinct levels of metabolism were identified corresponding to an "inactive" and "active" state, where the latter is probably also related to locomotion of the specimens inside the measurement chamber [Lamprecht and Becker, 1988, Rees and Hand, 1990]. The analysis of regular patterns showed that snails are still more or less following a daily rhythm of activity and inactivity that is, however, undergoing a shift towards longer phases of inactivity the longer the phases of water and food deprivation during a measurement are (Figure 3.1 and Figure 3.6). A similar prolongation of phases of inactivity can be observed for larger specimens corresponding to the results of Dieterich et al. [2013] who have shown a down regulation of stress proteins in older individuals of *X. derbentina* that need to save resources.

The mean value of total energy consumption (Figure 3.3) showed that the small individuals react much more sensitive to a temperature increase with regard to the overall energy turnover showing a distinct regulation of metabolism. It was stated that the reason for this size-specific difference may be the higher specific surface of small specimens since the heat flux is higher when exerted on smaller specific surfaces.

The division of "active" and "inactive" metabolic energy fractions (Figure 3.4) revealed that "active" metabolic energy is saved for both size groups when temperature increases, which was especially significant for the small individuals. That is probably the most basic and efficient mechanism of this snail species in order to save energy at difficult thermal conditions. However, the cross-comparison of "active" energy fraction for each temperature only revealed a distinct decrease for larger specimen at the lower temperature of 20 °C. It was concluded that the reason for this may be due to the existence of a lower limit of activity phases before snails pass into estivation. Individuals at the higher temperature may still try to follow their more or less fixed activity cycles of feeding time and liquid intake in such a way that a further reduction of activity is restricted. Therefore, by having this limit already reached no additional decrease of "active" energy can be observed at the higher temperature.

The time share of activity (Table 3.1) showed that large individuals of *X. derbentina* spent more time in the state of activity than small ones do at 20 °C. This matches the results of the "active" and "inactive" energy fractions at 20 °C. Larger individuals reduce their "active" metabolic turnover compared to smaller ones and, therefore, are able to spend a longer time in the "active" state. The fact that this time share subsequently decreases again at the higher temperature indicates an anomalous behavior of *X. derbentina* since poikilothermic animals usually become more active at higher temperatures. However, this has been reported before and found to be transient until the expected behavior adjusts again [Kerkut and Taylor, 1958].

By approaching the mean surfaces of both size groups by a sphere the corresponding mass ratio was compared to the ratio of the change of time spent in activity when temperature increases from 20 °C to 30 °C and it was found that both are approximately inversely proportional to each other. This is indicative for the fact that their body weight and the exposition to ambient temperature have a direct influence on the behavior of *X. derbentina*.

The frequency analysis of the metabolic signal during the "inactive" state revealed the existence of increased frequency components for the higher test temperature. The identified oscillations most probably represent muscular activity of the animal as these processes contribute most to the overall thermal output measured by the calorimeter. Crozier and Stier [1925] as well as Bailey and Lazaridou-Dimitriadou [1991] reported an increased heart beat frequency for higher temperatures in three different snail species that may likely be a cause for the observed frequency increase due to a higher metabolic effort at higher temperatures. This may represent indices for thermal stress.

Detailed NMR measurements performed at the facilities of Bruker BioSpin GmbH in Rheinstetten with an Avance II 400 MHz Wide Bore System, 9.4 T, equipped with a Micro2.5 Gradient System and a 10 mm 1H resonator provided valuable data of the inner organic structure of a 0.95 cm diameter sized specimen of *X. derbentina*. The data was used to reconstruct the hepatopancreas, the kidney, the intestine, the heart, and the lung with its overlying vein system. The geometrical volume of the lung and the heart facilitated the calculation of further physiological details that complement the measured oxygen consumption and energy turnover. Using the size of the lung and combining

both datasets of oxygen consumption and energy turnover a response surfaces was calculated for a medium sized snail of 0.95 cm diameter in its aerobic state with a heat output of approximately 70 µW at 30 °C and 49 µW at 25 °C (Figure 5.1). The resulting surfaces show "oxygen reduction per breath" vs. "lung volume/breathing volume" and "breathing frequency". By reasonably setting the limits of "oxygen reduction per breath" to be in between 1–3 % a delimited remaining area described all possible physiological states of *X. derbentina*. The resulting range of "breathing frequency" of 1–5 min^{-1} fitted very well to the ones found for *H. pomatia* reported by Maas [1939].

Based on reported oxygen partial pressures of *H. pomatia* from [Mikkelsen and Weber, 1992] oxygen concentrations in artery and vein of *X. derbentina* were calculated that are based on the sole physical solubility of oxygen in the snail's blood. The definition of a variable factor Φ by which the oxygen concentration raises due to the chemical bonding onto hemocyanin facilitated the calculation of a range of absorbed oxygen concentration. Its definition combined with the physiological structure of *X. derbentina*'s heart, which consists of a single auricle and a single ventricle, yielded a range for the heartbeat frequency of $f = 2.7 - 5.4\,\mathrm{min}^{-1}$ for inactive specimens of 0.9–0.95 cm diameter size at 25°C.

Based on the performed NMR measurements a surrogate model of *X. derbentina*'s vein system was constructed. Therein, the diameters of all 37 capillaries (0.15 mm) and of the main vein (0.35 mm) are the result of their respective mean values of all capillary and main vein sections (Figure 6.1). By the definition of a perimeter fraction of 50 % for capillaries and main vein that are actually participating on the diffusive exchange of oxygen between the lung and the blood an active diffusive surface of 53.9 mm^2 was calculated from the surrogate model. Fick's first law of diffusion yielded the analytical value for the amount of active diffusive surface based on the measured oxygen consumption and the oxygen partial pressures of *H. pomatia*. This calculation assumed that the diffusive length is the surface averaged mean membrane thickness of capillaries and main vein. Furthermore the venous oxygen partial pressure was chosen to be the mean value of artery and vein since the partial pressure is continually increasing as the blood passes through the vein. Under these assumptions Fick's law resulted in a value of 56.2 mm^2 for the active diffusive

surface, which is in close accordance to the value obtained geometrically from the surrogate model.

A model approach was presented to validate the measured oxygen concentration by utilizing an adjusted version of the Colburn analogy between wall shear stress inside the surrogate vein system and mass transfer of oxygen into *X. derbentina*'s blood. This pragmatic approach requires a much lower computational effort compared to a complex CFD simulation that directly takes the diffusive processes of oxygen into account. In order to achieve this each capillary and the main vein was divided into segments of finite lengths. For the first segment of each capillary as well as for the first segment of the main vein the oxygen mass fraction inside the hemolymph was chosen to be zero as a starting condition. Subsequently the oxygen mass fraction at the inner membrane wall of the first segment was calculated using the aforementioned Colburn analogy in combination with the constant and known value of oxygen mass fraction inside the snail's lung. Fick's law was then utilized to obtain the absolute transferred diffusion mass flow of oxygen inside the segment. By passing this value to the next segment and relating it to the mass flow of blood in this segment a new value for oxygen mass fraction inside the snail's hemolymph was calculated for the second element. This again facilitated the calculation of the oxygen mass fraction at the membrane wall for the second element and provides the necessary value to start the iteration process again. By successively passing the local oxygen diffusion mass flows to the next segment and relating the summarized oxygen diffusion mass flows to the mass flow of blood in the following segment a marching solution algorithm was obtained. This algorithm depends on the choice of appropriate starting and boundary conditions and was used to present a course for oxygen mass fractions as well as the transferred oxygen diffusion mass flows along each capillary and main vein segment. The evaluation of the absolute transferred oxygen mass flow obtained by the presented method reveals a very good agreement with the measured oxygen consumption of medium-sized specimens at 25 °C and is a good indicator for the correctness of the method.

Finally, the cardiac performance of *X. derbentina* was investigated by an interspecific extrapolation of the pressure difference generated by the hearts of a set of terrestrial snails. Combining this result with the calculated cardiac out-

put of the "inactive" animal, which was based on the mean heartbeat frequency and ventricle volume, yielded the value of $P = 1.97 \times 10^{-7}\,\mathrm{W}$ for the cardiac performance. This performance was compared to the one of *B. canaliculatum* and found to be in a reasonable range. The equivalent oxygen consumption to deliver this cardiac performance was related to the overall oxygen consumption resulting in a fraction of $0.37\,\%$ of energy attributable to the sole cardiac performance of the animal. This comparably low value was justified by the slower lifestyle of the "inactive" snail compared to human beings.

Further work on the metabolic regulation processes of *X. derbentina* should involve a higher number of individuals for calorimetric investigations since some statistical uncertainties are still remaining in this study. The additional inclusion of a larger temperature range up to a critical limit of approximately $40\,^{\circ}\mathrm{C}$ for these measurements will yield even more information on the transitional shift between the amount and duration of "active" and "inactive" phases of the animal. Additionally more work should be carried out on the geometrical data of *X. derbentina*'s organs by utilizing a higher resolution for further NMR measurements. Thereby some of the taken assumptions in the present work should be ensured or revised. This should eventually lead to a complex 3D model of the animal that facilitates sophisticated simulations of internal heat fluxes that should take the individual energy consumptions of the most important organs into account. Therefore, the paths of blood flow need to be either acquired by the NMR measurements or constructed by a modelling approach. As a consequence thereof the presented Colburn analogy should be adapted to this three-dimensional model to predict oxygen diffusion mass flows from the snail's blood to the specific organs. The energetic requirements of the most important organs should, therefore, correlate with the paths of blood flowing around them resulting in proper values of shear stress to ensure a sufficient mass transfer to the organs.

Bibliography

J. D. Anderson. *Computational Fluid Dynamics: The Basics with Applications*. Tata McGraw-Hill International Edition, New Dehli, 2012.

Z. Astolfi-Filho, E. B. de Oliveira, J. S. d. R. Coimbra, and J. Telis-Romero. Friction factors, convective heat transfer coefficients and the colburn analogy for industrial sugarcane juices. *Biochemical Engineering Journal*, 60 (0):111–118, 2012. ISSN 1369-703X. doi: http://dx.doi.org/10.1016/j.bej.2011.10.011. URL `http://www.sciencedirect.com/science/article/pii/S1369703X11002889`.

S. Aubry, C. Labaune, F. Magnin, P. Roche, and L. Kiss. Active and passive dispersal of an invading land snail in mediterranean france. *Journal of Animal Ecology*, 75:802–813, 2006. doi: 10.1111/j.1365-2656.2006.01100.x.

H. Baehr and K. Stephan. *Wärme- und Stoffübertragung*. Springer Berlin Heidelberg, 2013. ISBN 9783642365584. URL `https://books.google.de/books?id=ztYoBAAAQBAJ`.

S. E. R. Bailey and M. Lazaridou-Dimitriadou. Inverse temperature acclimation of heart rate in hibernating land snails. *Journal of Comparative Physiology B*, 160(6):677–681, 1991. ISSN 0174-1578. doi: 10.1007/BF00571267. URL `http://dx.doi.org/10.1007/BF00571267`.

M. C. Barnhart. Gas permeability of the epiphragm of a terrestrial snail, otala lactea. *Physiological Zoology*, 56(3):436–444, 1983. ISSN 0031935X. URL `http://www.jstor.org/stable/30152609`.

M. C. Barnhart and B. R. McMahon. Discontinuous carbon dioxide release and metabolic depression in dormant land snails. *Journal of Experimental Biology*, 128:123–138, 1987.

W. Becker. Microcalorimetric studies in biomphalaria glabrata: The influence of schistosoma mansoni on the basal metabolism. *Journal of comparative physiology*, 135(2):101–105, 1980. ISSN 0340-7594. doi: 10.1007/BF00691199. URL http://dx.doi.org/10.1007/BF00691199.

W. Becker and I. Lamprecht. Mikrokalorimetrische untersuchungen zum wirt-parasit-verhältnis zwischen biomphalaria glabrata und schistosoma mansoni. *Zeitschrift für Parasitenkunde*, 53(3):297–305, 1977. ISSN 0044-3255. doi: 10.1007/BF00389947. URL http://dx.doi.org/10.1007/BF00389947.

K. Berg and K. W. Ockelmann. The respiration of freshwater snails. *Journal of Experimental Biology*, 36(4):690–708, 1959.

L. v. Bertalanffy. Quantitative laws in metabolism and growth. *Quart. Rev. Biol.*, 32(3):217–231, 1957.

L. v. Bertalanffy and I. Müller. Untersuchungen über die gesetzlichkeit des wachstums. viii: Die abhängigkeit des stoffwechsels von der körpergröße und der zusammenhang von stoffwechseltypen und wachstumstypen. *Riv. Biol.*, 35:48–95, 1943.

P. Blazka. Temperaturadaption des gesamtmetabolismus bei der weinbergschnecke helix pomatia l. *Zool. Jb., Abt. allg. Zool. u. Physiol.*, 65:430–438, 1955.

F. Bloch. Nuclear induction. *Physical Review*, 70(7-8):460–474, 1946. URL http://link.aps.org/doi/10.1103/PhysRev.70.460. PR.

P. Böckh and T. Wetzel. *Wärmeübertragung. Grundlagen und Praxis. 2., bearb. Aufl.* Springer, 2014.

S. L. Chown, E. Marais, J. S. Terblanche, C. J. Klok, J. R. B. Lighton, and T. M. Blackburn. Scaling of insect metabolic rate is inconsistent with the nutrient supply network model. *Functional Ecology*, 21(2):282–290, 2007. ISSN 1365-2435. doi: 10.1111/j.1365-2435.2007.01245.x. URL http://dx.doi.org/10.1111/j.1365-2435.2007.01245.x.

W. J. Crozier and T. B. Stier. Temperature characteristic for heart beat frequency in limax. *The Journal of General Physiology*, 7(6):705–708, 1925.

doi: 10.1085/jgp.7.6.705. URL http://jgp.rupress.org/content/7/6/705.abstract.

E. Cussler. *Diffusion: Mass Transfer in Fluid Systems*. Cambridge University Press, 2009. ISBN 9781139474214. URL https://books.google.de/books?id=w_RXbN61PrEC.

M. Czarnołęski, J. Kozłowski, G. Dumiot, J.-C. Bonnet, J. Mallard, and M. Dupont-Nivet. Scaling of metabolism in helix aspersa snails: changes through ontogeny and response to selection for increased size. *Journal of Experimental Biology*, 211(3):391–400, 2008. doi: 10.1242/jeb.013169. URL http://jeb.biologists.org/content/211/3/391.abstract.

B. Dale. The eco-physiological significance of the circulatory mechanics of lymnaea stagnalis l. *Comparative Biochemistry and Physiology Part A: Physiology*, 47(3):1105–1113, 1974. ISSN 0300-9629. doi: http://dx.doi.org/10.1016/0300-9629(74)90483-6. URL http://www.sciencedirect.com/science/article/pii/0300962974904836.

A. S. Dalkilic, B. Kundu, and S. Wongwises. An experimental investigation of the reynolds analogy and its modifications applied to annular condensation laminar flow of r134a in a vertical tube. *Arabian Journal for Science and Engineering*, 38(6):1493–1507, 2013. ISSN 1319-8025. doi: 10.1007/s13369-013-0595-0. URL http://dx.doi.org/10.1007/s13369-013-0595-0.

H. F. Dallas, B. A. Curtis, and D. Ward. Water exchange, temperature tolerance, oxygen consumption and activity of the namib desert snail, trigonephrus sp. *J. Moll. Stud.*, 57(3):359–366, 1991. doi: 10.1093/mollus/57.3.359.

P. L. DeFur and C. P. Mangum. The effects of environmental variables on the heart rates of invertebrates. *Comparative Biochemistry and Physiology Part A: Physiology*, 62(2):283–294, 1979. ISSN 0300-9629. doi: http://dx.doi.org/10.1016/0300-9629(79)90058-6. URL http://www.sciencedirect.com/science/article/pii/0300962979900586.

M. H. Depledge and D. J. H. Phillips. Circulation, respiration and fluid dynamics in the gastropod mollusc, hemifusus tuba (gmelin). *Journal of Experimental Marine Biology and Ecology*, 95(1):1–13, 1986. ISSN 0022-0981. doi: http://dx.doi.org/10.1016/0022-0981(86)90083-3. URL `http://www.sciencedirect.com/science/article/pii/0022098186900833`.

A. Dieterich. *Ökophysiologische Konsequenzen und Bewältigung hoher Habitattemperaturen bei mediterranen Landschnecken*. PhD thesis, University of Tübingen, 2015.

A. Dieterich, U. Fischbach, M. Ludwig, M. A. Di Lellis, S. Troschinski, U. Gärtner, R. Triebskorn, and H. R. Köhler. Daily and seasonal changes in heat exposure and the hsp70 level of individuals from a field population of xeropicta derbentina (krynicki 1836) (pulmonata, hygromiidae) in southern france. *Cell Stress and Chaperones*, 18(4):405–414, 2013. ISSN 1355-8145. doi: 10.1007/s12192-012-0393-8.

A. Dieterich, S. Troschinski, S. Schwarz, M. A. Di Lellis, A. Henneberg, U. Fischbach, M. Ludwig, U. Gärtner, R. Triebskorn, and H. R. Köhler. Hsp70 and lipid peroxide levels following heat stress in xeropicta derbentina (krynicki 1836) (gastropoda, pulmonata) with regard to different colour morphs. *Cell Stress and Chaperones*, pages 1–10, 2014. ISSN 1355-8145. doi: 10.1007/s12192-014-0534-3.

K. Drong and I. Lamprecht. Toxicological studies of energy flows in ecological systems. *Pure and Applied Chemistry*, 65(9):1967–1972, 1993. doi: 10.1351/pac199365091967.

F. G. Duerr. Changes in the size-metabolic rate relationship of lymnaea stagnalis appressa say produced by digenetic trematode parasitism. *Comparative Biochemistry and Physiology*, 20(2):391–398, 1967. ISSN 0010-406X. doi: dx.doi.org/10.1016/0010-406X(67)90255-1. URL `http://www.sciencedirect.com/science/article/pii/0010406X67902551`.

H. Eckwert, G. Alberti, and H.-R. Köhler. The induction of stress proteins (hsp) in oniscus asellus (isopoda) as a molecular marker of multiple heavy metal exposure: I. principles and toxicological assessment. *Ecotoxicology*, 6 (5):249–262, 1997. ISSN 0963-9292. doi: 10.1023/A:1018682928839.

L. Fahrenholz, I. Lamprecht, and B. Schricker. Microcalorimetric investigations of the energy metabolism of honeybee workers, apis mellifera carnica. *Thermochimica Acta*, 151(0):13–21, 1989. ISSN 0040-6031. doi: dx.doi.org/10.1016/0040-6031(89)85333-X. URL http://www.sciencedirect.com/science/article/pii/004060318985333X.

R. L. Fournier. *Basic transport phenomena in biomedical engineering*. Taylor and Francis Ltd, New York [u.a.], 2. edition, 2007. ISBN 1-59169-026-9. URL http://digitool.hbz-nrw.de:1801/webclient/DeliveryManager?pid=2098188&custom_att_2=simple_viewer.

J. D. Gaitán-Espitia, A. Bruning, F. Mondaca, and R. F. Nespolo. Intraspecific variation in the metabolic scaling exponent in ectotherms: Testing the effect of latitudinal cline, ontogeny and transgenerational change in the land snail cornu aspersum. *Comparative Biochemistry and Physiology. Part A, Physiology*, 165(2):169–177, 2013. ISSN 1095-6433. doi: 10.1016/j.cbpa.2013.03.002. URL http://www.sciencedirect.com/science/article/pii/S1095643313000603.

D. S. Glazier. Beyond the '3/4-power law': variation in the intra-and interspecific scaling of metabolic rate in animals. *Biological Reviews*, 80(4):611–662, 2005. ISSN 1469-185X. doi: 10.1017/S1464793105006834. URL http://dx.doi.org/10.1017/S1464793105006834.

D. S. Glazier. The 3/4-power law is not universal: Evolution of isometric, ontogenetic metabolic scaling in pelagic animals. *BioScience*, 56(4):325–332, 2006. doi: 10.1641/0006-3568(2006)56[325:tplinu]2.0.co;2. URL http://bioscience.oxfordjournals.org/content/56/4/325.abstract.

D. S. Glazier. Activity affects intraspecific body-size scaling of metabolic rate in ectothermic animals. *Journal of Comparative Physiology. B, Biochemical, Systemic, and Environmental Physiology*, 179(7):821–828, 2009. ISSN 0174-1578. doi: 10.1007/s00360-009-0363-3. URL http://dx.doi.org/10.1007/s00360-009-0363-3.

E. Gnaiger. Das kalorische äquivalent des atp-umsatzes im aeroben und anoxischen metabolismus. *Thermochimica Acta*, 40(1):195–223, 1980. ISSN

0040-6031. doi: dx.doi.org/10.1016/0040-6031(80)87186-3. URL http://www.sciencedirect.com/science/article/pii/0040603180871863.

E. Gnaiger, J. M. Shick, and J. Widdows. Metabolic microcalorimetry and respirometry of aquatic animals. *Techniques in comparative respiratory physiology: an experimental approach. Cambridge University Press, Cambridge*, pages 113–135, 1989.

J. N. R. Grainger. *Quantitative Biology of Metabolism: Models of Metabolism, Metabolic Parameters, Damage to Metabolism, Metabolic Control*, chapter The Relation between Heat Production, Oxygen Consumption and Temperature in Some Poikilotherms, pages 86–90. Springer Berlin Heidelberg, Berlin, Heidelberg, 1968. ISBN 978-3-642-51065-6. doi: 10.1007/978-3-642-51065-6_11. URL http://dx.doi.org/10.1007/978-3-642-51065-6_11.

J. Grote. Die sauerstoffdiffusionskonstanten im lungengewebe und wasser und ihre temperaturabhängigkeit. *Pflüger's Archiv für die gesamte Physiologie des Menschen und der Tiere*, 295(3):245–254, 1967. ISSN 0365-267x. doi: 10.1007/BF01844104. URL http://dx.doi.org/10.1007/BF01844104.

E. L. Hahn. Spin echoes. *Physical Review*, 80(4):580–594, 1950. URL http://link.aps.org/doi/10.1103/PhysRev.80.580. PR.

C. S. Hammen. Metabolic rates of marine bivalve molluscs determined by calorimetry. *Comparative Biochemistry and Physiology Part A: Physiology*, 62(4):955–959, 1979. ISSN 0300-9629. doi: dx.doi.org/10.1016/0300-9629(79)90034-3. URL http://www.sciencedirect.com/science/article/pii/0300962979900343.

C. S. Hammen. Total energy metabolism of marine bivalve mollusks in anaerobic and aerobic states. *Comparative Biochemistry and Physiology Part A: Physiology*, 67(4):617–621, 1980. ISSN 0300-9629. doi: dx.doi.org/10.1016/0300-9629(80)90250-9. URL http://www.sciencedirect.com/science/article/pii/0300962980902509.

L. G. Hanson. Is quantum mechanics necessary for understanding magnetic resonance? *Concepts in Magnetic Resonance Part A*, 32A(5):329–340, 2008.

ISSN 1552-5023. doi: 10.1002/cmr.a.20123. URL http://dx.doi.org/10.1002/cmr.a.20123.

R. Hashemi, W. Bradley, and C. Lisanti. *MRI: The Basics*. Lippincott Williams and Wilkins, 2010. ISBN 9781608311156.

K. Hausser and H. Kalbitzer. *NMR für Mediziner und Biologen: Strukturbestimmung, Bildgebung, In-vivo-Spektroskopie*. Springer, 1989.

J. P. Herold. Myocardial efficiency in the isolated ventricle of the snail, helix pomatia l. *Comparative Biochemistry and Physiology Part A: Physiology*, 52(3):435–440, 1975. ISSN 0300-9629. doi: http://dx.doi.org/10.1016/S0300-9629(75)80061-2. URL http://www.sciencedirect.com/science/article/pii/S0300962975800612.

C. F. Herreid. Metabolism of land snails (otala lactea) during dormancy, arousal, and activity. *Journal of Experimental Biology*, 55:385–398, 1977. doi: 10.1016/0300-9629(77)90187-6.

R. Hill and J. Welsh. *Physiology of Mollusca*, volume 2. Academic Press, New York, 2013. ISBN 9781483275857. URL https://books.google.de/books?id=XTLgBAAAQBAJ.

J. P. Hornak. The basics of mri, 1996. URL http://www.cis.rit.edu/htbooks/mri/.

F. R. Horne. The utilization of foodstuffs and urea production by a land snail during estivation. *Biological Bulletin*, 144(2):321–330, 1973. ISSN 00063185. doi: 10.2307/1540011. URL http://www.jstor.org/stable/1540011.

F. Incropera. *Fundamentals of heat and mass transfer*. John Wiley, 6th edition, 2007. ISBN 9780471457282. URL https://books.google.de/books?id=_P9QAAAAMAAJ.

M. Jischa. *Konvektiver Impuls-, Wärme- und Stoffaustausch*. Vieweg+Teubner Verlag, 1982. ISBN 9783528081447. URL https://books.google.de/books?id=ATQbAAAACAAJ.

G. B. Joachimsohn, I. Lamprecht, and B. Schaarschmidt. Cadmium induced changes of the metabolic activity of the freshwater snailplanorbis corneus estimated by direct calorimetry. *Journal of thermal analysis*, 35(2):659–669, 1989. ISSN 0022-5215. doi: 10.1007/BF01904466. URL http://dx.doi.org/10.1007/BF01904466.

H. D. Jones. Hydrostatic pressures within the heart and pericardium of patella vulgata l. *Comparative Biochemistry and Physiology*, 34(2):263–272, 1970. ISSN 0010-406X. doi: http://dx.doi.org/10.1016/0010-406X(70)90165-9. URL http://www.sciencedirect.com/science/article/pii/0010406X70901659.

H. D. Jones. Circulatory pressures in helix pomatia l. *Comparative Biochemistry and Physiology Part A: Physiology*, 39(2):289–295, 1971. ISSN 0300-9629. doi: http://dx.doi.org/10.1016/0300-9629(71)90085-5. URL http://www.sciencedirect.com/science/article/pii/0300962971900855.

G. A. Kerkut and R. M. A. P. Ridge. The effect of temperature changes on the activity on the neurones of the snail helix aspersa. *Comparative Biochemistry and Physiology*, 5(4):283–295, 1962. ISSN 0010-406X. doi: dx.doi.org/10.1016/0010-406X(62)90057-9. URL http://www.sciencedirect.com/science/article/pii/0010406X62900579.

G. A. Kerkut and B. J. R. Taylor. The effect of temperature changes on the activity of poikilotherms. *Behaviour*, 13(3/4):259–279, 1958. ISSN 00057959. doi: 10.2307/4532903. URL http://www.jstor.org/stable/4532903.

M.-L. Kienle. Körpergröße, körperzeiten und energiebilanz. xiii: Über beziehungen zwischen körpergröße, lungengröße und energiekonsum bei pulmonaten, insbesondere helix pomatia l. und zebrina detrita müll. *Z. vergl. Physiol.*, 40(4):440–450, 1957. doi: 10.1007/BF00340371.

M.-L. Kienle and W. Ludwig. Körperzeiten, körpergröße und energiebilanz. xi: Die beziehung zwischen körpergröße und sauerstoffverbrauch bei landpulmonaten. *Z. vergl. Physiol.*, 39:102–118, 1956.

L. Kiss, C. Labaune, F. Magnin, and S. Aubry. Plasticity of the life cycle of

xeropicta derbentina (krynicki, 1836), a recently introduced snail in mediterranean france. *J. Moll. Stud.*, 71:221–231, 2005. doi: 10.1093/mollus/eyi030.

M. Kleiber. Body size and metabolic rate. *Physiological Reviews*, 27(4):511–541, 1947.

H. R. Köhler. Die rolle von stressproteinen bei der anpassung an umweltbedingungen: Ökophysiologische, ökotoxikologische und evolutionsbiologische implikationen. *Environmental Sciences Europe*, 21(2):150–159, 2009. doi: 10.1007/s12302-009-0041-9.

H.-R. Köhler, R. Triebskorn, W. Stöcker, P.-M. Kloetzel, and G. Alberti. The 70 kd heat shock protein (hsp 70) in soil invertebrates: A possible tool for monitoring environmental toxicants. *Archives of Environmental Contamination and Toxicology*, 22(3):334–338, 1992. ISSN 0090-4341. doi: 10.1007/BF00212095.

H.-R. Köhler, R. Lazzara, N. Dittbrenner, Y. Capowiez, C. Mazzia, and R. Triebskorn. Snail phenotypic variation and stress proteins: do different heat response strategies contribute to waddington's widget in field populations? *Journal of Experimental Zoology Part B: Molecular and Developmental Evolution*, 312B(2):136–147, 2009. ISSN 1552-5015. doi: 10.1002/jez.b.21253. URL `http://dx.doi.org/10.1002/jez.b.21253`.

J. Kozłowski, M. Konarzewski, and A. T. Gawelczyk. Cell size as a link between noncoding dna and metabolic rate scaling. *Proc. Natl. Acad. Sci.*, 100(24):14080–14085, 2003. doi: 10.1073/pnas.2334605100. URL `http://www.pnas.org/content/100/24/14080.abstract`.

U. Krämer. Säure-basen-status und blutgase, 2005. URL `http://mtaschule-os.de/media/8976a2dd1f07d516ffff80dfac14422f.pdf`.

M. Kraume. *Transportvorgänge in der Verfahrenstechnik: Grundlagen und apparative Umsetzungen*. Springer Berlin Heidelberg, 2012. ISBN 9783642251481. URL `https://books.google.de/books?id=wXRLLwEACAAJ`.

I. Lamprecht. Monitoring metabolic activities of small animals by means of microcalorimetry. *Pure and Applied Chemistry*, 70(3):695–700, 1998. doi: dx.doi.org/10.1351/pac199870030695.

I. Lamprecht and W. Becker. Combination of calorimetry and endoscopy for monitoring locomotor activities of small animals. *Thermochimica Acta*, 130(0):87–93, 1988. ISSN 0040-6031. doi: 10.1016/0040-6031(88)87053-9. URL http://www.sciencedirect.com/science/article/pii/0040603188870539.

I. Lamprecht and F. R. Matuschka. Microcalorimetric investigations of the energy metabolism of some reptiles. *Thermochimica Acta*, 94(1):161–167, 1985. ISSN 0040-6031. doi: dx.doi.org/10.1016/0040-6031(85)85256-4. URL http://www.sciencedirect.com/science/article/pii/0040603185852564.

R. Larsen and T. Ziegenfuß. *Beatmung: Grundlagen und Praxis*. Springer, 2009. ISBN 9783540888116. URL https://books.google.de/books?id=FaYzy3Hfq-QC.

D. Lide. *CRC Handbook of Chemistry and Physics, 85th Edition*. Taylor and Francis, 2004. ISBN 9780849304859. URL https://books.google.de/books?id=WDll8hA006AC.

W. Liebsch. Über die atmung einiger heliciden. *Zool. Jb., Abt. allg. Zool. u. Physiol.*, 46:161–208, 1929.

M. Ludwig. private communication, 2012.

G. Lusk. Animal calorimetry: Twenty-fourth paper. analysis of the oxidation of mixtures of carbohydrate and fat. *Journal of Biological Chemistry*, 59(1):41–42, 1924. URL http://www.jbc.org/content/59/1/41.short.

J. A. Maas. Über die atmung von helix pomatia l. *Zeitschrift für vergleichende Physiologie*, 26(5):605–610, 1939. ISSN 0044-362x. doi: 10.1007/BF00341094. URL http://dx.doi.org/10.1007/BF00341094.

J. Markl. Blaues blut – struktur, funktion und evolution der hämocyanine. *Chemie in unserer Zeit*, 30(1):6–18, 1996. ISSN 1521-3781. doi: 10.1002/ciuz.19960300103. URL http://dx.doi.org/10.1002/ciuz.19960300103.

C. F. Mason. Respiration rates and population metabolism of woodland snails. *Oecologia*, 7(1):80–94, 1971. doi: 10.1007/BF00346295.

M. P. Mayer and B. Bukau. Hsp70 chaperones: Cellular functions and molecular mechanism. *Cellular and Molecular Life Sciences*, 62(6):670–684, 2005. doi: 10.1007/s00018-004-4464-6.

K. Mellanby. Low temperature and insect activity. *Proceedings of the Royal Society of London. Series B - Biological Sciences*, 127(849):473–487, 1939. doi: 10.1098/rspb.1939.0035. URL http://rspb.royalsocietypublishing.org/content/127/849/473.short.

F. F. Mikkelsen and R. E. Weber. Oxygen transport and hemocyanin function in the pulmonate land snail, helix pomatia: Physiological and molecular implications of polyphasic oxygen-binding curves. *Physiological Zoology*, 65 (6):1057–1073, 1992. ISSN 0031935X. doi: 10.2307/30158268. URL http://www.jstor.org/stable/30158268.

T. Mizrahi, J. Heller, S. Goldenberg, and Z. Arad. Heat shock protein expression in relation to reproductive cycle in land snails: Implications for survival. *Comparative Biochemistry and Physiology. Part A, Physiology*, 160(2):149–155, 2011. doi: 10.1016/j.cbpa2011.05.031.

R. Müller. Atmung, stoffwechsel und blutkreislauf. *Praxis der Naturwissenschaften - Physik in der Schule*, 50(8):23–26, 2001.

C. D. Murray. The physiological principle of minimum work: I. the vascular system and the cost of blood volume. *Proceedings of the National Academy of Sciences of the United States of America*, 12(3):207–214, 1926. ISSN 0027-8424 1091-6490. URL http://www.ncbi.nlm.nih.gov/pmc/articles/PMC1084489/. 16576980[pmid] Proc Natl Acad Sci U S A.

H. Nopp. Temperaturbezogene regulationen des sauerstoffverbrauchs und der herzschlagrate bei einigen landpulmonaten. *Z. vergl. Physiol.*, 50(6):641–659, 1965. doi: 10.1007/BF00365257.

M. M. Pamatmat. Oxygen uptake and heat production in a metabolic conformer (littorina irrorata) and a metabolic regulator (uca pugnax). *Marine Biology*, 48(4):317–325, 1978. ISSN 0025-3162. doi: 10.1007/BF00391635. URL `http://dx.doi.org/10.1007/BF00391635`.

M. M. Pamatmat. Measuring aerobic and anaerobic metabolism of benthic infauna under natural conditions. *Journal of Experimental Zoology*, 228 (3):405–413, 1983. ISSN 1097-010X. doi: 10.1002/jez.1402280303. URL `http://dx.doi.org/10.1002/jez.1402280303`.

G. J. Peakin. The measurement of the costs of maintenance in terrestrial poikilotherms: A comparison between respirometry and calorimetry. *Experientia*, 29(7):801–802, 1973. ISSN 0014-4754. doi: 10.1007/BF01946295. URL `http://dx.doi.org/10.1007/BF01946295`.

B. B. Rees and S. C. Hand. Heat dissipation, gas exchange and acid-base status in the land snail oreohelix during short-term estivation. *Journal of Experimental Biology*, 152(1):77–92, 1990. URL `http://jeb.biologists.org/content/152/1/77.abstract`.

A. Reuner, F. Brümmer, and R. O. Schill. Heat shock proteins (hsp70) and water content in the estivating mediterranean grunt snail (cantareus apertus). *Comparative Biochemistry and Physiology Part B: Biochemistry and Molecular Biology*, 151(1):28–31, 2008. ISSN 1096-4959. doi: dx.doi.org/10.1016/j.cbpb.2008.05.004.

W. A. Riddle. Water relations and humidity-related metabolism of the desert snail rabdotus schiedeanus (pfeiffer) (helicidae). *Comparative Biochemistry and Physiology. Part A, Physiology*, 51(3):579–583, 1975. doi: 10.1016/0300-9629(75)90344-8.

W. A. Riddle. Comparative respiratory physiology of a desert snail radbotus schiedeanus, and a garden snail, helix aspersa. *Comparative Biochemistry and Physiology. Part A, Physiology*, 56(3):369–373, 1977. doi: 10.1016/0300-9629(77)90251-1.

T. L. Rising and K. B. Armitage. Acclimation to temperature by the terrestrial gastropods, limax maximus and philomycus carolinianus: oxygen consump-

tion and temperature preferences. *Comparative Biochemistry and Physiology*, 30(6):1091–1114, 1969. doi: 10.1016/0010-406X(69)91047-0. URL http://www.ncbi.nlm.nih.gov/pubmed/5349635. Rising, T L Armitage, K B eng 1969/09/15 Comp Biochem Physiol. 1969 Sep 15;30(6):1091-114.

A. Rizzatti and S. Romero. Heart rate and body weight alterations in juvenile specimens of the tropical land snail megalobulimus sanctipauli during dormancy. *Brazilian Journal of Medical and Biological Research*, 34:959–967, 2001. ISSN 0100-879X.

M. Rubner. Über den einfluss der körpergrösse auf stoff- und kraftwechsel. *Z. Biol. Munich*, 19:535–562, 1883.

A. Saleuddin and K. Wilbur. *The Mollusca: Physiology*. Elsevier Science, 2012. ISBN 9780323139212. URL https://books.google.de/books?id=9yvtRJkyhU4C.

R. Sander. Compilation of henry's law constants for inorganic and organic species of potential importance in environmental chemistry, 1999.

R. Sander. Compilation of henry's law constants (version 4.0) for water as solvent. *Atmos. Chem. Phys.*, 15(8):4399–4981, 2015. ISSN 1680-7324. doi: 10.5194/acp-15-4399-2015. URL http://www.atmos-chem-phys.net/15/4399/2015/. ACP.

R. F. Schmidt, F. Lang, and M. Heckmann. *Physiologie Des Menschen: Mit Pathophysiologie*. Springer Medizin Verlag Heidelberg, 2005. ISBN 9783540264163. URL http://books.google.de/books?id=Ig0Ah9bpYfAC.

K. Schmidt-Nielsen, C. R. Taylor, and A. Shkolnik. Desert snails: problems of heat, water and food. *Journal of Experimental Biology*, 55:385–398, 1971.

J. Schwartzkopff. Das herzminutenvolumen von helix pomatia l. *Experientia*, 9(11):428–429, 1953. ISSN 0014-4754. doi: 10.1007/BF02175534. URL http://dx.doi.org/10.1007/BF02175534.

J. Schwartzkopff. Über die leistung des isolierten herzens der weinbergschnecke (helix pomatia l.) im künstlichen kreislauf. *Zeitschrift für vergle-*

ichende Physiologie, 36(6):543–594, 1954. ISSN 0044-362x. doi: 10.1007/BF00339387. URL http://dx.doi.org/10.1007/BF00339387.

E. Segal. Acclimation in molluscs. *Am. Zool.*, 1(2):235–244, 1961.

P. J. S. Smith. Cardiac performance in response to loading pressures in busycon canaliculatum (gastropoda) and mercenaria mercenaria (bivalvia). *Journal of Experimental Biology*, 119(1):301–320, 1985. URL http://jeb.biologists.org/content/119/1/301.abstract.

P. J. S. Smith. Cardiac output in the mollusca: Scope and regulation. *Experientia*, 43(9):956–965, 1987. ISSN 0014-4754. doi: 10.1007/BF01952210. URL http://dx.doi.org/10.1007/BF01952210.

P. J. S. Smith and R. B. Hill. Modulation of output from an isolated gastropod heart: Effects of acetylcholine and fmrfamide. *Journal of Experimental Biology*, 127(1):105–120, 1987. URL http://jeb.biologists.org/content/127/1/105.abstract.

D. Sonntag. Important new values of the physical constants of 1986, vapour pressure formulations based on the its-90, and psychrometer formulae. *Z. Meteorol.*, 70(5):340–344, 1990.

E. Specht. Grundlagen der Wärme- und Stoffübertragung. http://www.uni-magdeburg.de/isut/TV/Download/Waerme-_und_Stoffuebertragung_Kapitel_1+2_WS0809.pdf, 2008. Lecture given at the Univ. of Magdeburg.

A. L. Steigen. Temperature effects on energy metabolism in banded and unbanded morphs of the snail cepaea hortensis müll. *Oecologia*, 41(2):163–173, 1979. doi: 10.1007/BF00345000.

V. Storch, U. Welsch, and W. Kükenthal. *Kükenthal Zoologisches Praktikum*. Elsevier, Spektrum, Akad. Verlag, 2006. ISBN 9783827416438. URL https://books.google.de/books?id=TmHQAAAACAAJ.

R. S. Subramanian. Heat transfer in flow throug conduits, 2014. URL http://web2.clarkson.edu/projects/subramanian/ch330/notes/HeatTransferinFlowThoroughConduits.pdf.

R. Triebskorn, H.-R. Köhler, W. Honnen, M. Schramm, S. M. Adams, and E. Müller. Induction of heat shock proteins, changes in liver ultrastructure, and alterations of fish behavior: are these biomarkers related and are they useful to reflect the state of pollution in the field? *Journal of Aquatic Ecosystem Stress and Recovery*, 6(1):57–73, 1997. ISSN 1386-1980. doi: 10.1023/A:1008224301117.

S. Troschinski, M. A. Di Lellis, S. Sereda, T. Hauffe, T. Wilke, R. Triebskorn, and H.-R. Köhler. Intraspecific variation in cellular and biochemical heat response strategies of mediterranean xeropicta derbentina [pulmonata, hygromiidae]. *PLoS ONE*, 9(1):1–15, 2014. ISSN 19326203. doi: 10.1371/journal.pone.0086613.

C. O. Van Regteren Altena. On the occurrence of a species of xeropicta in france. *Basteria*, 24:21–26, 1960.

R. L. Webb. A critical evaluation of analytical solutions and reynolds analogy equations for turbulent heat and mass transfer in smooth tubes. *Wärme - und Stoffübertragung*, 4(4):197–204, 1971. ISSN 0042-9929. doi: 10.1007/BF01002474. URL `http://dx.doi.org/10.1007/BF01002474`.

H. Wesemeier. Untersuchungen über die stoffwechselreduktion. ein intra- und interspezifischer vergleich an 17 molluskenarten. *Z. vergl. Physiol.*, 43(1): 1–28, 1960. doi: 10.1007/BF00351199.

G. B. West and J. H. Brown. The origin of allometric scaling laws in biology from genomes to ecosystems: towards a quantitative unifying theory of biological structure and organization. *Journal of Experimental Biology*, 208(9): 1575–1592, 2005. doi: 10.1242/jeb.01589. URL `http://jeb.biologists.org/content/208/9/1575.abstract`.

G. B. West, J. H. Brown, and B. J. Enquist. A general model for the origin of allometric scaling laws in biology. *Science*, 276(5309):122–126, 1997. doi: 10.1126/science.276.5309.122. URL `http://www.sciencemag.org/content/276/5309/122.abstract`.

S. Yengkokpam, A. Pal, N. Sahu, K. Jain, R. Dalvi, S. Misra, and D. Debnath. Metabolic modulation in labeo rohita fingerlings during starvation: Hsp70

expression and oxygen consumption. *Aquaculture*, 285(1-4):234–237, 2008. doi: 10.1016/j.aquaculture.2008.08.034.